ML-TDR-64-125
VOLUME II

IMPROVED GRAPHITE MATERIALS FOR HIGH-TEMPERATURE AEROSPACE USE

VOLUME II — DEVELOPMENT OF GRAPHITE-REFRACTORY COMPOSITES

TECHNICAL DOCUMENTARY REPORT No. ML-TDR-64-125, VOL. II

UNION CARBIDE CORPORATION
LAWRENCEBURG, TENNESSEE

OCTOBER 1964

AIR FORCE MATERIALS LABORATORY
RESEARCH AND TECHNOLOGY DIVISION
AIR FORCE SYSTEMS COMMAND
WRIGHT-PATTERSON AIR FORCE BASE, OHIO

Blank Page

NOTICES

When Government drawings, specifications, or other data are used for any purpose other than in connection with a definitely related Government procurement operation, the United States Government thereby incurs no responsibility nor any obligation whatsoever; and the fact that the Government may have formulated, furnished, or in any way supplied the said drawings, specifications, or other data, is not to be regarded by implication or otherwise as in any manner licensing the holder or any other person or corporation, or conveying any rights or permission to manufacture, use, or sell any patented invention that may in any way be related thereto.

Qualified requesters may obtain copies of this report from the Defense Documentation Center (DDC), (formerly ASTIA), Cameron Station, Bldg. 5, 5010 Duke Street, Alexandria, Virginia, 22314.

This report has been released to the Office of Technical Services, U.S. Department of Commerce, Washington 25, D. C., for sale to the general public.

Copies of this report should not be returned to the Research and Technology Division, Wright-Patterson Air Force Base, Ohio, unless return is required by security considerations, contractual obligations, or notice on a specific document.

300 - December 1964 - 448-17-439

Blank Page

FOREWORD

This report was prepared by the Union Carbide Corporation, Carbon Products Division, under Contract No. AF 33(657)-11171. The contract was initiated under Project No. 7350, "Refractory Inorganic Nonmetallic Materials," Task No. 735002, "Refractory Nonmetallic Materials: Graphitic." The research and development program was accomplished at the Carbon Products Division, Advanced Materials Laboratory, Lawrenceburg, Tennessee, and the Carbon Products Research Laboratory, Parma, Ohio. The work was administered under the direction of the Air Force Materials Laboratory, Research and Technology Division; Major R. H. Wilson and C. A. Pratt, Jr., were the project engineers.

Volume I of this report covers work conducted from 1 May 1963 to 31 March 1964 on Task 1, "Research and Development for Improved Graphite Materials." Volume II covers work conducted from 1 May 1963 to 30 April 1964 on Task 2, "Development of Graphite-Refractory Composites."

The program has been under the direction of Mr. R. M. Bushong. Work at the Carbon Products Research Laboratory was under the supervision of Mr. J. C. Bowman, with Dr. W. W. Lozier serving as Project Coordinator. Scientists at the Research Laboratory were Messrs. M. Janes, I. C. Lewis, T. Edstrom, C. V. Mitchell, L. S. Singer, M. Haun, A. R. Cherry, C. E. Lowell and Mrs. S. B. Wallon. Work at the Advanced Materials Laboratory was under the supervision of Mr. R. C. Stroup, with Mr. M. B. Carter serving as Project Coordinator. "Task 1" experimentalists were Messrs. C. F. Stout (Group Leader), G. C. Tolley, E. R. McHenry, and J. H. Turner. "Task 2" experimentalists were Messrs. K. J. Zeitsch (Group Leader), W. C. Beasley, W. E. Biles, and J. D. Cannon, with testing, processing and applications support by Dr. R. B. Dull and Messrs. C. W. Waters and D. C. Hiler.

ABSTRACT

New graphite-base refractory composites were developed through the selective substitution of the components in grade JTA. Studies were conducted on the following composite changes: zirconium, silicon and niobium replacement of boron; and niobium, cerium and lanthanum replacement of silicon. Studies of graphite-oxide reactions have provided information concerning the stability of oxide coatings in contact with carbon bodies. Insight was gained into the mechanisms of such reactions when their limits of stability are exceeded. A high-temperature apparatus was developed to supplement existing oxidation tests at this laboratory. Cyclic tests of short duration were completed on grade ATJ, SiC-coated RVC and grade JTA. Additional tests using exposures of 5, 15, 30, and 60 minutes over the temperature range of 1400° to 1800°C were performed on grade JTA. These data were used as a basis for screening new composites. The most oxidation-resistant composite was JT-0981 in which the boron was completely replaced with silicon. This material exhibited excellent performance at 1700, 1800, 1900, and 2000°C; however, at lower temperatures, no protective coating was formed and the performance was poor. Plasma tests conducted at 1900°C on the front face of JTA samples shows its excellent oxidation resistance. Similar tests on JT-0981 were stopped when the low temperature areas on the samples were losing material faster than the hot face.

W. G. RAMKE
Chief, Ceramics and Graphite Branch
Metals and Ceramics Division
AF Materials Laboratory

TABLE OF CONTENTS

PAGE

1. INTRODUCTION 1

2. SUMMARY 3

3. FUNDAMENTAL INVESTIGATIONS 4

3.1. Gas Development from Graphite-Oxide Powder Reactions 4

3.1.1. Description of Apparatus and Experimental Procedure 4
3.1.2. Results 10

3.2. Studies of Massive Graphite-Oxide Systems 43

3.2.1. Oxide Spheres Embedded in Graphite 44

3.3. Conclusions 64

4. COMPOSITIONAL STUDIES ON GRAPHITE-BASE REFRACTORY COMPOSITES 66

4.1. Fabrication 66

4.2. Preliminary Screening for Oxidation Resistance 66

4.3. Results 68

4.3.1. Effect of Replacing Boron in JTA 69
4.3.2. Effect of Replacing Silicon in JTA 73
4.3.3. Effect of Multiple Replacements in JTA 77
4.3.4. Effect of Increasing the Carbon Content of JTA 80
4.3.5. Graphite-Oxide-Silicon Composites 80

5. CHARACTERIZATION OF SELECTED MATERIALS 85

5.1. Oxidation Resistance 85

5.1.1. Testing at Atmospheric Pressure 85
5.1.2. Pressure Effects on Oxidation Rates 106

5.2. Physical Properties 110

5.2.1. JTA 110
5.2.2. JT-0981 114

TABLE OF CONTENTS (CONT'D)

PAGE

6. APPLICATION TESTING OF SELECTED MATERIALS 118

6.1. Performance of ATJ Graphite, JTA, JT-0965, and JT-0981 in High-Velocity Air Plasma. 118

6.1.1. ATJ and JTA Testing 118
6.1.2. JT-0965 and JT-0981 Testing 123

6.2. Performance of JTA in Rocket Motors 124

7. RECOMMENDATIONS FOR FUTURE WORK 127

8. REFERENCES 128

ILLUSTRATIONS

FIGURE		PAGE
1.	The Reaction of Graphite with Refractory Oxides, CO Equilibrium Pressure Versus Temperature	5
2.	Torsional Effusion Apparatus, Cross Section	6
3.	Torsional Effusion Apparatus, Overall View	7
4.	Calibration of the Torsional Effusion Apparatus with Germanium	9
5.	Change of Zero Drift with Time, Bell Jar Pressure, 1.3×10^{-6} Atm, Initial Azimuth, 135 Degrees	11
6.	The Reaction of Graphite with Aluminum Sesquioxide, Scanning Experiment	12
7.	The Reaction of Graphite with Beryllium Monoxide, Scanning Experiment	13
8.	The Reaction of Graphite with Calcium Zirconate, Scanning Experiment	14
9.	The Reaction of Graphite with Cerium Dioxide, Scanning Experiment	15
10.	The Reaction of Graphite with Dysprosium Sesquioxide, Scanning Experiment	16
11.	The Reaction of Graphite with Erbium Sesquioxide, Scanning Experiment	17
12.	The Reaction of Graphite with Europium Sesquioxide, Scanning Experiment	18
13.	The Reaction of Graphite with Gadolinium Sesquioxide, Scanning Experiment	19
14.	The Reaction of Graphite with Hafnium Dioxide, Scanning Experiment	20
15.	The Reaction of Graphite with Holmium Sesquioxide, Scanning Experiment	21
16.	The Reaction of Graphite with Lanthanum Sesquioxide, Scanning Experiment	22
17.	The Reaction of Graphite with Lutecium Sesquioxide, Scanning Experiment	23

ILLUSTRATIONS (CONT'D)

FIGURE		PAGE
18.	The Reaction of Graphite with Magnesium Zirconate, Scanning Experiment	24
19.	The Reaction of Graphite with Niobium Sesquioxide, Scanning Experiment	25
20.	The Reaction of Graphite with Niobium Pentoxide, Scanning Experiment	26
21.	The Reaction of Graphite with Neodymium Sesquioxide, Scanning Experiment	27
22.	The Reaction of Graphite with Praseodymium Sesquioxide, Scanning Experiment	28
23.	The Reaction of Graphite with Scandium Sesquioxide, Scanning Experiment	29
24.	The Reaction of Graphite with Silicon Dioxide, Scanning Experiment	30
25.	The Reaction of Graphite with Samarium Sesquioxide, Scanning Experiment	31
26.	The Reaction of Graphite with Strontium Zirconate, Scanning Experiment	32
27.	The Reaction of Graphite with Terbium Sesquioxide, Scanning Experiment	33
28.	The Reaction of Graphite with Thorium Dioxide, Scanning Experiment	34
29.	The Reaction of Graphite with Thulium Sesquioxide, Scanning Experiment	35
30.	The Reaction of Graphite with Uranium Dioxide, Scanning Experiment	36
31.	The Reaction of Graphite with Yttrium Sesquioxide, Scanning Experiment	37
32.	The Reaction of Graphite with Ytterbium Sesquioxide, Scanning Experiment	38
33.	The Reaction of Graphite with Zirconium Dioxide, Scanning Experiment	39

ILLUSTRATIONS (CONT'D)

FIGURE		PAGE
34.	Reactions Between Graphite and Refractory Oxides, Comparison of Scanning Experiments, Pressure Isotherms for an Equilibrium Temperature of 1465°C	40
35.	Reactions Between Graphite and Refractory Oxides, Comparison of Scanning Experiments, Pressure Isotherms for an Equilibrium Temperature of 1575°C	41
36.	Reactions Between Graphite and Refractory Oxides, Comparison of Scanning Experiments, Pressure Isotherms for an Equilibrium Temperature of 1675°C	42
37.	Apparatus for Stability Studies on Massive Graphite-Oxide Systems	45
38.	Graphite-Alumina Systems After Exposure to High Temperature	46
39.	Graphite-Beryllia Systems After Exposure to High Temperature	48
40.	Graphite-Ceria Systems After Exposure to High Temperature	50
41.	Graphite-Hafnia Systems After Exposure to High Temperature	51
42.	Graphite-Strontium Zirconate Systems After Exposure to High Temperature	52
43.	Graphite-Thoria Systems After Exposure to High Temperature	54
44.	Graphite-Yttria Systems After Exposure to High Temperature	55
45.	Graphite-Zirconia Systems After Exposure to High Temperature	57
46.	ZrC Coating on ZrO_2, Produced by ZrO_2 in Contact with Massive Graphite at 2400°C for a Period of 1 Hour, Magnification: 7.75X	58
47.	Graphite-Zirconium Silicate Systems After Exposure to High Temperature	59

ILLUSTRATIONS (CONT'D)

FIGURE		PAGE
48.	Apparatus for Heating Oxide Pellets on a Graphite Pedestal	62
49.	SiO_2 Pellets After Being Heated on Graphite to Various Temperatures	63
50.	Y_2O_3 Pellets After Being Heated on Graphite to Various Temperatures	63
51.	Dy_2O_3 Pellets After Being Heated on Graphite to Various Temperatures	64
52.	Cross Sections of JTA and JT-0950 Test Samples After 10-Minute Exposures, Actual Size of Each Cross Section, $\frac{1}{4}$ Inch by $\frac{1}{4}$ Inch	68
53.	The Effect of Replacing Boron by Zirconium in JTA on the Cross Section of Test Samples Exposed for 10 Minutes, Actual Size of Cross Section, $\frac{1}{4}$ Inch by $\frac{1}{4}$ Inch	70
54.	The Effect of Replacing Boron by Silicon in JTA on the Cross Section of Test Samples Exposed for 10 Minutes, Actual Size of Cross Section, $\frac{1}{4}$ Inch by $\frac{1}{4}$ Inch	71
55.	The Effect of Replacing Boron by Niobium in JTA on the Cross Section of Test Samples Exposed for 10 Minutes, Actual Size of Cross Section, $\frac{1}{4}$ Inch by $\frac{1}{4}$ Inch	72
56.	The Effect of Replacing Silicon by Niobium in JTA on the Cross Section of Test Samples Exposed for 10 Minutes, Actual Size of Cross Section, $\frac{1}{4}$ Inch by $\frac{1}{4}$ Inch	74
57.	The Effect of Replacing Silicon by Lanthanum in JTA, Appearance of Samples After 10-Minute Exposures	75
58.	The Effect of Replacing Silicon by Cerium in JTA, Appearance of Samples After 10-Minute Exposures	76
59.	Cross Sections of JT-0974 After 10-Minute Exposures, Actual Size of Cross Section, $\frac{1}{4}$ Inch by $\frac{1}{4}$ Inch	77

FIGURE		PAGE
60.	The Effect of Varying the Ratio of Silicon to Zirconium in C/Zr/Si Composites with a Carbon Content of 48 Per Cent on the Cross Section of Test Samples Exposed for 10 Minutes, Actual Size of Cross Section, $\frac{1}{4}$ Inch by $\frac{1}{4}$ Inch	78
61.	Cross Sections of JTA and JT-0965 After 10-Minute Exposures, Actual Size of Cross Section, $\frac{1}{4}$ Inch by $\frac{1}{4}$ Inch	79
62.	Hot Zone Cross Sections of JT-0001 and JT-0005 After 10-Minute Exposures	82
63.	Hot Zone Cross Sections of JT-0030, JT-0040, and JT-0080 After 10-Minute Exposures	84
64.	High-Temperature Oxidation Apparatus, Cross Section	87
65.	Electromagnetic Rotation of Sample Sphere	88
66.	High-Temperature Oxidation Apparatus	88
67.	SiC-Coated RVC Graphite Before and After Oxidation at 1700°C	90
68.	JTA Sample After 5 Minutes of Oxidation at 1700°C	91
69.	JTA Sample Demonstrating Uniform Coating After 20 Minutes (4 Cycles) Oxidation at 1700°C	91
70.	Surface of JTA Sample Opposite Air Impingement After 80 Seconds at 2000°C	93
71.	Weight Loss Versus Exposure Time of JTA Between 1400° and 1800°C	93
72.	Appearance of JTA Samples After Testing, Upper Numbers Indicating Time of Exposure in Minutes	94
73.	Mean Oxidation Rate Versus Exposure Time for Grade JTA	95
74.	Appearance of JTA Sample After Being Tested for 11 Minutes at 1900°C	95

ILLUSTRATIONS (CONT'D)

FIGURE		PAGE
75.	Oxidation Characteristics of JTA Between 1400 and 1900°C, Relative Weight Loss Versus Time of Exposure	97
76.	Oxidation Characteristics of JTA Between 1400 and 1900°C, Mean Oxidation Rate Versus Time of Exposure	98
77.	Appearance of JTA Samples After Testing, Upper Numbers Indicating Time of Exposure in Minutes	99
78.	Effect of the Silicon Level on the Oxidation Behavior of C/Zr/Si Composites With a Carbon Content of 48 Per Cent	101
79.	Appearance of JT-0961 After 15 Minutes of Oxidation at 1800°C	101
80.	Coating Appearance of C/Hf/Si Composites as Compared with JTA and JT-0981 After 15 Minutes of Oxidation at 1800°C	102
81.	Oxidation Characteristics of JT-0981 Between 1400 and 2000°C, Relative Weight Loss Versus Time of Exposure	103
82.	Oxidation Characteristics of JT-0981 Between 1400 and 2000°C, Mean Oxidation Rate Versus Time of Exposure	103
83.	Appearance of JT-0981 Samples After Testing, Upper Numbers Indicating Time of Exposure in Minutes	104
84.	Comparison Between JTA and JT-0981, Mean Oxidation Rate Over 15 Minutes of Exposure Versus Temperature	105
85.	Oxidation Apparatus for Tests at Reduced and Elevated Pressures, Cross Section	107
86.	Oxidation Apparatus for Tests at Reduced and Elevated Pressures, Overall View	108
87.	Oxidation Characteristics of ATJ Graphite as a Function of the Ambient Pressure	109

ILLUSTRATIONS (CONT'D)

FIGURE		PAGE
88.	Oxidation Characteristics of JTA as a Function of the Ambient Pressure	109
89.	The Effect of Ambient Pressure on the Oxidation Behavior of JTA, Cross Sections of Samples After 10-Minute Exposures	111
90.	The Effect of Ambient Pressure on the Oxidation Behavior of JT-0981, Cross Sections of Samples After 10-Minute Exposures	112
91.	Tensile Stress-Strain Relationships for JTA at Room Temperature	114
92.	Flexural Strength of JTA Versus Temperature	115
93.	Thermal Expansion of JTA Versus Temperature	116
94.	Sample Configuration Employed in Plasma Tests	119
95.	Cross Section of JTA Sample After Four 6-Minute Air Plasma Exposures at a Front Surface Temperature of 1740°C	119
96.	JTA Sample After Four 6-Minute Air Plasma Exposures at a Front Surface Temperature of 1740°C, Interface Between Coating and Parent Material, 4X	120
97.	Appearance of ATJ and JTA Samples After Subsonic Exposures at Surface Temperatures of Approximately 1900°C	121
98.	Appearance of ATJ and JTA Samples After Sonic Exposures at Surface Temperatures of Approximately 1900°C	122
99.	Side View of JT-0965 After Sonic Air Plasma Exposure at a Front Surface Temperature of 2300°C, Test Duration, 200 Sec.	124
100.	Front View of JT-0965 After Sonic Air Plasma Exposures at a Front Surface Temperature of 2300°C, Test Duration, 200 Sec.	124
101.	Side View of JT-0981 After Sonic Air Plasma Exposure at a Front Surface Temperature of 2300°C, Test Duration, 200 Sec.	125

ILLUSTRATIONS (CONT'D)

FIGURE		PAGE
102.	Front View of JT-0981 After Sonic Air Plasma Exposure at a Front Surface Temperature of 2300°C, Test Duration, 200 Sec.	125
103.	Performance of JTA as a Throat Insert in a Liquid Fuel Rocket Motor as Compared to Silica Cloth Phenolic Used Under Identical Conditions	126

TABLES

TABLE		PAGE
1.	Summary of Compositions Investigated.	67
2.	Oxidation Results for Increases in Carbon Content of Grade JTA	80
3.	Oxidation Characteristics of C/Y_2O_3/Si Composites, Performance as a Function of the Silicon Content at a Constant Carbon Level of 48 Per Cent.	81
4.	Oxidation Characteristics of Various Graphite-Oxide-Silicon Composites, Carbon Content - 48 Per Cent, Silicon Content - 18.5 Per Cent	83
5.	Oxidation Characteristics of ATJ Graphite	89
6.	Mean Oxidation Rates of Grade JTA Using Cyclic Exposure	92
7.	Effect of Upstream Pressure on the Oxidation Characteristics of JTA at 1800°C	96
8.	Oxidation Characteristics of Selected New Composites	100
9.	Comparison of Silicized and Unsilicized JT-0981	106
10.	Room-Temperature Physical Properties of JTA	113
11.	Room-Temperature Physical Properties of JT-0981	117
12.	High Velocity Experiments with JTA and ATJ at 1900°C	120
13.	High Velocity (Mach 3.5) Experiments With JTA and ATJ at 1500°C	123

CLEARINGHOUSE FOR FEDERAL SCIENTIFIC AND TECHNICAL INFORMATION CFSTI
DOCUMENT MANAGEMENT BRANCH 410.11

LIMITATIONS IN REPRODUCTION QUALITY

ACCESSION # AD 609247

☐ 1. LEGIBILITY OF THIS DOCUMENT IS IN PART UNSATISFACTORY. REPRODUCTION HAS BEEN MADE FROM THE BEST AVAILABLE COPY.

☐ 2. ORIGINAL DOCUMENT CONTAINS COLOR OTHER THAN BLACK AND WHITE AND IS AVAILABLE IN LIMITED SUPPLY. AFTER PRESENT STOCK IS EXHAUSTED, IT WILL BE AVAILABLE IN BLACK-AND-WHITE ONLY.

☐ 3. THE REPRODUCIBLE QUALITY OF THIS DOCUMENT IS NOT ADEQUATE FOR PUBLIC SALE. AVAILABLE TO CUSTOMERS OF THE DEFENSE DOCUMENTATION CENTER ONLY.

☐ 4. DOCUMENT AVAILABLE FROM CLEARINGHOUSE ON LOAN ONLY (TECHNICAL TRANSLATIONS).

PROCESSOR: W. Patterson

TSL-107-12-64

BLANK PAGE

1. INTRODUCTION

This volume covers the one-year program on Task 2, "Development of Graphite-Refractory Composites," of a program to provide graphite materials for high-temperature aerospace use. This development effort is a continuation of selected portions of the program for studies leading to the understanding required for development of uniform reproducible carbon-based materials capable of being tailored to meet high-temperature materials requirements in advanced aerospace systems conducted under Contract No. AF 33(615)-6915. This earlier work included scale-up, characterization, and evaluation of graphites to permit their successful use as engineering materials. Major emphasis was placed on acquiring a better understanding of the specific chemistry and pyrolysis reaction of raw materials; the limiting properties of single crystals; the relationship between the basic chemical and physical processes and processing techniques; and improved testing methods. The work conducted under Contract No. AF 33(615)-6915 is covered in the various volumes of WADD TR 61-72.

Our effort under the previous contract has served as a basis for the present development program on graphite-refractory composites and the empirical approach to selective modification was continued. JT-0832 (Grade JTA) was used as a reference base for evaluating new composites. Studies were performed to improve oxidation resistance and to establish the contribution of individual additives as well as replacement constituents to the overall performance of the composite.

These composites, upon exposure to oxygen at elevated temperatures, enclose themselves with a protective oxide coating. In this fashion, they represent an improvement over coated systems by providing oxidation protection in depth. Should processes such as erosion, chemical reaction, or vaporization result in local or general loss of the protective coating, oxidation of the base material will regenerate the protective layer.

At the interface between coating and parent material, refractory oxides confront a highly carbonaceous material of generally more than 70 volume per cent carbon. While some of this carbon is bonded in carbides and in solid solutions, the bulk appears as free carbon or graphite. Since graphite reacts with oxides to form carbides at high temperatures, studies of these reactions were considered essential in the development of graphite-base refractory composites.

An apparatus was developed which would provide oxidation data up to 2000°C. This apparatus was used to determine the oxidation characteristics of grade JTA for comparison with promising new experimental composites.

Contact with Air Force Contractors and Subcontractors was maintained to expedite the dispersal of information on improved materials developed under this program, and to coordinate the evaluation of materials from this program at other locations.

2. SUMMARY

Studies of the oxidation resistance of grade JTA have disclosed the contribution of each of the component materials. Boron forms a low-melting oxide which provides excellent protection below 1400°C. Above 1600°C, the boron appears to be detrimental. Silicon provides its best oxidation protection in the 1500° to 2000°C temperature range. Zirconium produces the most refractory oxide of the three but, to be effective, must be used in combination with other additives to produce liquid phases in the low and intermediate temperature ranges. New graphite-base refractory composites were developed through the selective substitution of the components in grade JTA. Studies were conducted on the following composite changes: zirconium, silicon and niobium replacement of boron; and niobium, cerium and lanthanum replacement of silicon.

Studies of graphite-oxide reactions indicate the stability of oxide coatings in contact with carbon bodies. In most cases, the first occurrence in the sequence of reaction is a solid-state diffusion of carbon into the oxide. If a solid material, such as the carbide, interrupts contact between reactants, stability between coating and matrix is continued. If a liquid phase which provides a transport medium between reactants is formed, lasting stability is terminated.

A high-temperature oxidation apparatus employing aerodynamic suspension and induction heating of an electromagnetically rotated spherical sample was developed. Cyclic tests of short duration were completed on grade ATJ, SiC-coated RVC and grade JTA. The oxidation of grade ATJ is diffusion controlled in this apparatus above 1600°C. The SiC coating on RVC limits this material to temperatures below approximately 1700°C. Coating scale-off, characteristic of the cyclic tests on JTA, prevented use of this data to establish mean oxidation rates as a function of time.

Additional tests using exposures of 5, 15, 30, and 60 minutes over the temperature range of 1400° to 1800°C were performed on grade JTA. In these tests, JTA exhibits excellent oxidation resistance up to 1700°C and diminished, but still impressive, stability at 1800°C. The actual temperature in the sample is somewhat higher than the surface temperatures reported in these tests.

Outstanding composites revealed in the preliminary screening tests were selected for testing in the high-temperature oxidation apparatus. The most oxidation-resistant composite, JT-0981, in which the boron was completely replaced with silicon, exhibited excellent performance at 1700, 1800, 1900, and 2000°C.

Plasma tests were performed on grade JTA at 1900°C surface temperature compared to grade ATJ under subsonic, sonic and supersonic flow conditions. In each case, the performance of the composite was excellent. Similar tests with grades JT-0965 and JT-0981 were stopped when it was noted that the protective coating did not form on the low-temperature portion of the sample.

3. FUNDAMENTAL INVESTIGATIONS

The high-temperature oxidation resistance of graphite-base refractory composites is provided by a protective oxide coating formed on the exposed surfaces. At the interface between coating and substrate material, refractory oxides are in contact with a highly carbonaceous material of generally more than 70 volume per cent carbon. Although some of this carbon is bonded in carbides and in solid solutions the bulk appears as free graphite. The contact of refractory oxides with the base stock permits reactions of the following type:

Graphite + Oxide → Carbon Monoxide + Carbide.

Studies of graphite-oxide reactions are considered an essential foundation for the development of graphite-base refractory composites with high-temperature oxidation resistance.

3.1. Gas Development from Graphite-Oxide Powder Reactions

The production of CO gas from graphite-oxide reactions has a decisive bearing on the oxidation characteristics of graphite-base refractory composites. Whenever the CO pressure in the interface between coating and parent material exceeds the ambient pressure, three cases have to be considered: (1) If the coating is impervious and solid, it is likely to be blasted off the parent material; (2) If the coating is impervious and liquid, bubbles are formed; (3) If the coating is somewhat porous, diffusion occurs through the pores. Conditions which permit the formation within a composite of CO reaction pressures above the ambient may end successful protection.

Figure 1 illustrates CO equilibrium pressures for various graphite-oxide reactions as a function of temperature.[1,2] Such equilibrium pressures as calculated from thermochemical functions represent the maximum possible CO pressures which could be delivered by the reactions. This does not mean, however, that these pressures are actually reached. Wherever solid reactants are involved, calculation of equilibrium pressures is generally of little practical value since many such reactions are entirely dormant because the solid reaction products are reaction barriers. To get an accurate picture, it is necessary to actually measure the reaction pressure of interest.

3.1.1. Description of Apparatus and Experimental Procedure

A torsional effusion apparatus was constructed to measure the reaction pressure. The suspension is illustrated in Figure 2. Two graphite effusion cells arranged horizontally are attached to a series of graphite and aluminum rods, and the latter in turn are suspended on a very fine tungsten wire clamped to the cover plate of a glass tower. Gases leaving the effusion cells provide a thrust which turns the cells until the torque is countered by the twisted wire. A mirror in the upper aluminum rod

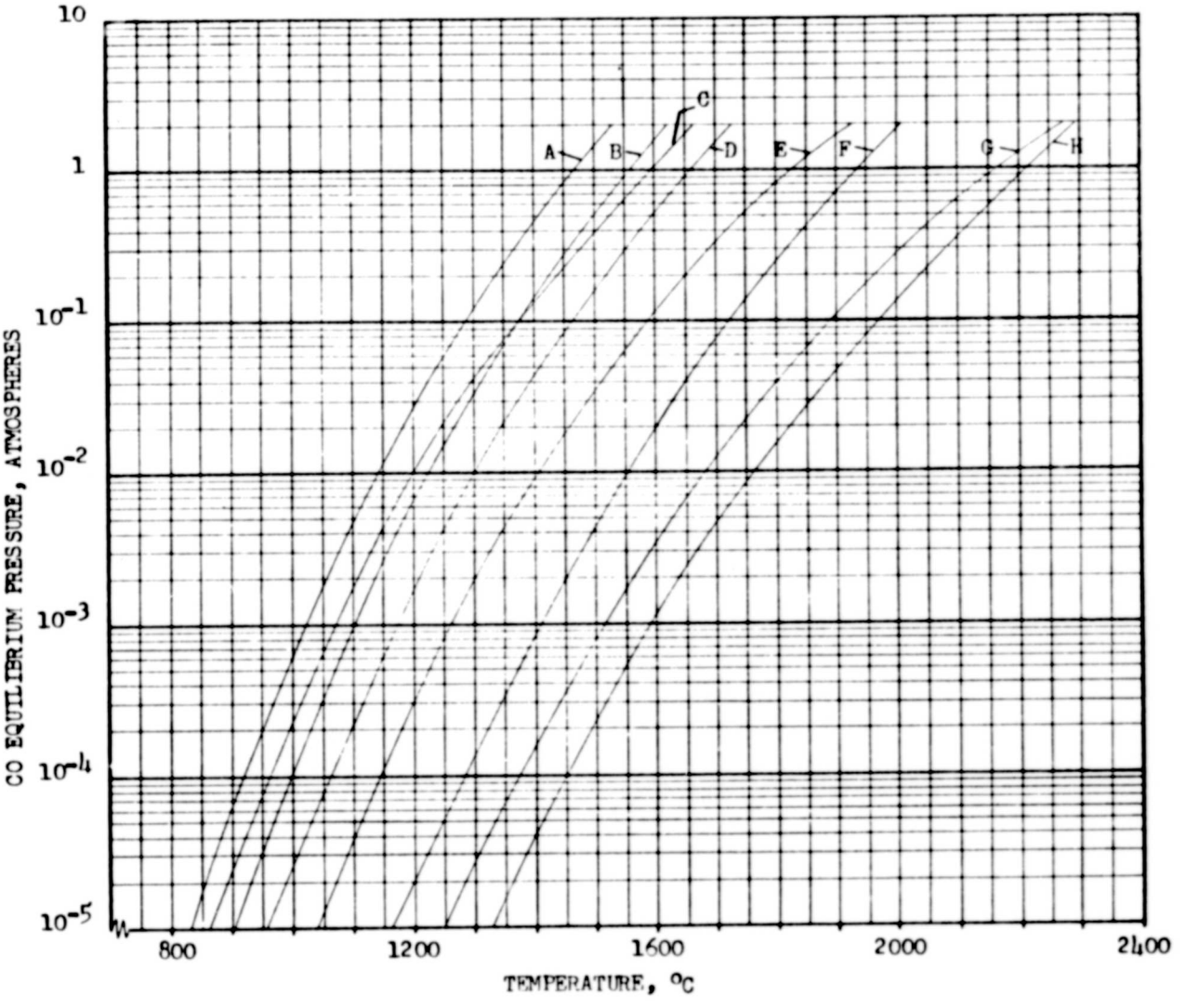

A) $SiO_2 + 3C \rightarrow SiC + 2CO$

B) $ZrSiO_4 + 6C \rightarrow ZrC + SiC + 4CO$

C) $2B_2O_3 + 7C \rightarrow B_4C + 6CO$

D) $ZrO_2 + 3C \rightarrow ZrC + 2CO$

E) $UO_2 + 4C \rightarrow UC_2 + 2CO$

F) $2Al_2O_3 + 9C \rightarrow Al_4C_3 + 6CO$

G) $ThO_2 + 4C \rightarrow ThC_2 + 2CO$

H) $2BeO + 3C \rightarrow Be_2C + 2CO$

L-821

Figure 1. The Reaction of Graphite with Refractory Oxides, CO Equilibrium Pressure Versus Temperature

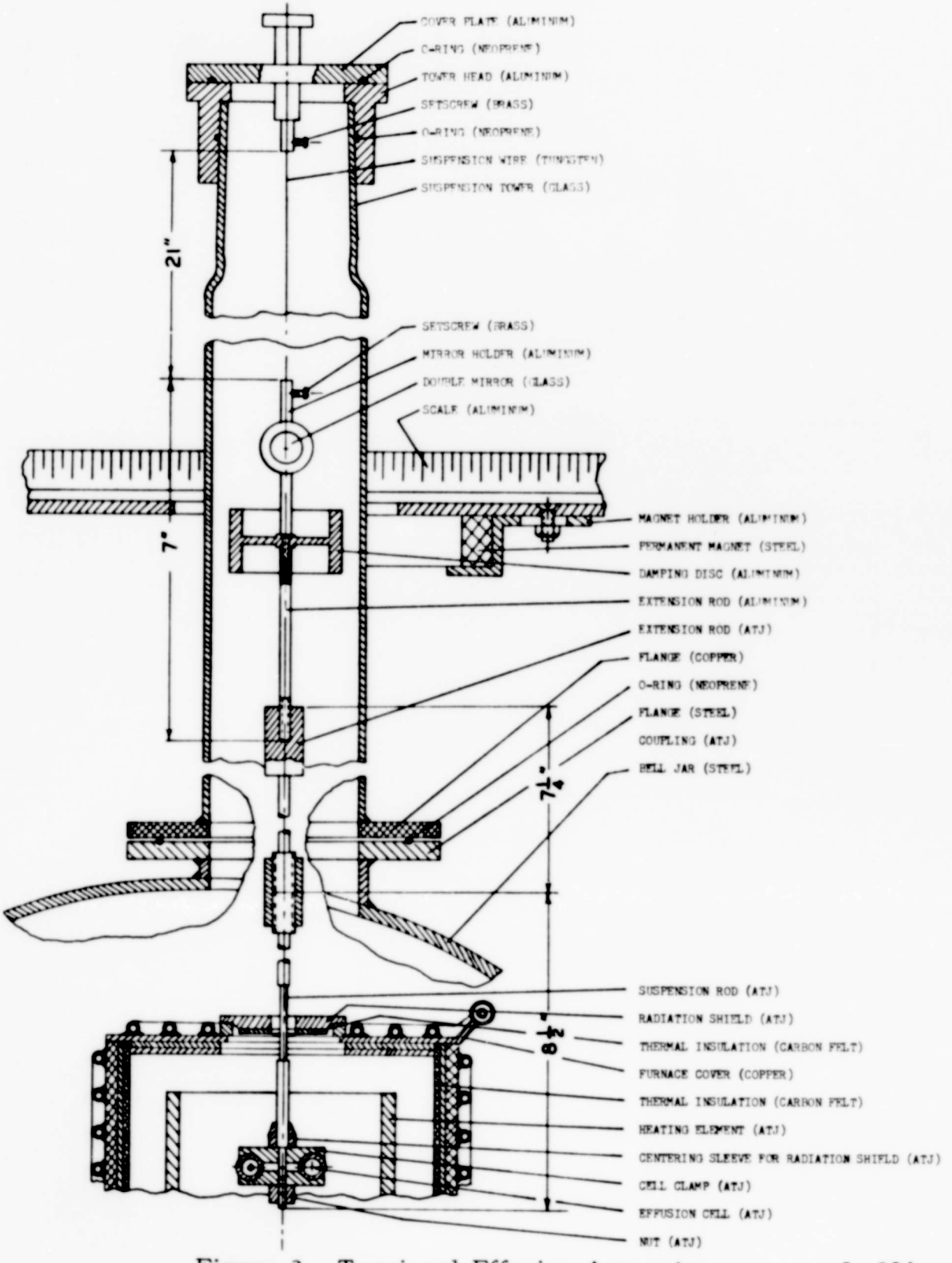

Figure 2. Torsional Effusion Apparatus, Cross Section L-201

reflects a light beam, thus indicating the torsional deflection. To prevent oscillations, the system is electromagnetically dampened. The effusion cells are mounted in the bell jar of a high-vacuum system and heated by radiation from graphite-resistance elements. Carbon felt insulation and a water-cooled furnace chamber protect the bell jar from heat.

The cells are brought into position by lowering the entire suspension train through the glass tower. The furnace chamber has an opening large enough to let the two effusion cells pass. During operation, this hole is covered by a graphite radiation shield. The overall appearance of the apparatus is illustrated in Figure 3.

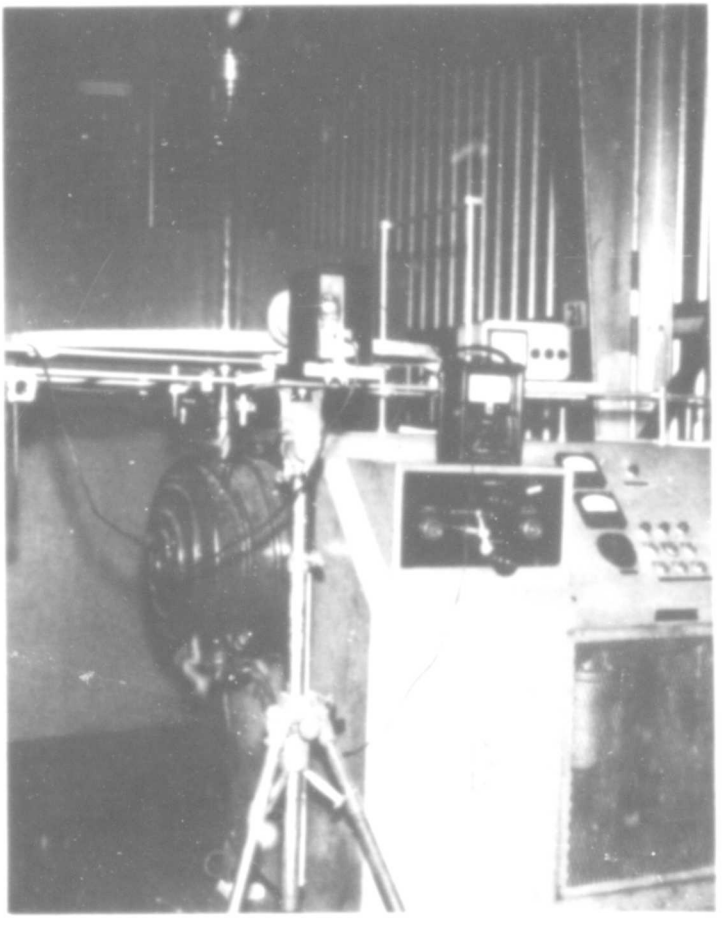

Figure 3. Torsional Effusion Apparatus, Overall View

The area of the hole in each effusion cell is small as compared with the area of the cell interior, and the mean free path of the gas is large when compared to cell dimensions. The resulting torque is then proportional to the partial pressure developed by the reaction in the cells. The orifice size was chosen to be $\frac{1}{64}$ inch diameter and molecular flow conditions applied with good approximation as long as the total pressure in the cells did not exceed 10^{-2} atm.

All tests were carried out under the following conditions:

Diameter of Tungsten Wire	- 0.002 inch
Free Length of Tungsten Wire	- 21 inches
Cell Capacity	- $\frac{3}{8}$ inch dia. x $\frac{7}{16}$
Cell Orifice Diameter	- $\frac{1}{64}$ inch
Distance between Orifice Centers	- 1.25 inches
Ambient Pressure	- $\leq$ 1.3 x 10^{-6} atm.

To obtain a measure of the partial pressure caused by a reaction in the cells, a calibration is necessary. The cells are loaded with a material for which the vapor pressure is known as a function of temperature, and the mirror deflections are obtained at various temperatures. The deflections can be translated into reaction pressures. The calibration material must not react with the cell walls and must yield sizable deflections while at an optically measurable temperature. From the few materials satisfying both requirements, germanium was chosen. The calibration curve is shown in Figure 4.

The cells were filled with a powdery blend consisting of graphite and one of the oxides in a ratio of 1:1 by volume.

The procedure consists of one long experiment in which temperature is increased in a step-wise fashion in a standard temperature-time program. With such a method the reaction pressure at each temperature level is effected by whatever happened at previous lower temperature levels; however, a qualitative measure of relative reactivity is indicated.

A significant aspect of the scanning procedure is that it allows clean separation of the effects of outgassing or decomposition from reactions. Scanning experiments have shown that many oxides exhibit significant outgassing peaks between 800 and 1100°C.

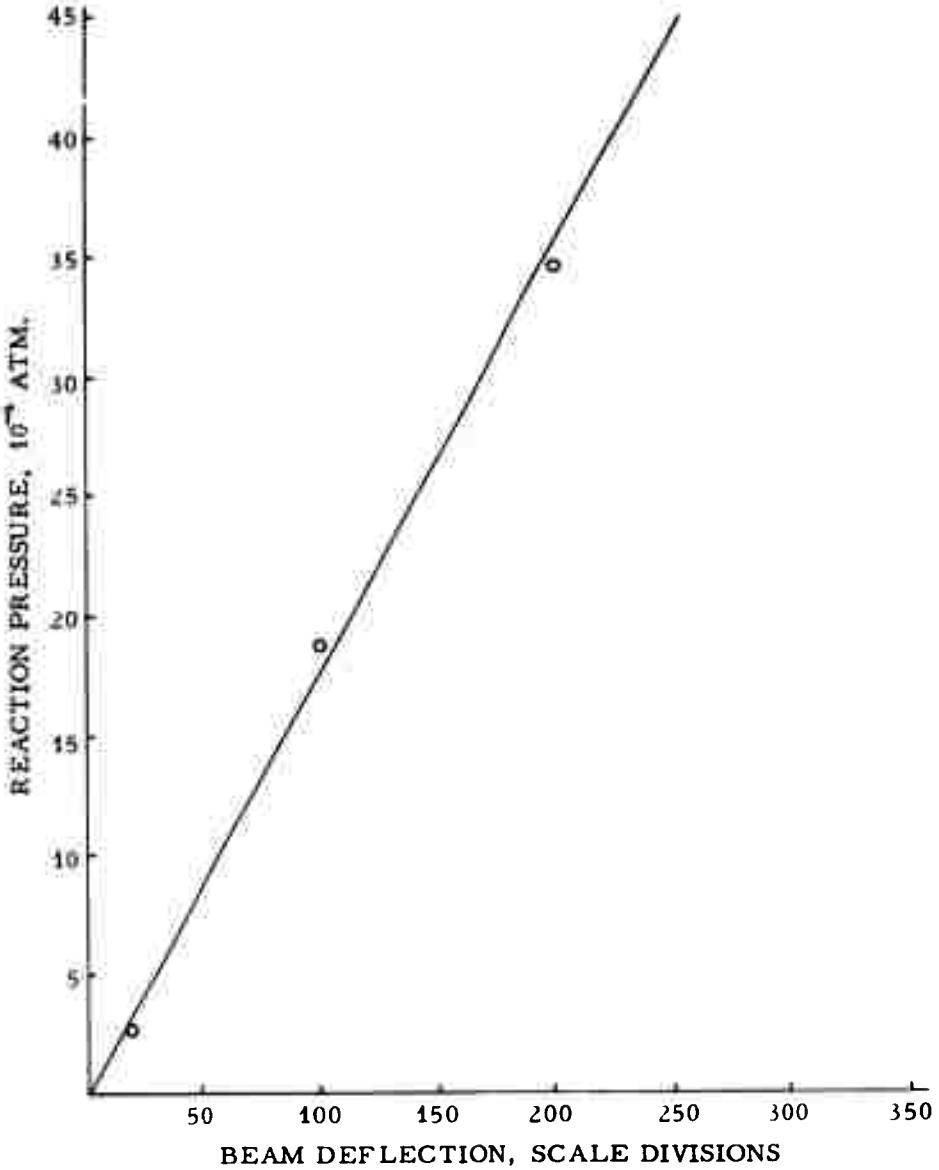

Figure 4. Calibration of the Torsional Effusion Apparatus with Germanium L-171

During scanning experiments, a small zero drift toward negative reaction pressures was observed whenever the reaction pressure was below the sensitivity of the instrument (approximately 0.1×10^{-4} atm.). This effect was found to be due to small temperature differences on the effusion cell housing. The change of the resulting zero drift with time is shown in Figure 5.

3.1.2. Results

So far the given technique has been applied to the reactions of graphite with Al_2O_3, BeO, $CaZrO_3$, CeO_2, Dy_2O_3, Er_2O_3, Eu_2O_3, Gd_2O_3, HfO_2, Ho_2O_3, La_2O_3, Lu_2O_3, $MgZrO_3$, Nb_2O_3, Nb_2O_5, Nd_2O_3, Pr_2O_3, Sc_2O_3, SiO_2, Sm_2O_3, $SrZrO_3$, Tb_2O_3, ThO_2, Tm_2O_3, UO_2, Y_2O_3, Yb_2O_3, and ZrO_2. The individual results for each of the reactions are shown in Figures 6 through 33. The holding time at each temperature level was chosen to be 15 minutes. The equilibrium temperatures reached at each level (generally after no more than 5 minutes) are given in the top part of each graph. Comparisons at arbitrarily chosen temperature levels of 1465, 1575, and 1675°C are presented in Figures 34 to 36.

The following summarizes these findings:

1) Of the oxides so far investigated, the following approximate order of increasing stability with respect to carbon has been established: Nb_2O_5, Eu_2O_3, UO_2, Nb_2O_3, Gd_2O_3, $MgZrO_3$, CeO_2, SiO_2, Al_2O_3, $CaZrO_3$, Sm_2O_3, HfO_2, Yb_2O_3, $SrZrO_3$, La_2O_3, ZrO_2, Nd_2O_3, Pr_2O_3, Tb_2O_3, ThO_2, Dy_2O_3, Ho_2O_3, Er_2O_3, Tm_2O_3, Sc_2O_3, Y_2O_3, Lu_2O_3 and BeO. The order changes slightly with temperature as can be seen by comparing the individual reaction experiments, but the basic grouping remains unaltered.

2) The drooping characteristics of all pressure isotherms is considered evidence that the solid products of the reactions studied; namely the carbides, are capable of functioning as reaction barriers between the reagents.

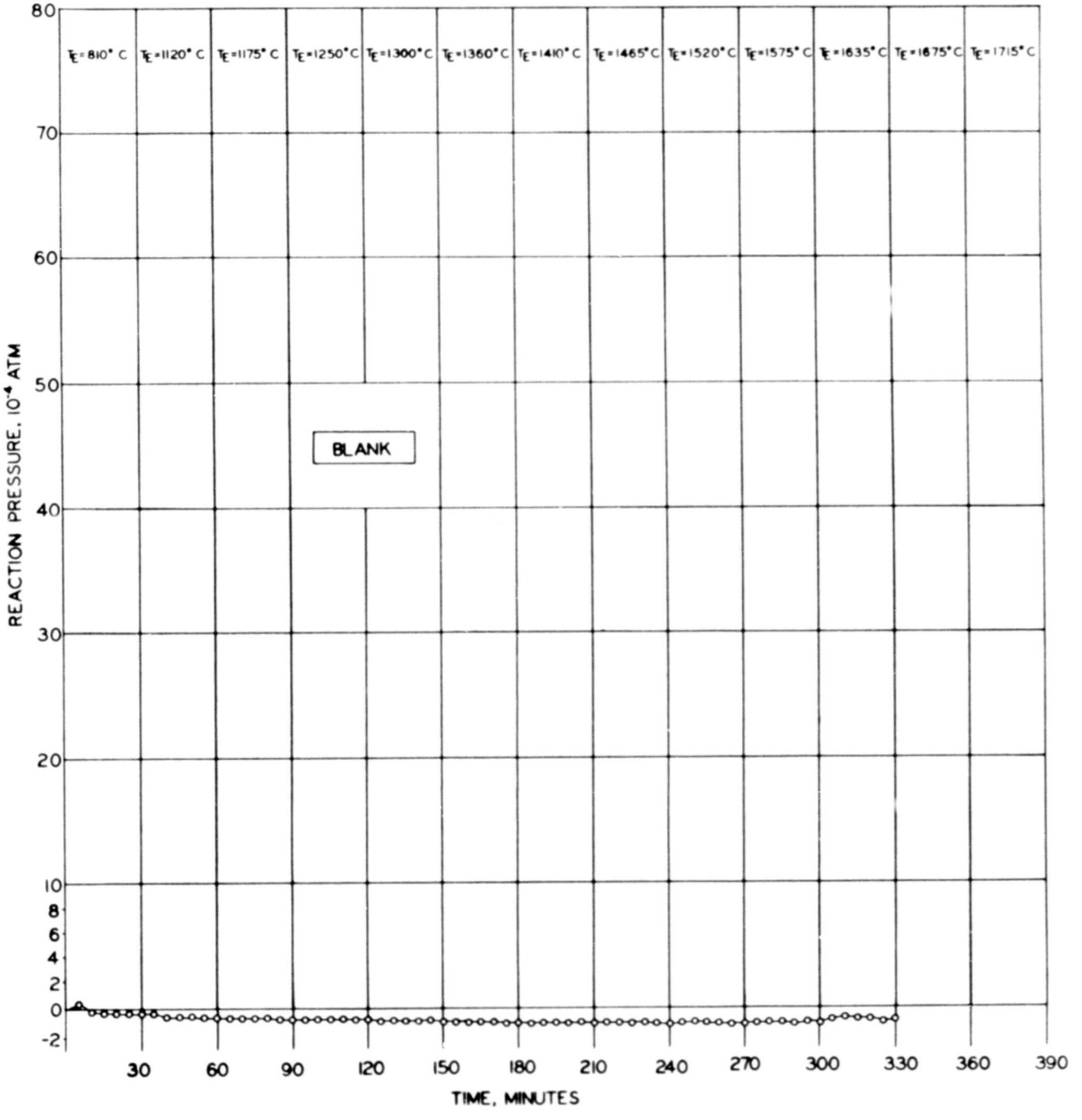

L-269

Figure 5. Change of Zero Drift with Time, Bell Jar Pressure, 1.3×10^{-6} ATM, Initial Azimuth, 135 Degrees

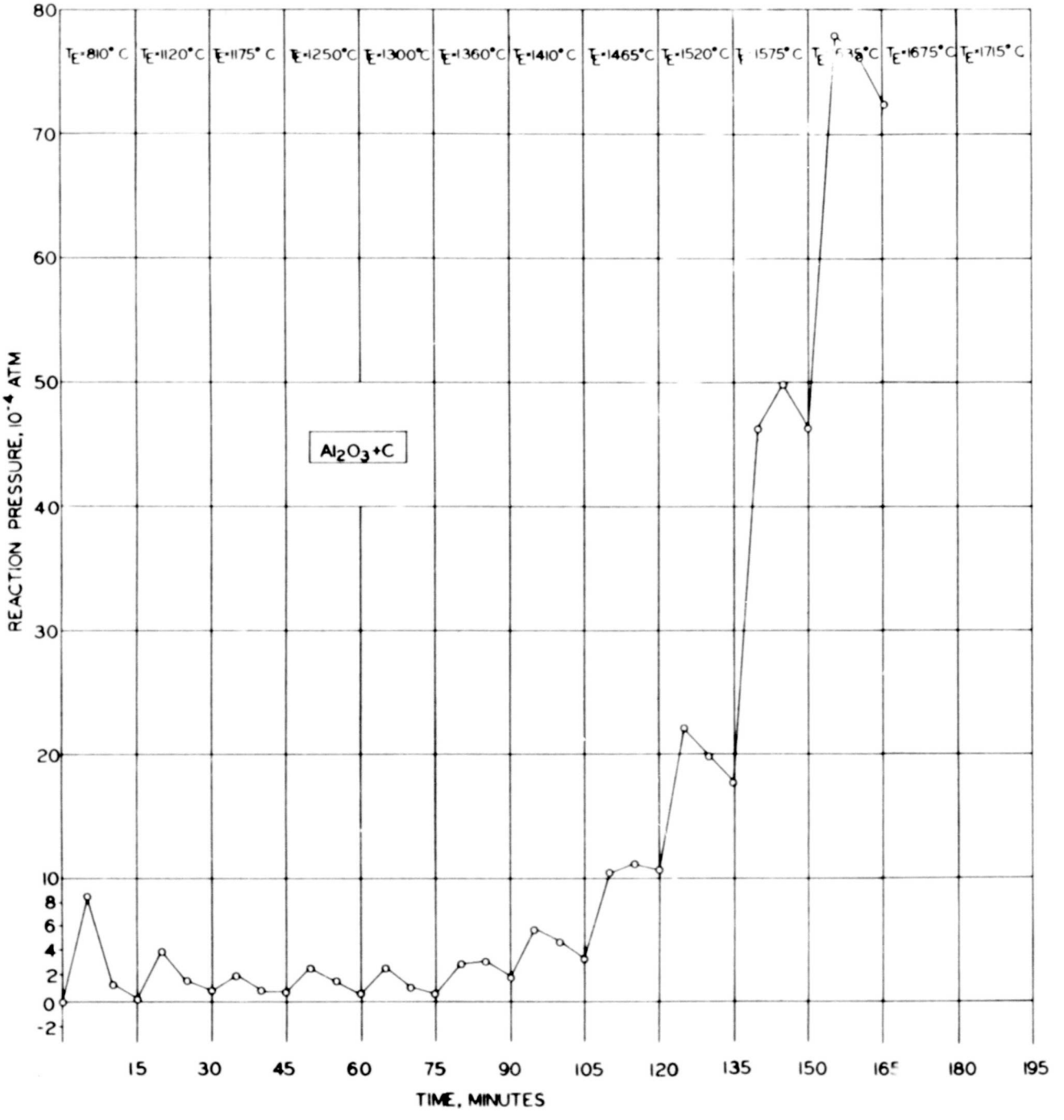

Figure 6. The Reaction of Graphite with Aluminum Sesquioxide, Scanning Experiment L-873

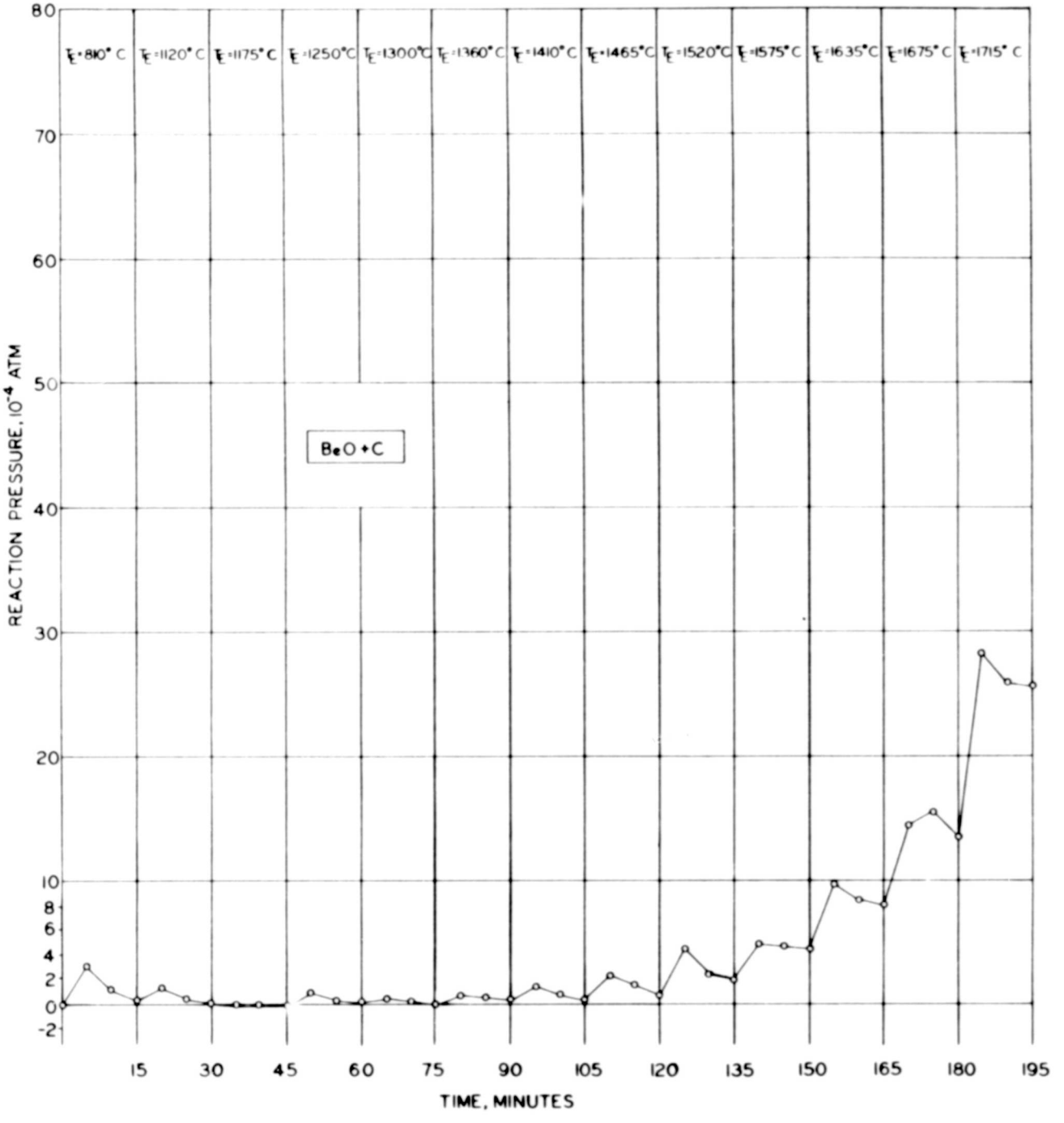

Figure 7. The Reaction of Graphite with Beryllium Monoxide, Scanning Experiment L-874

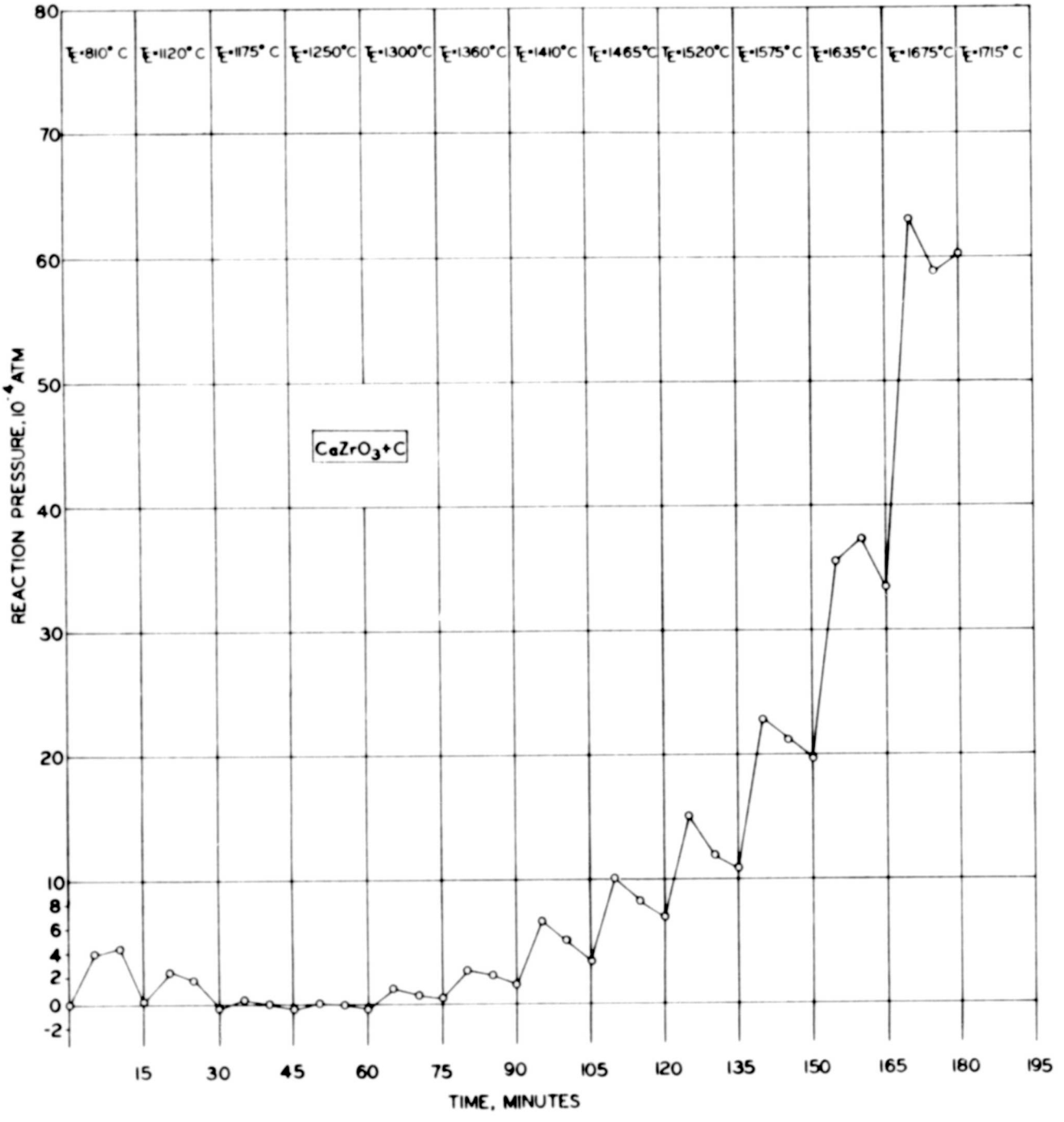

Figure 8. The Reaction of Graphite with Calcium Zirconate, Scanning Experiment L-875

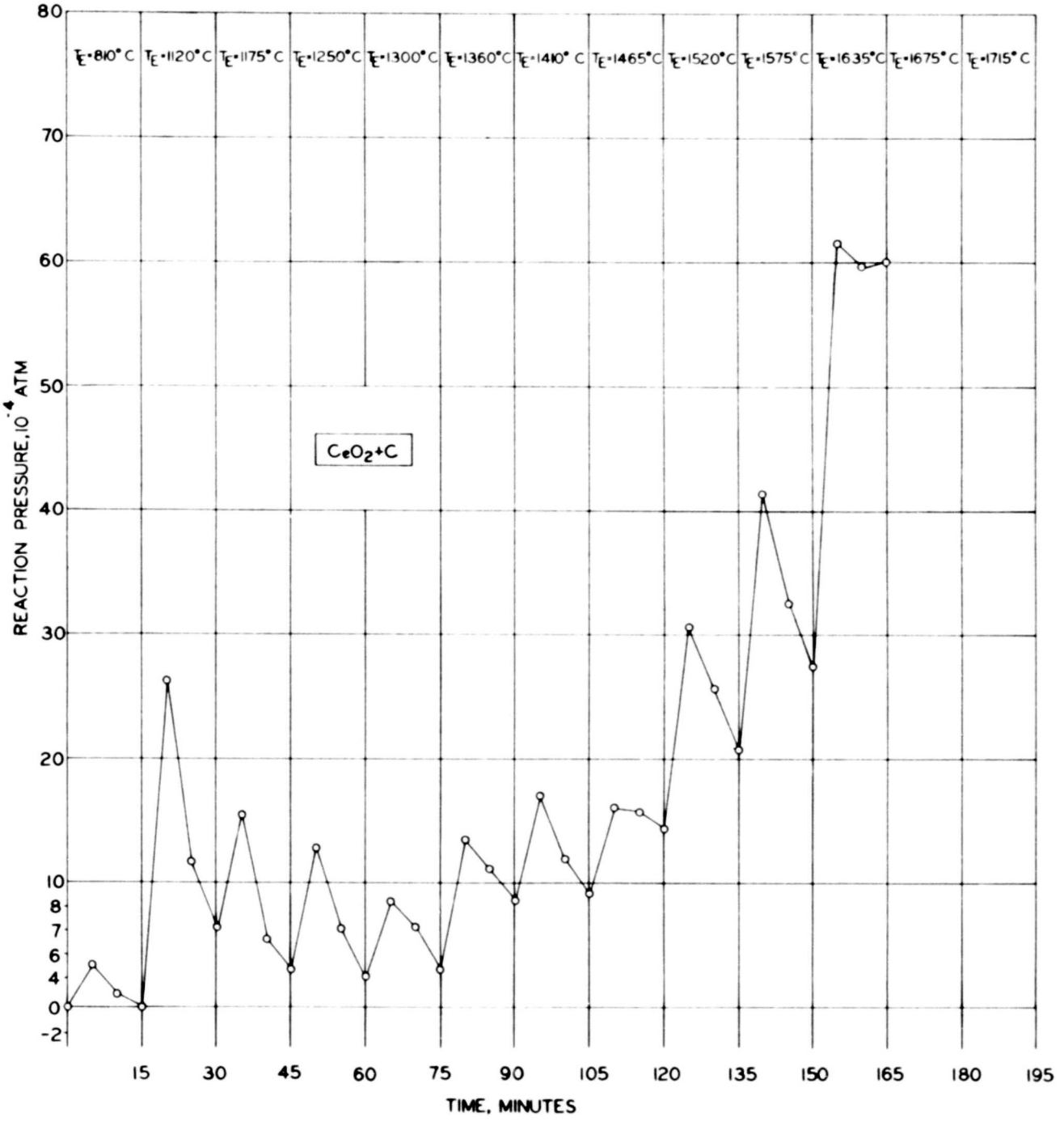

Figure 9. The Reaction of Graphite with Cerium Dioxide, Scanning Experiment

L-870

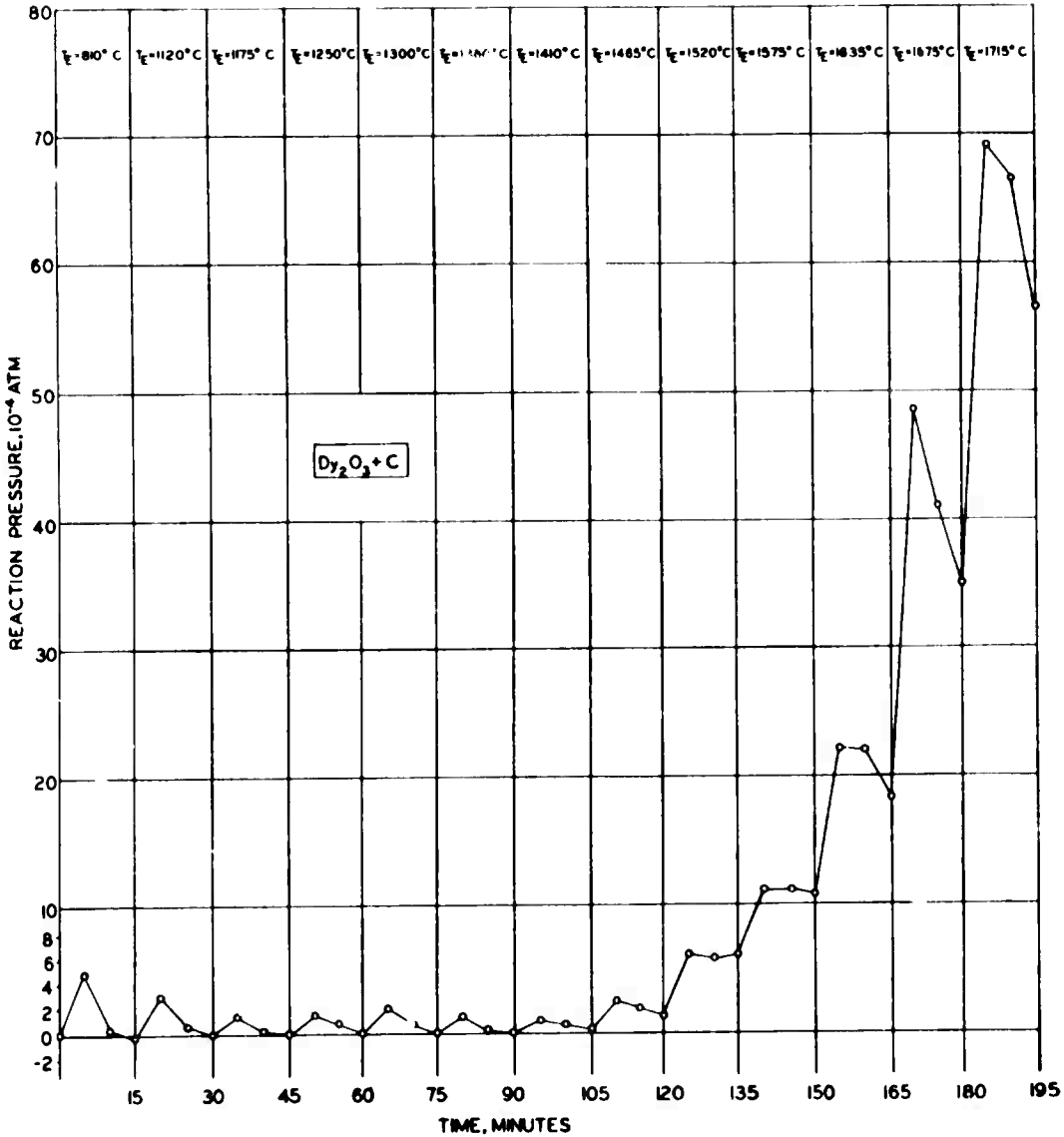

Figure 10. The Reaction of Graphite with Dysprosium Sesquioxide, Scanning Experiment L-274

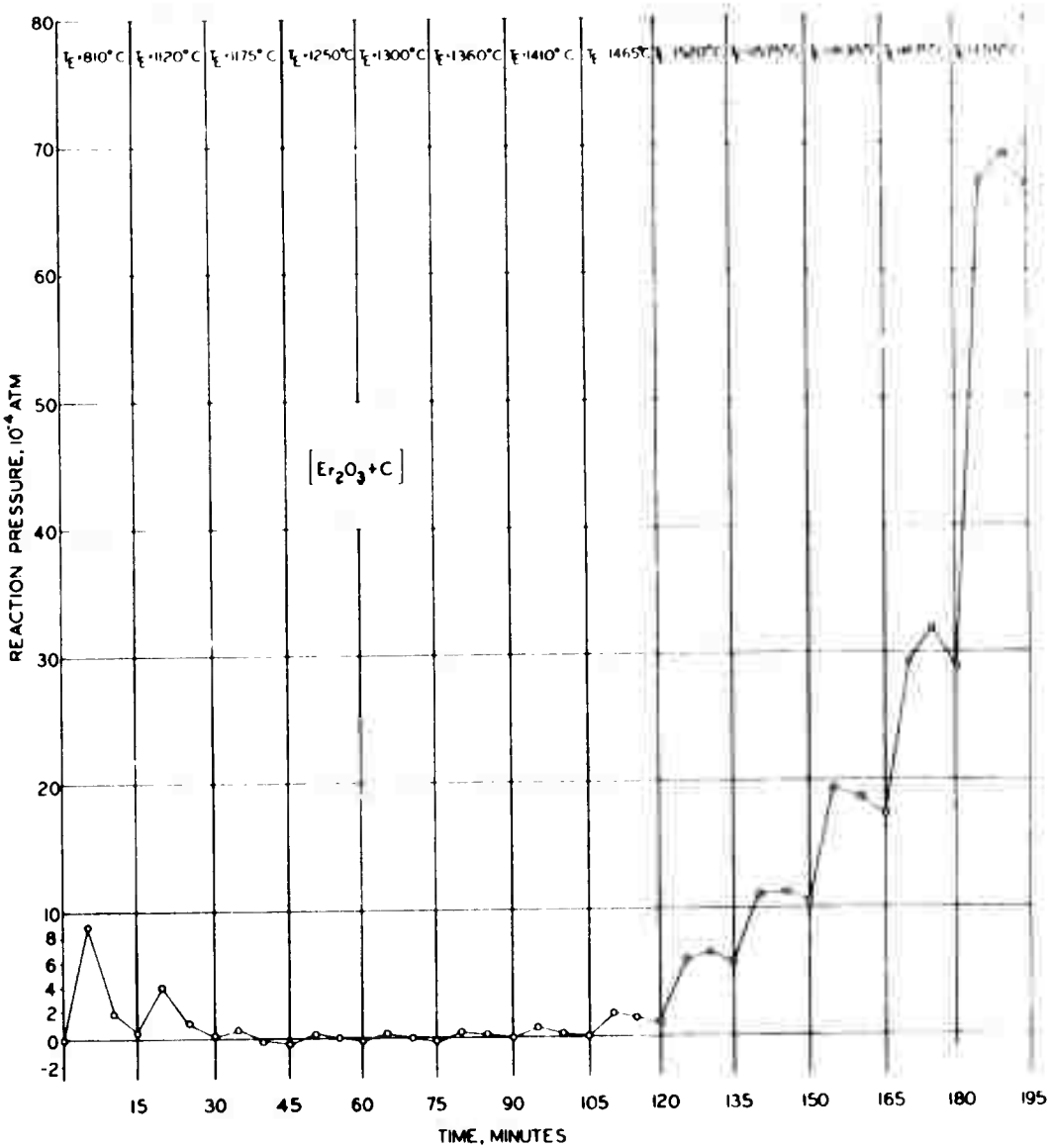

Figure 11. The Reaction of Graphite with Erbium Sesquioxide, Scanning Experiment L-877

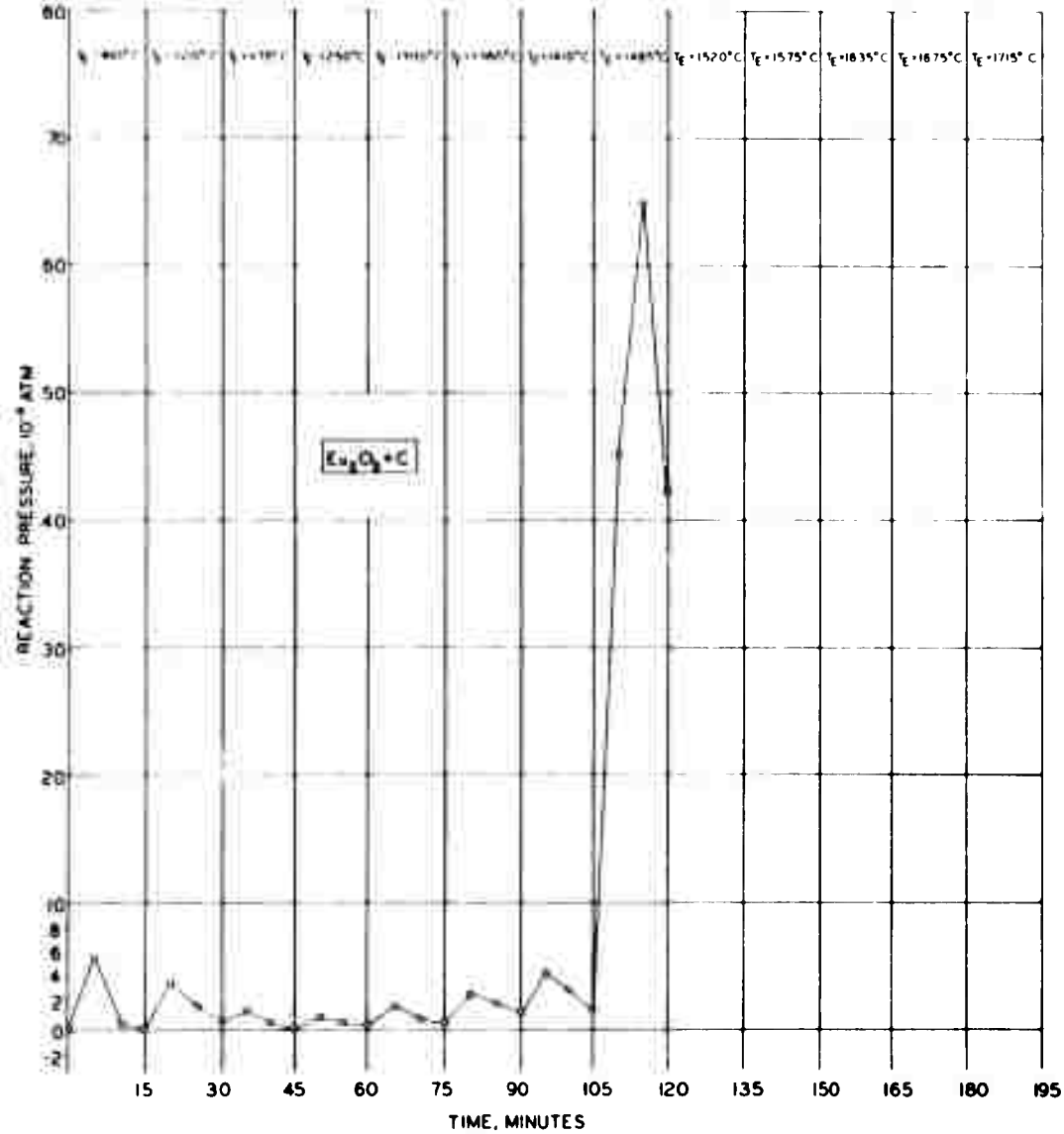

Figure 12. The Reaction of Graphite with Europium Sesquioxide, Scanning Experiment L-276

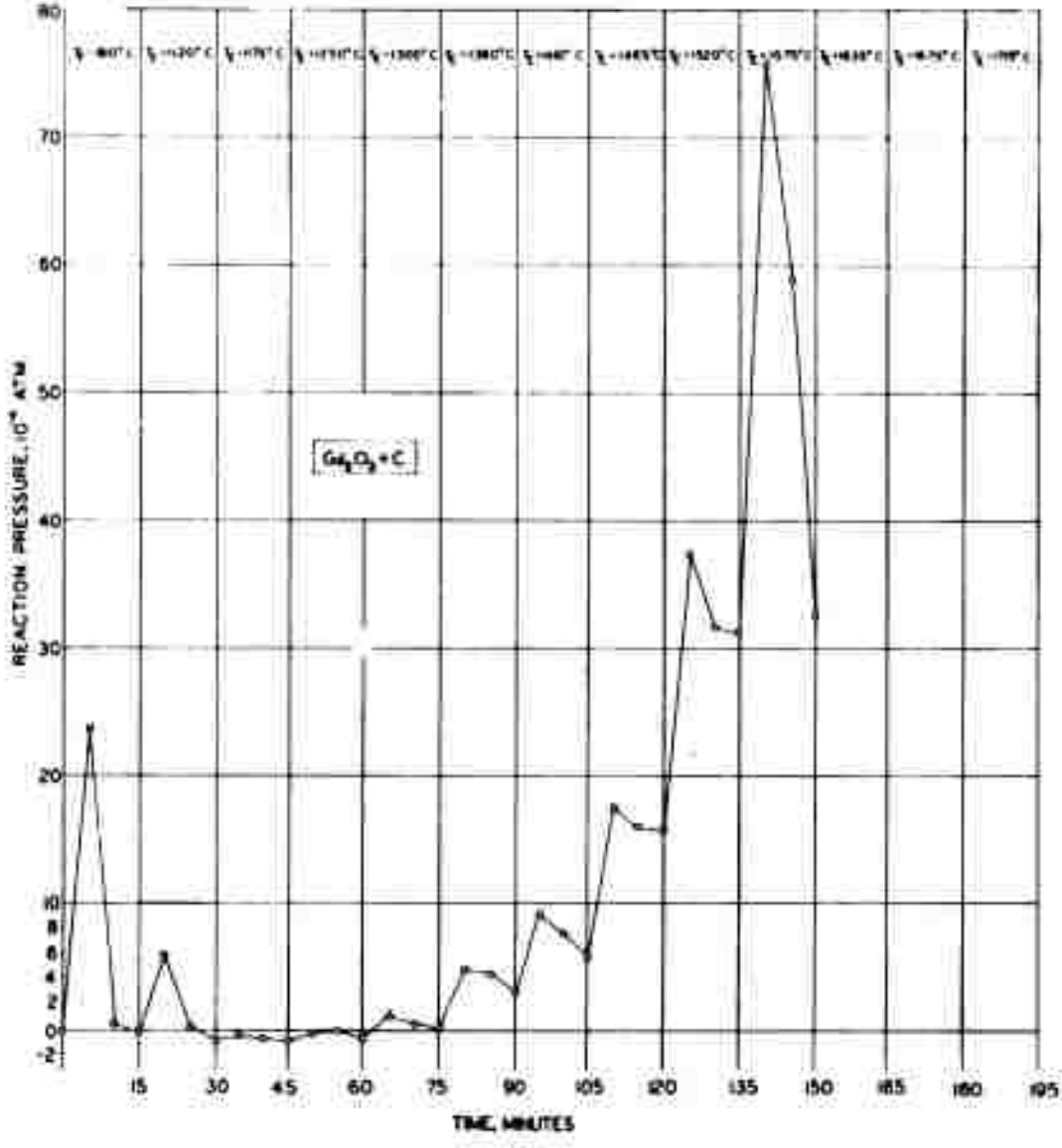

Figure 13. The Reaction of Graphite with Gadolinium Sesquioxide, Scanning Experiment L-277

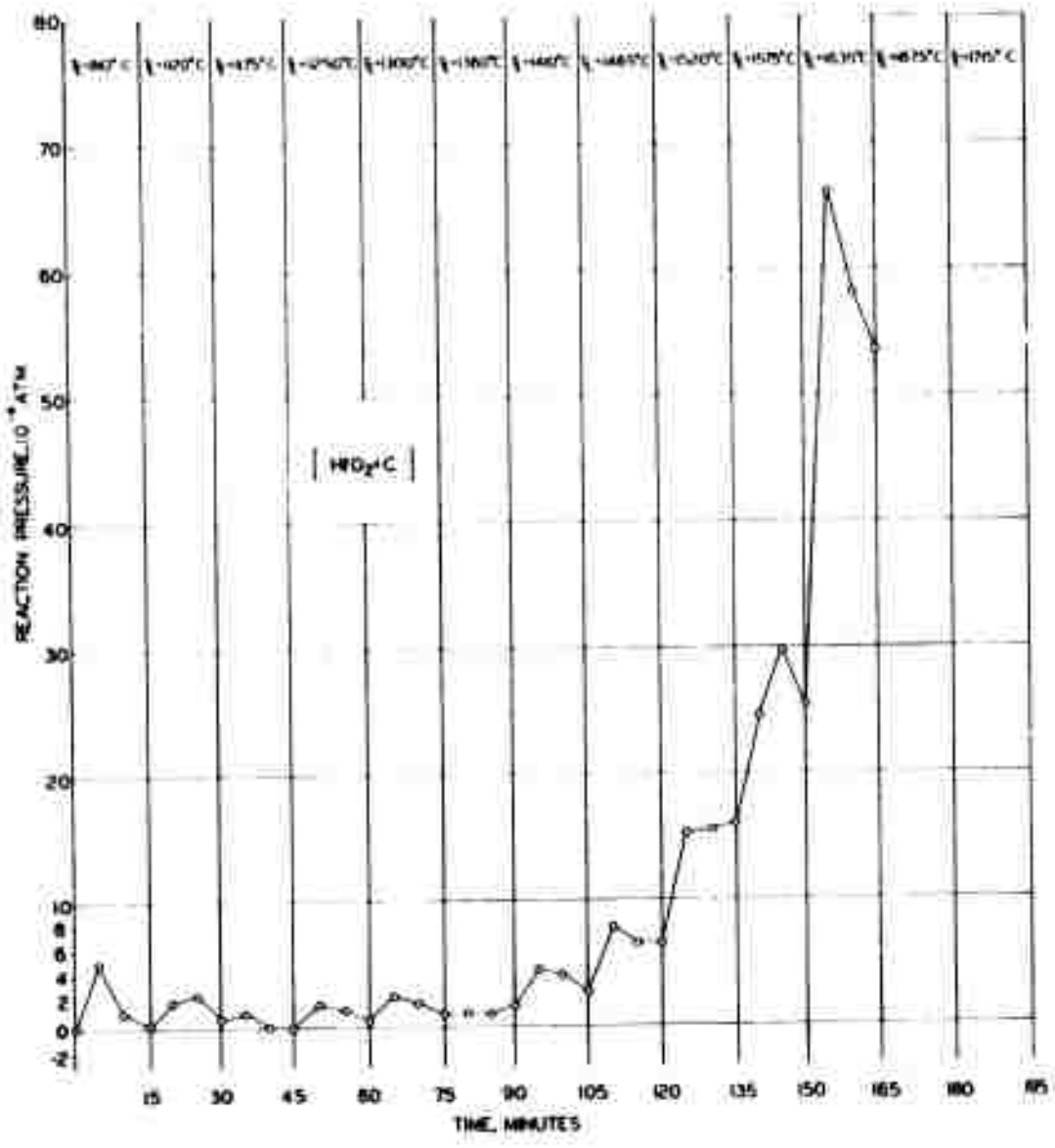

Figure 14. The Reaction of Graphite with Hafnium Dioxide, Scanning Experiment

L-878

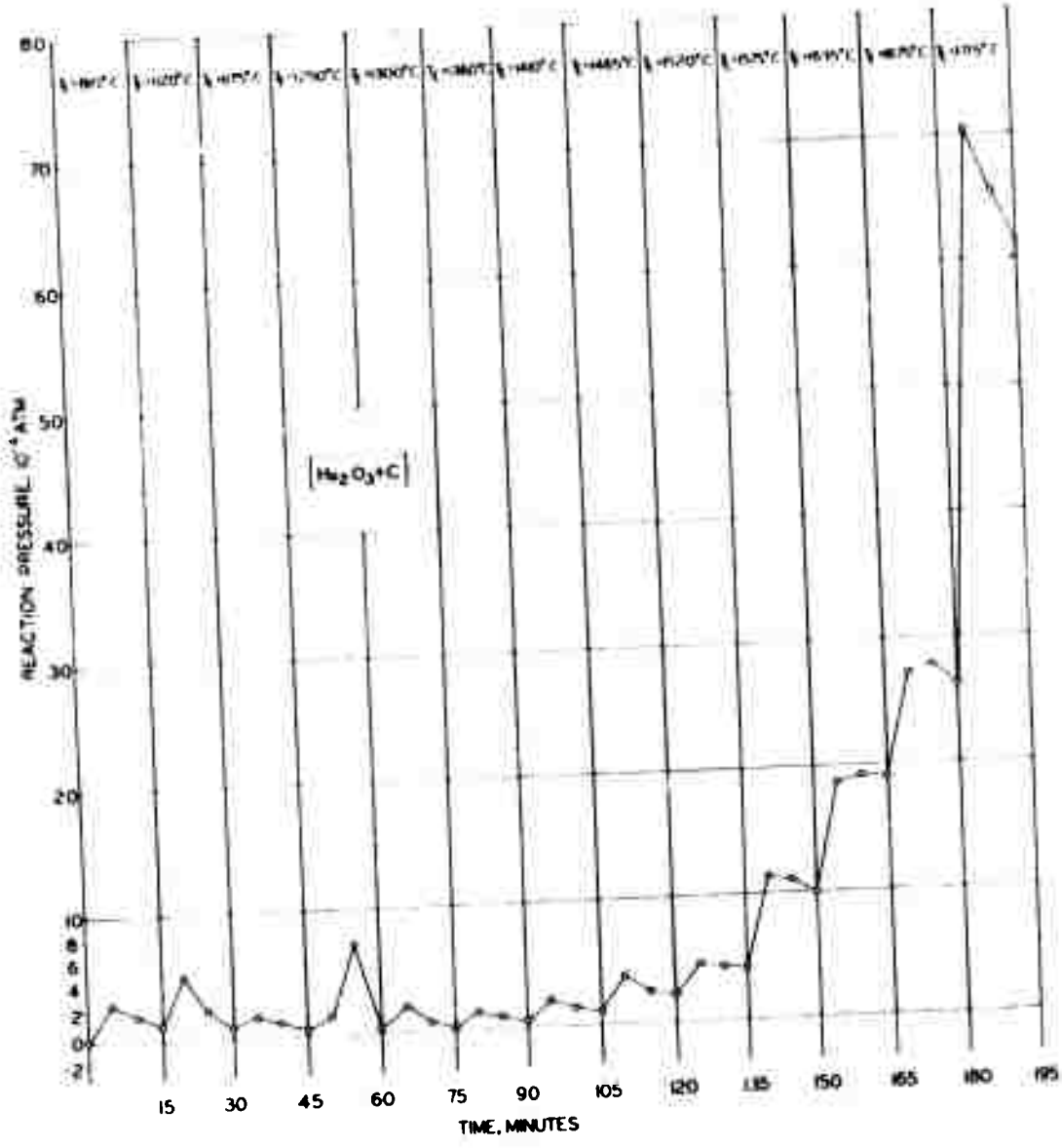

L-879

Figure 15. The Reaction of Graphite with Holmium Sesquioxide, Scanning Experiment

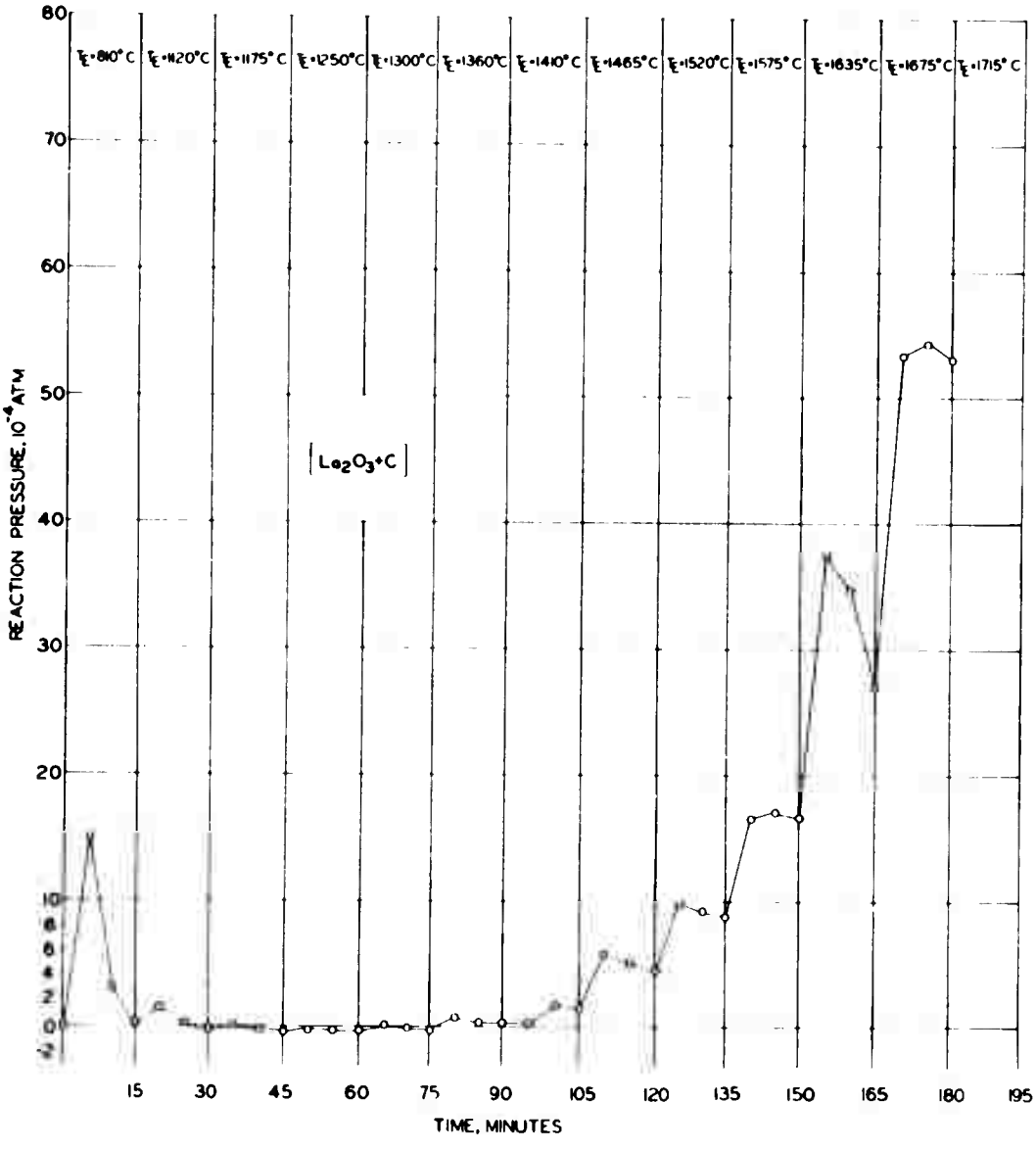

Figure 16. The Reaction of Graphite with Lanthanum Sesquioxide, Scanning Experiment L-880

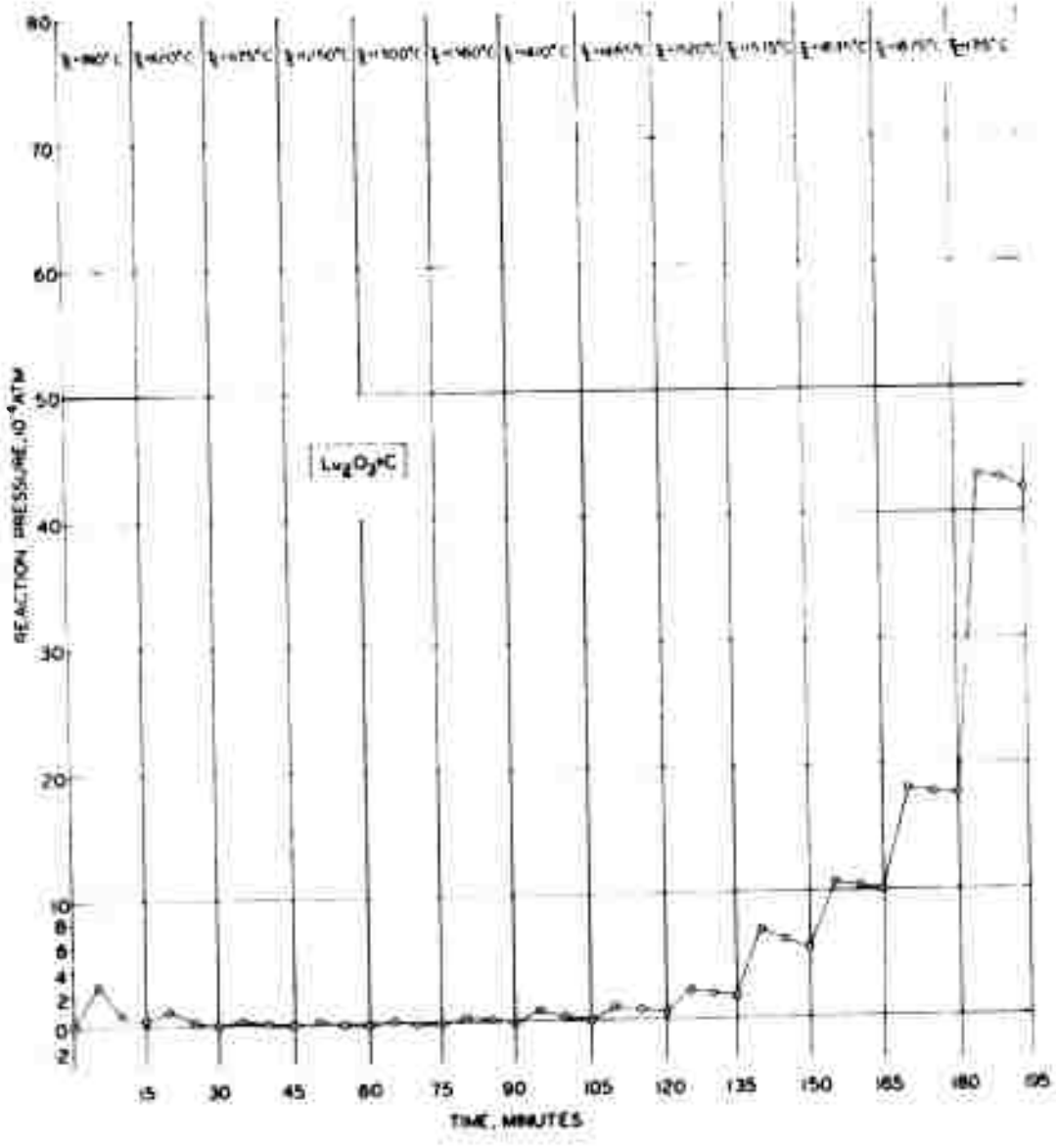

Figure 17. The Reaction of Graphite with Lutecium Sesquioxide, Scanning Experiment L-881

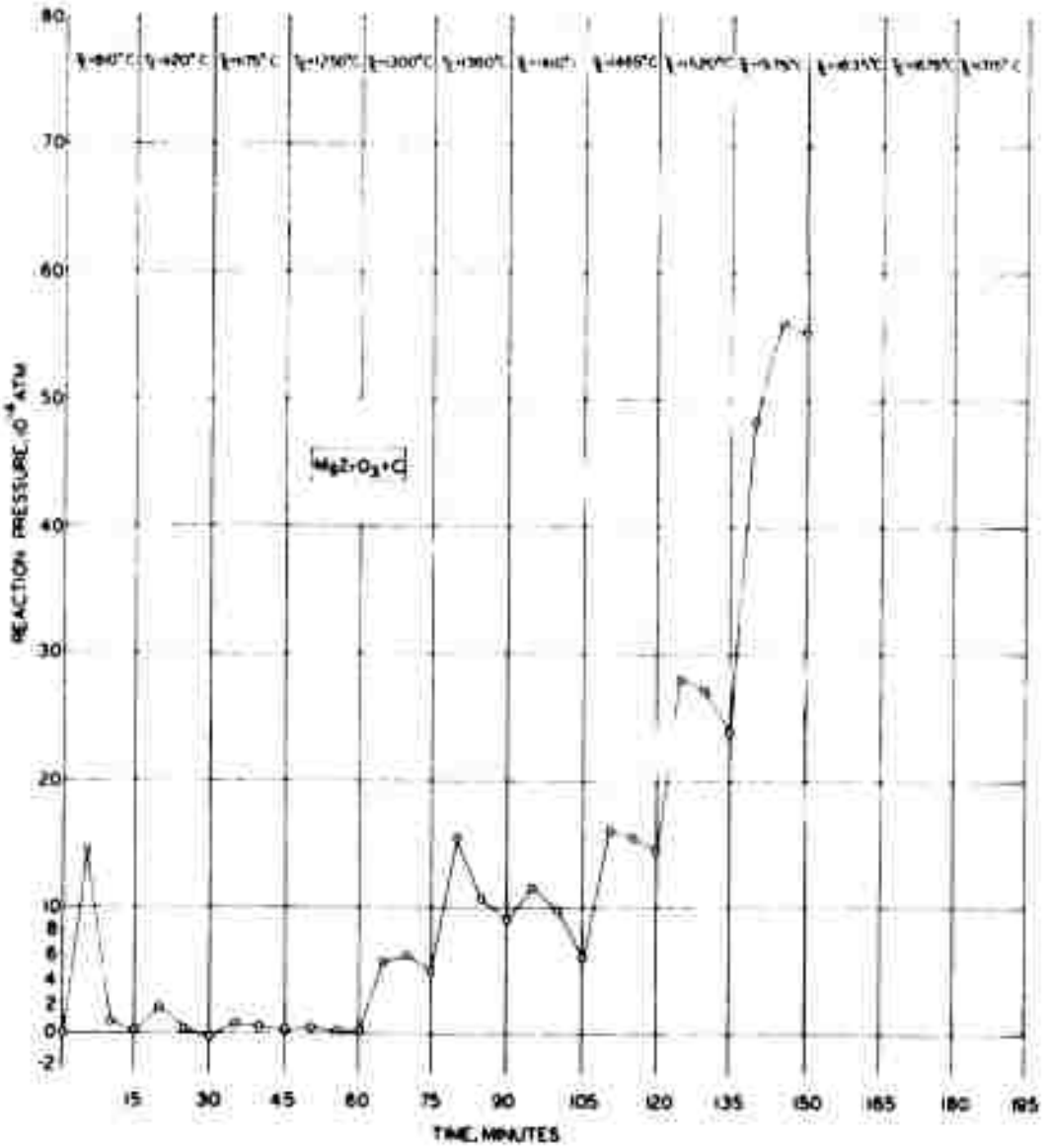

Figure 18. The Reaction of Graphite with Magnesium Zirconate, Scanning Experiment L-882

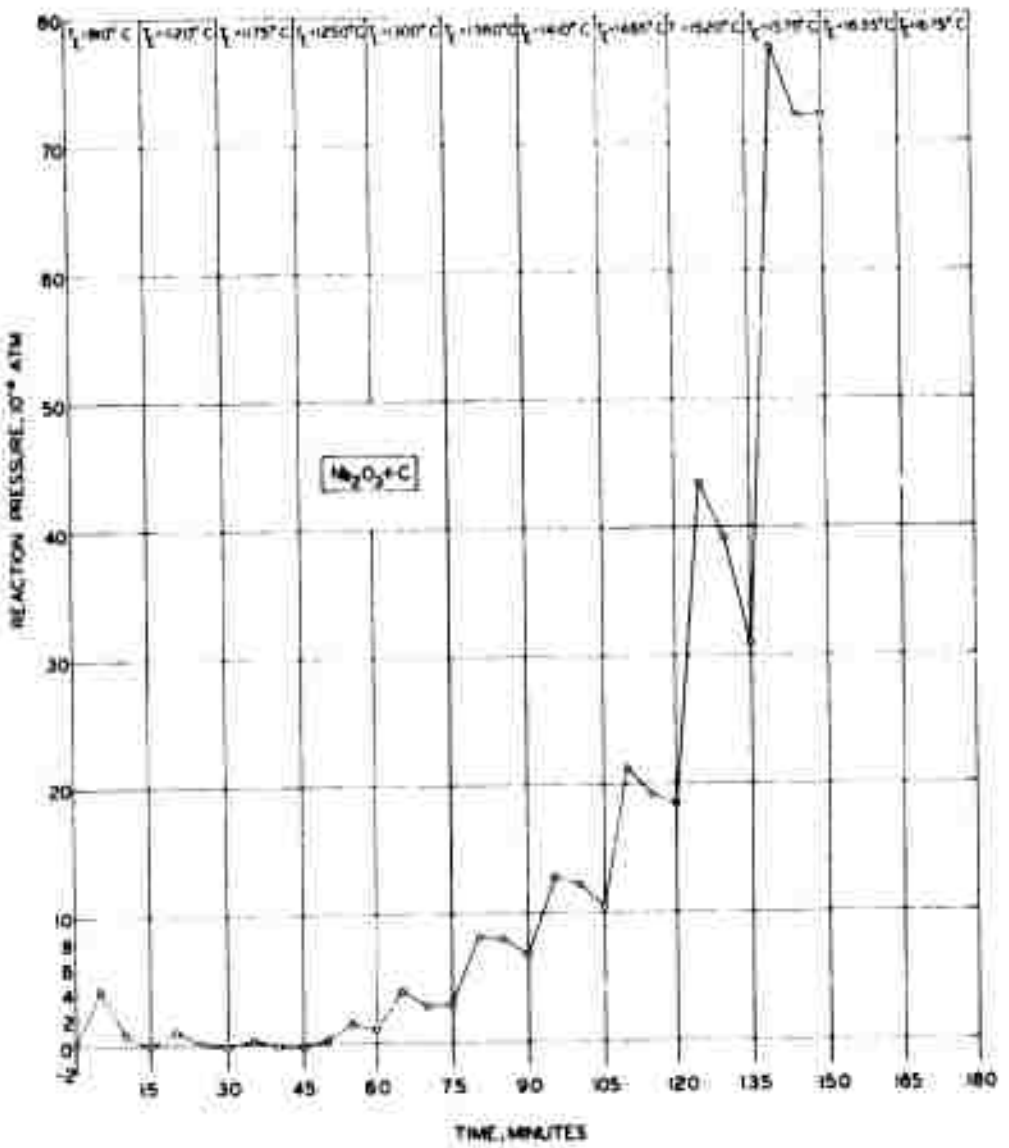

Figure 19. The Reaction of Graphite with Niobium Sesquioxide, Scanning Experiment L-883

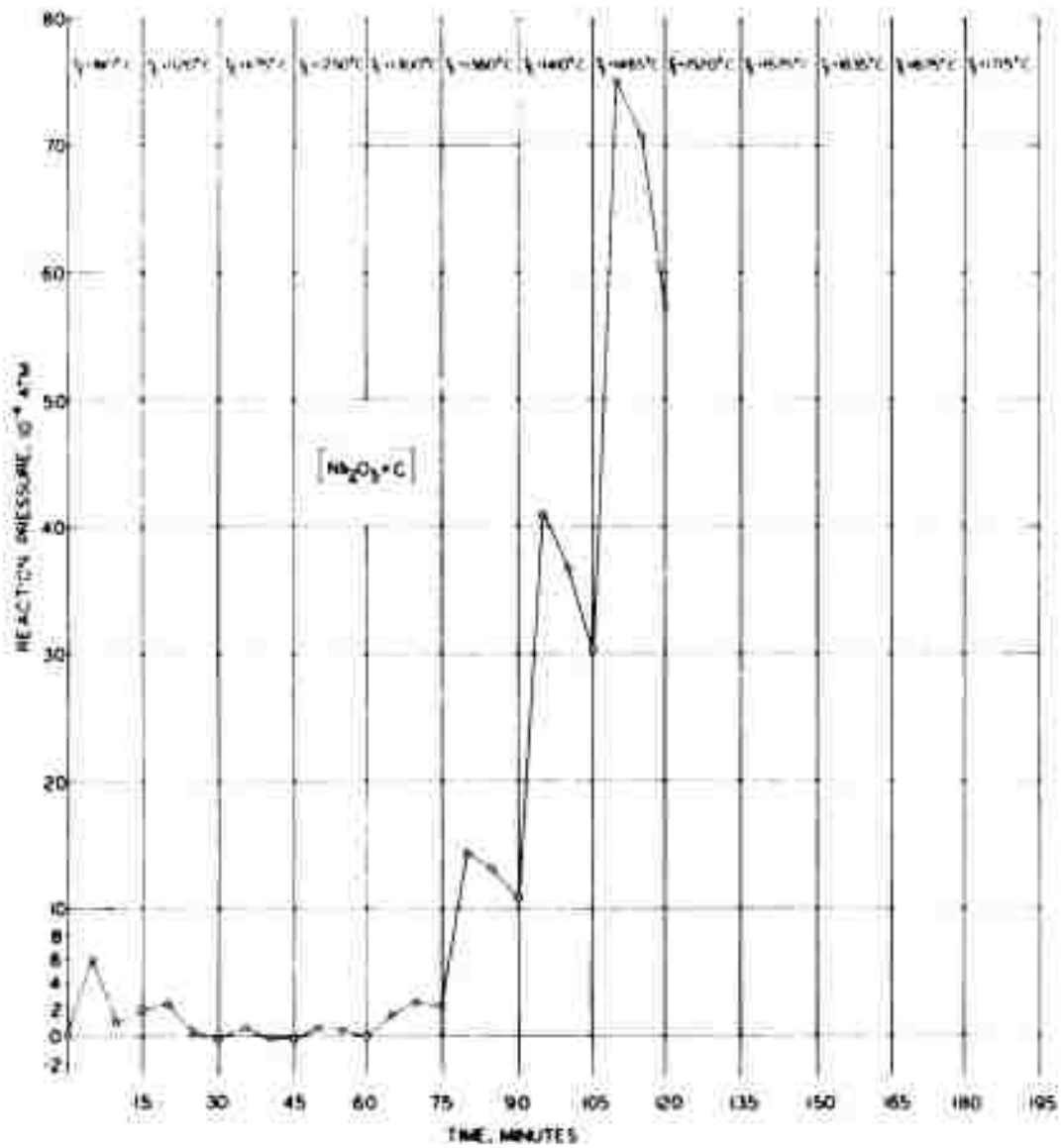

Figure 20. The Reaction of Graphite with Niobium Pentoxide, Scanning Experiment L-884

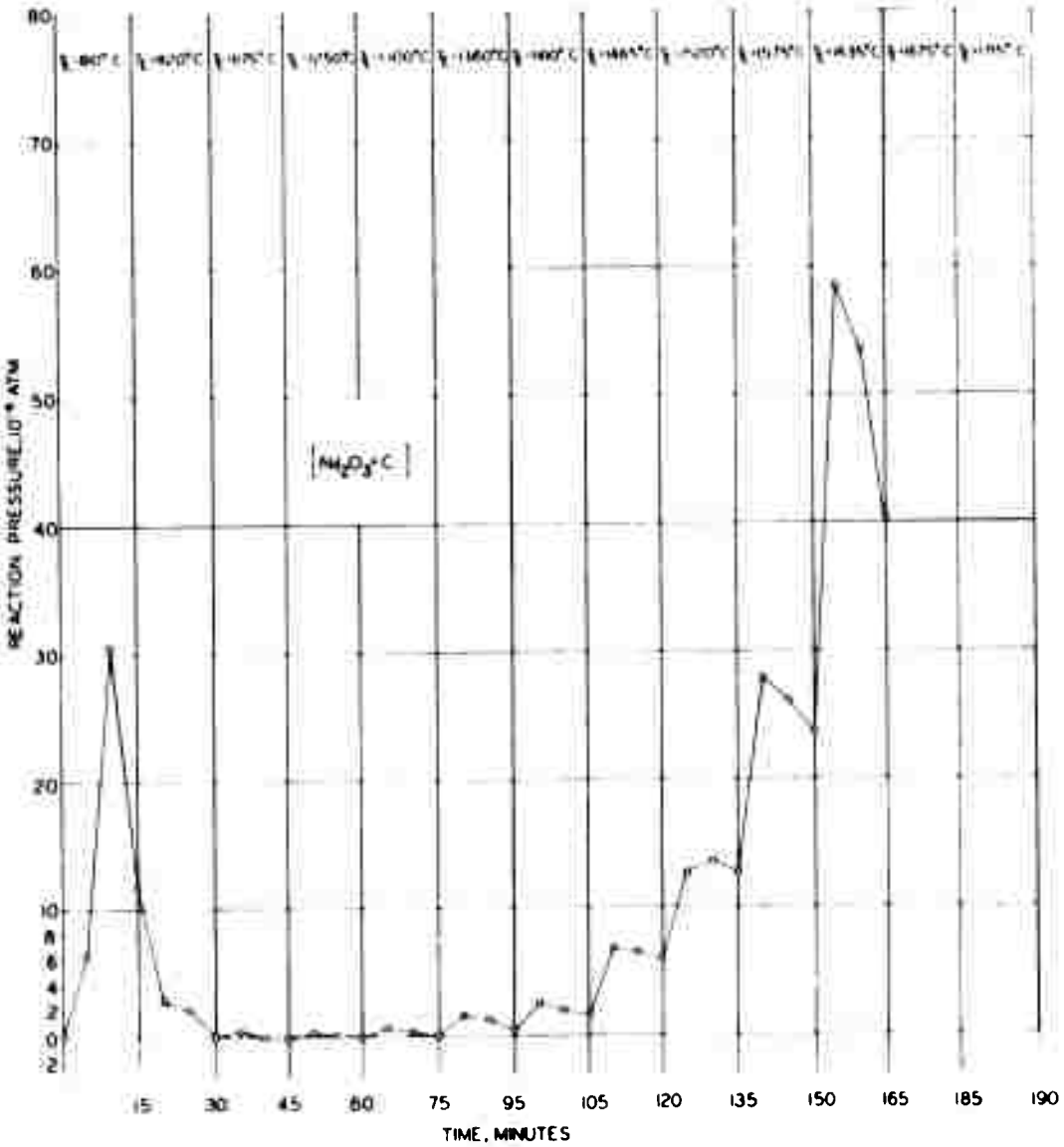

Figure 21. The Reaction of Graphite with Neodymium Sesquioxide, Scanning Experiment L-885

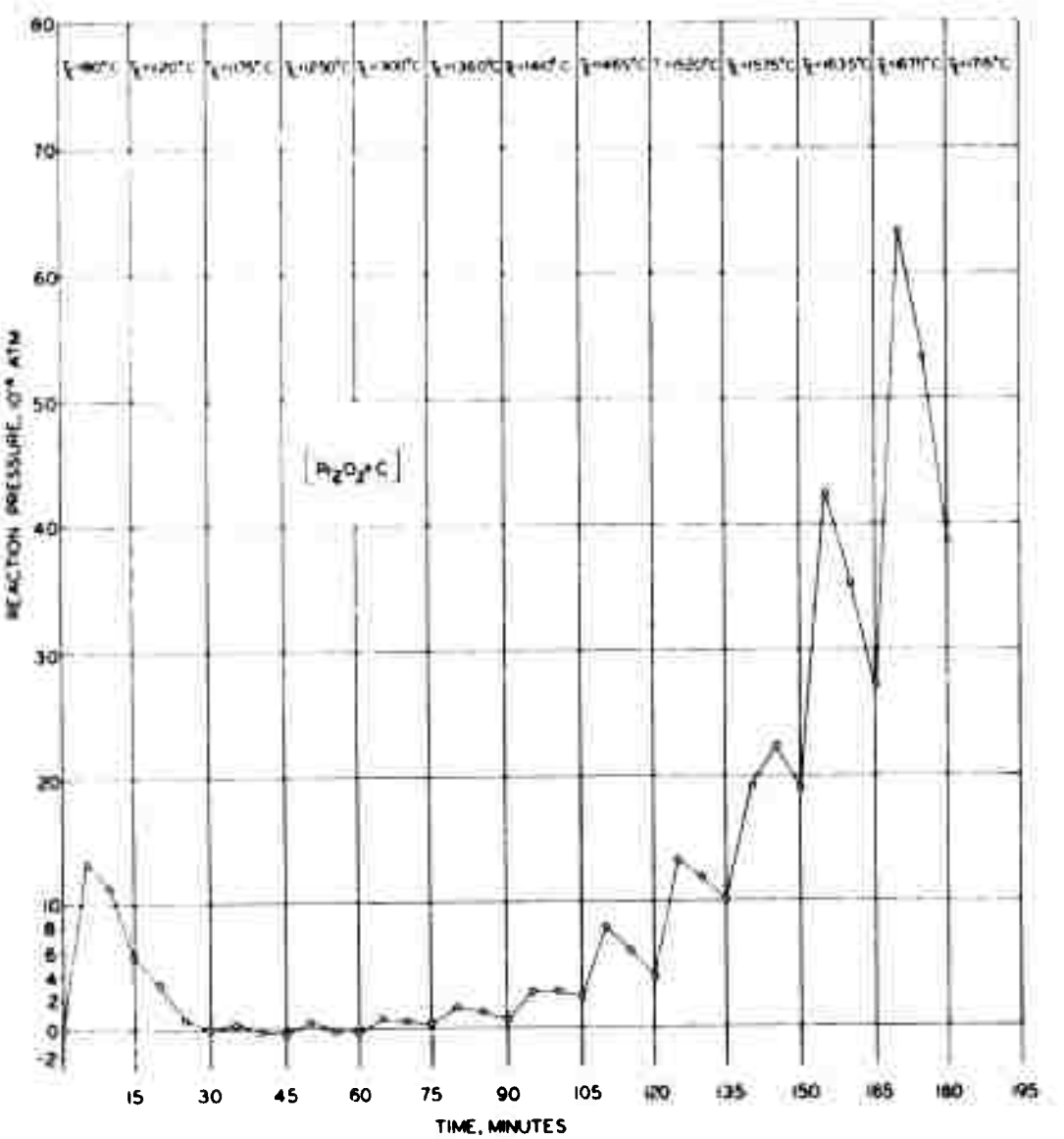

Figure 22. The Reaction of Graphite with Praseodymium Sesquioxide, Scanning Experiment

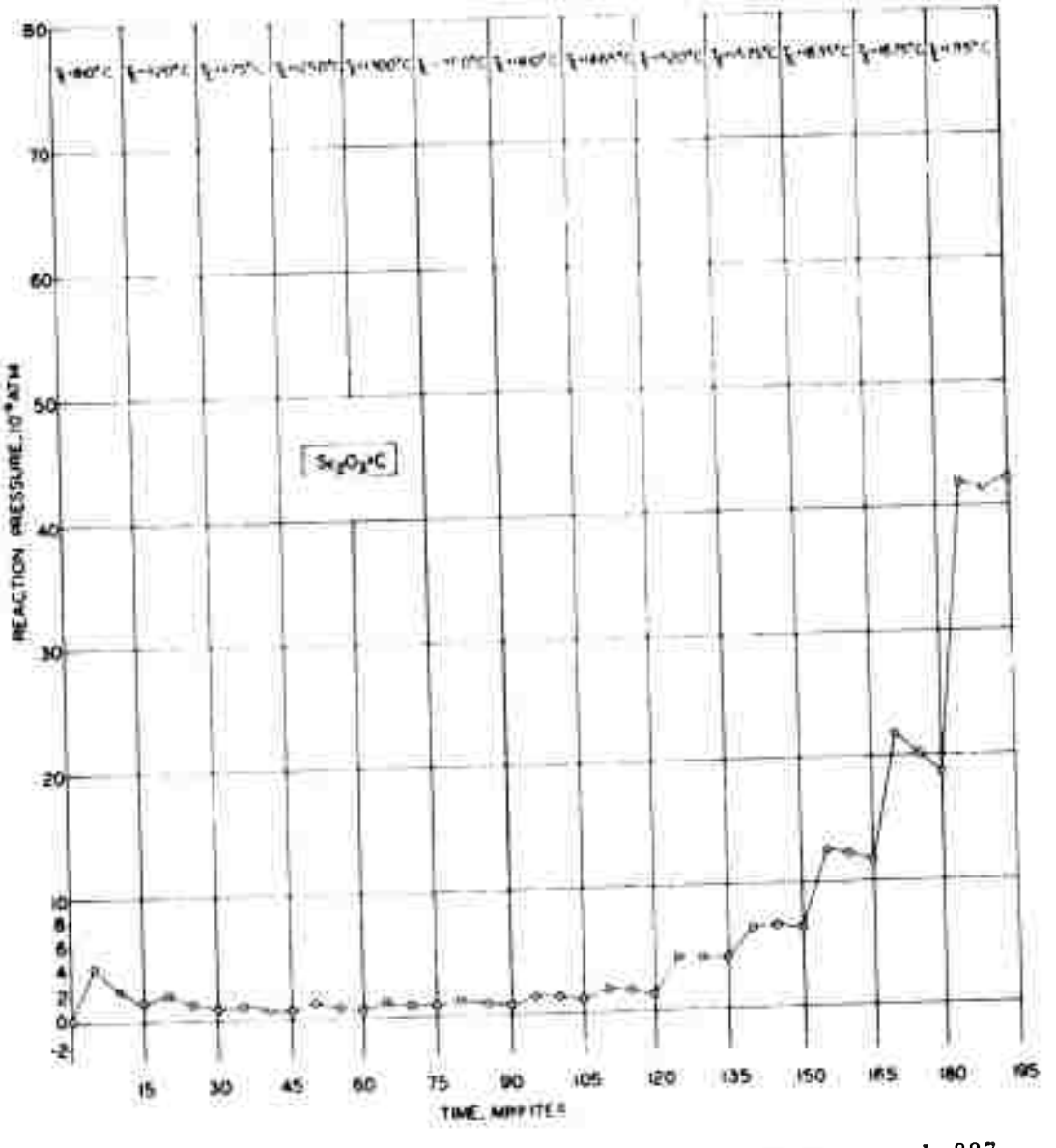

Figure 23. The Reaction of Graphite with Scandium Sesquioxide, Scanning Experiment L-887

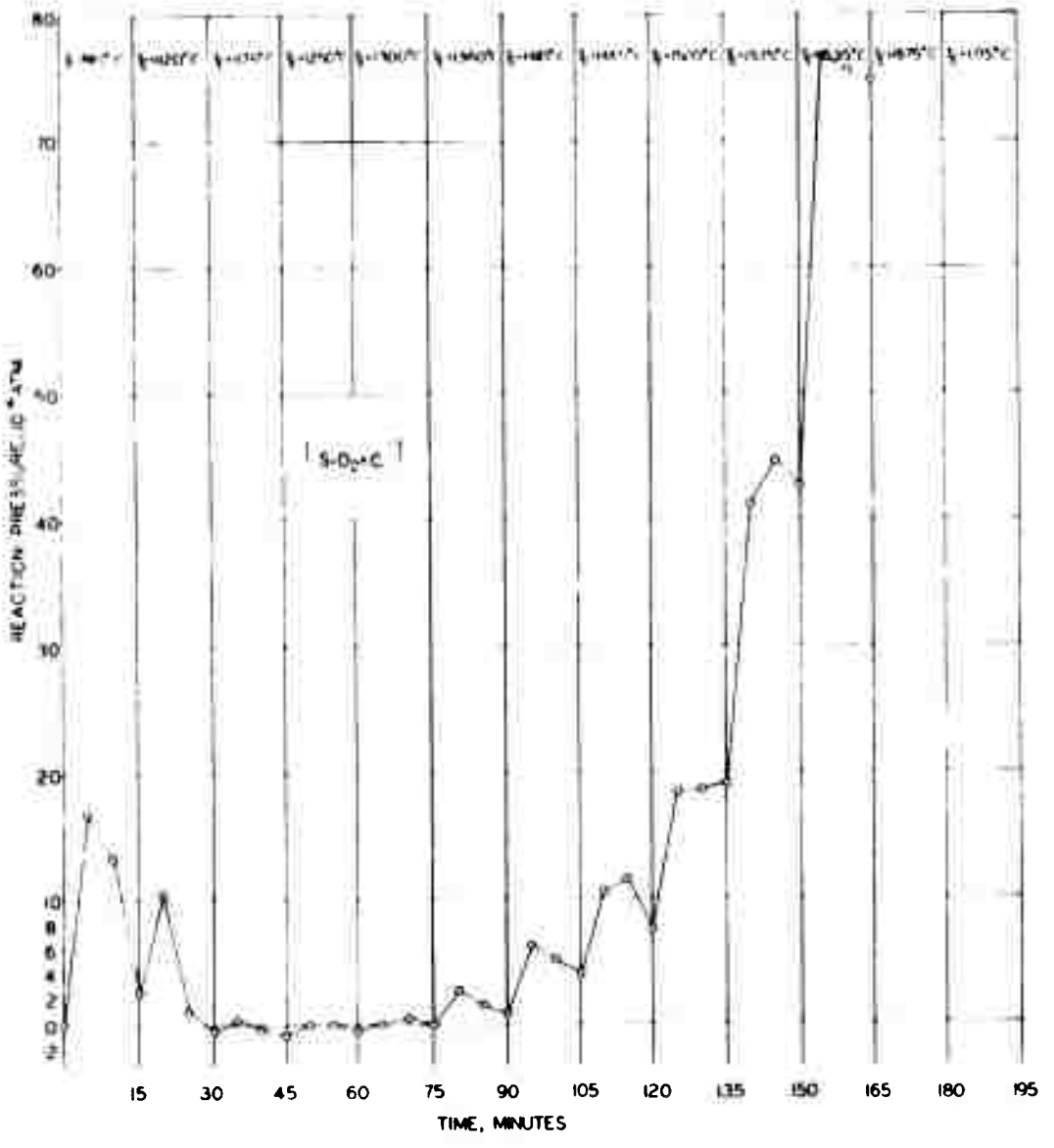

Figure 24. The Reaction of Graphite with Silicon Dioxide, Scanning Experiment

L-888

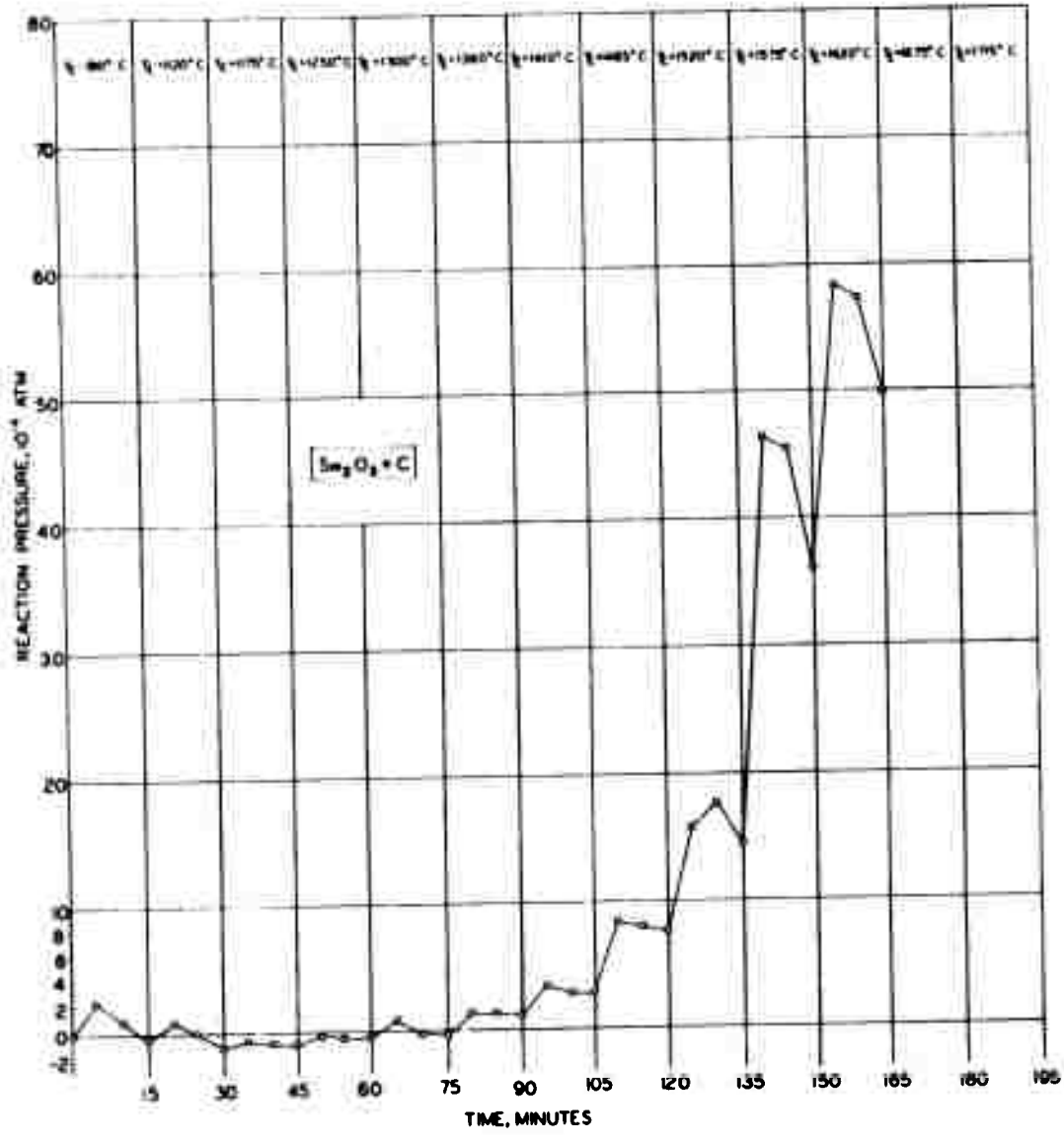

Figure 25. The Reaction of Graphite with Samarium Sesquioxide, Scanning Experiment L-282

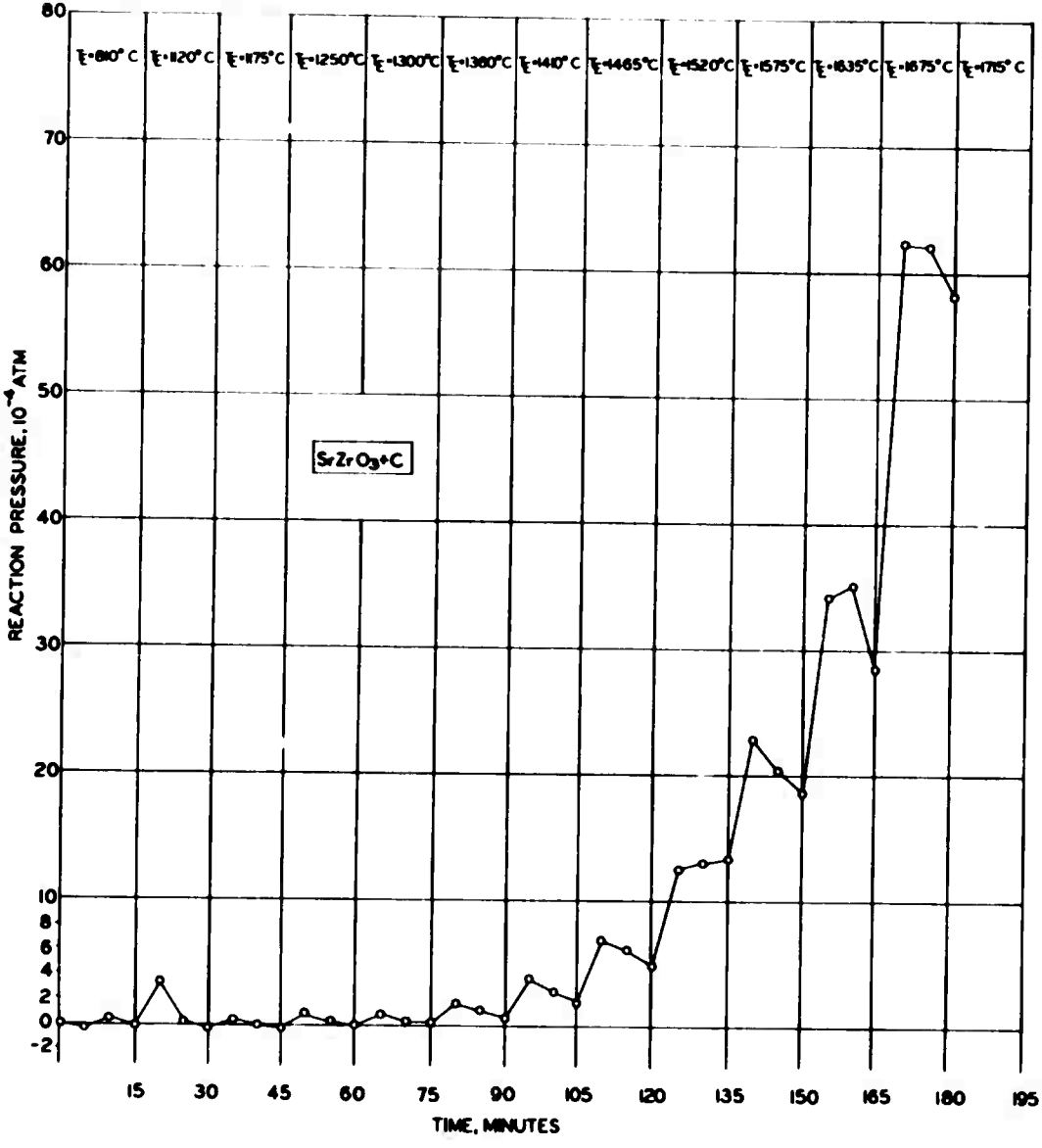

Figure 26. The Reaction of Graphite with Strontium Zirconate, Scanning Experiment L-889

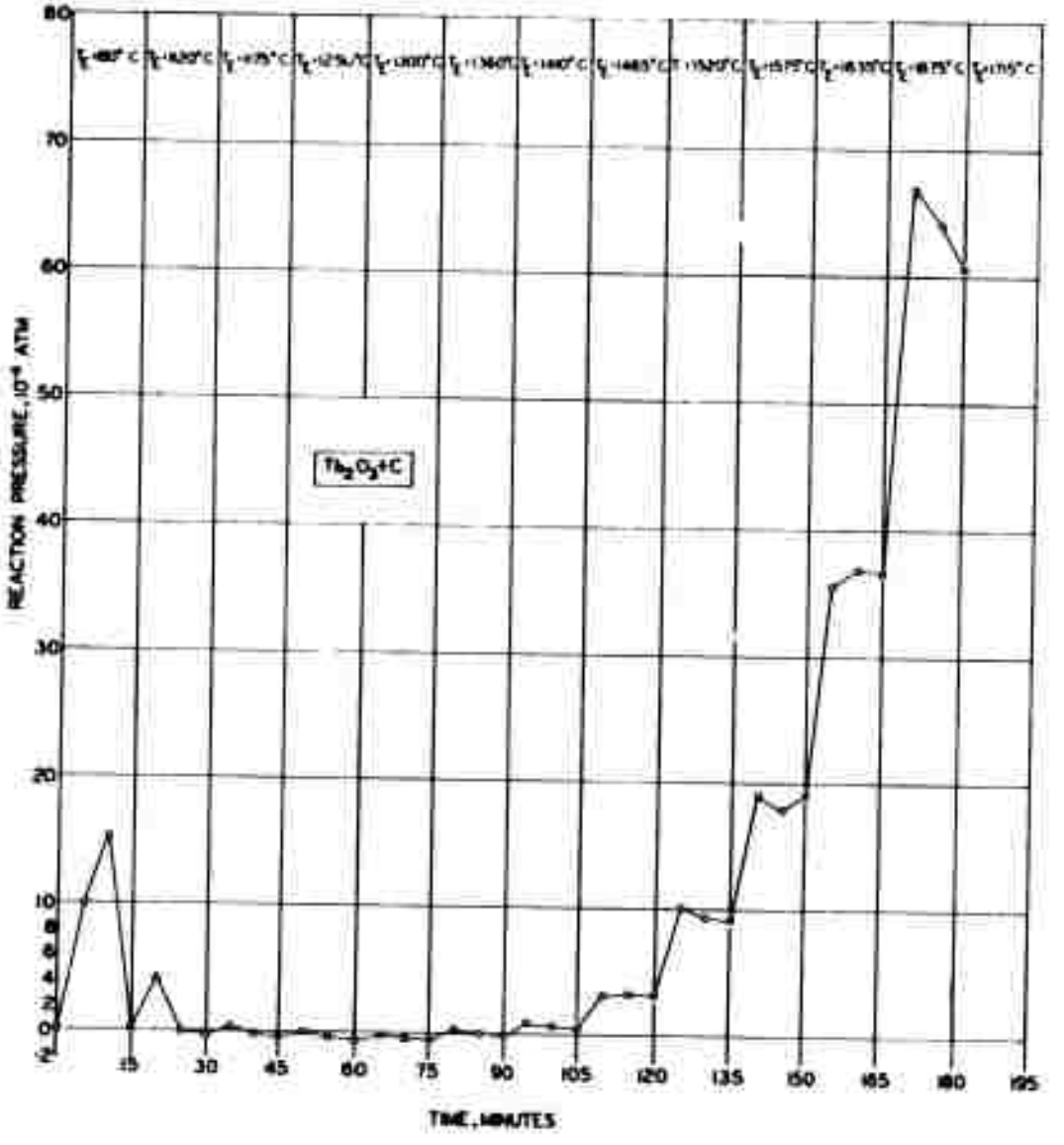

Figure 27. The Reaction of Graphite with Terbium Sesquioxide, Scanning Experiment L-890

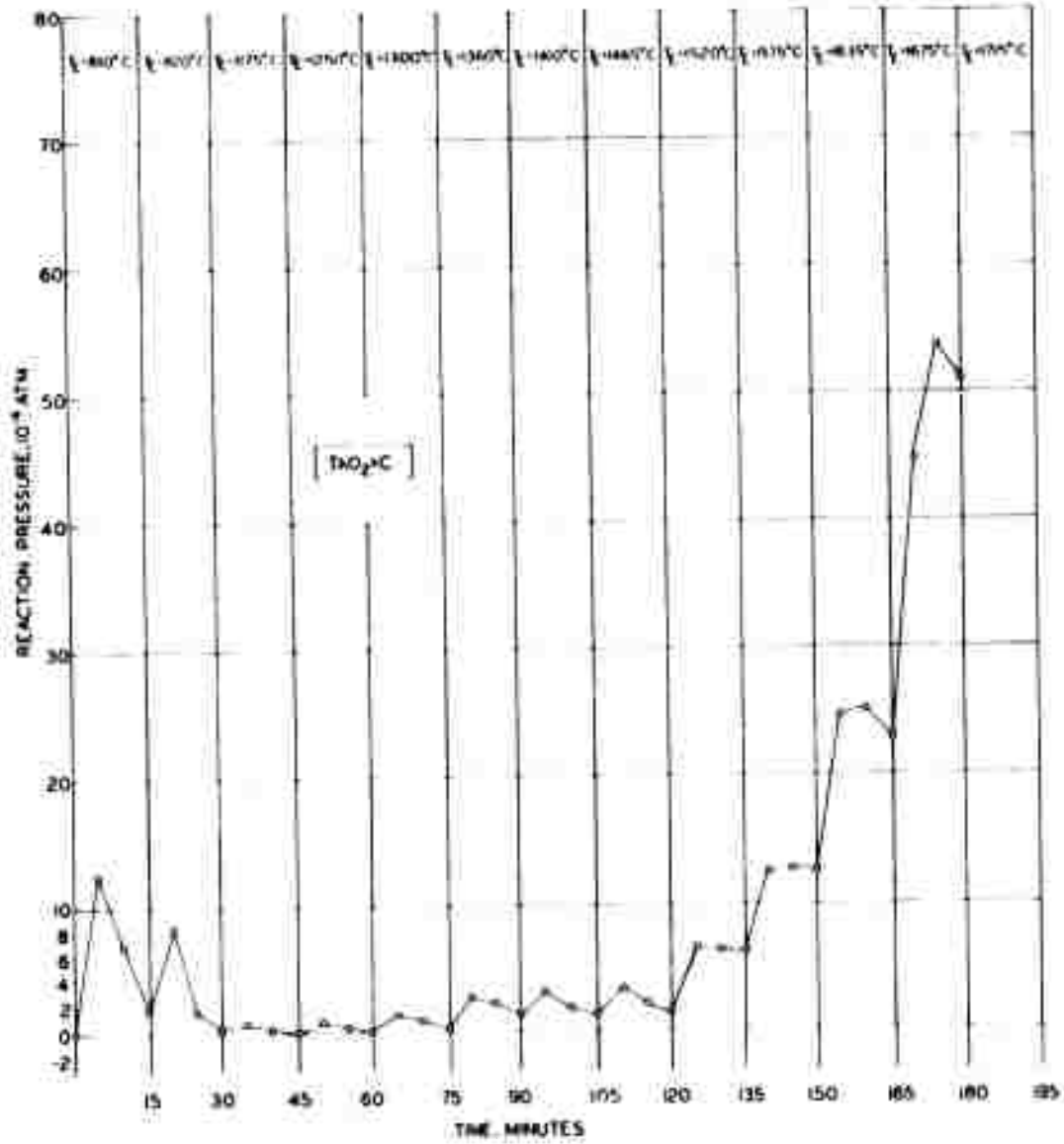

Figure 28. The Reaction of Graphite with Thorium Dioxide, Scanning Experiment L-891

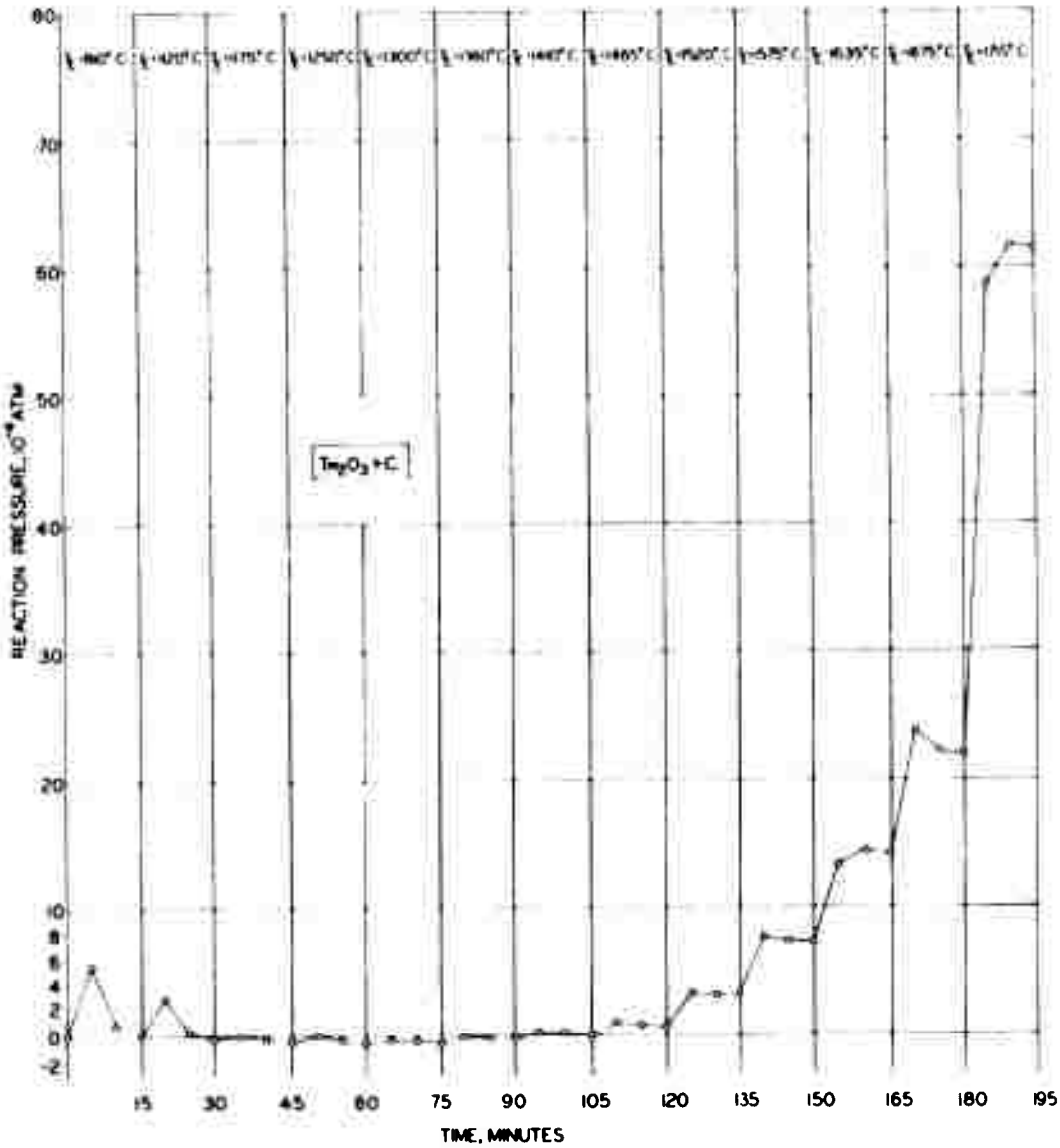

Figure 29. The Reaction of Graphite with Thulium Sesquioxide, Scanning Experiment L-892

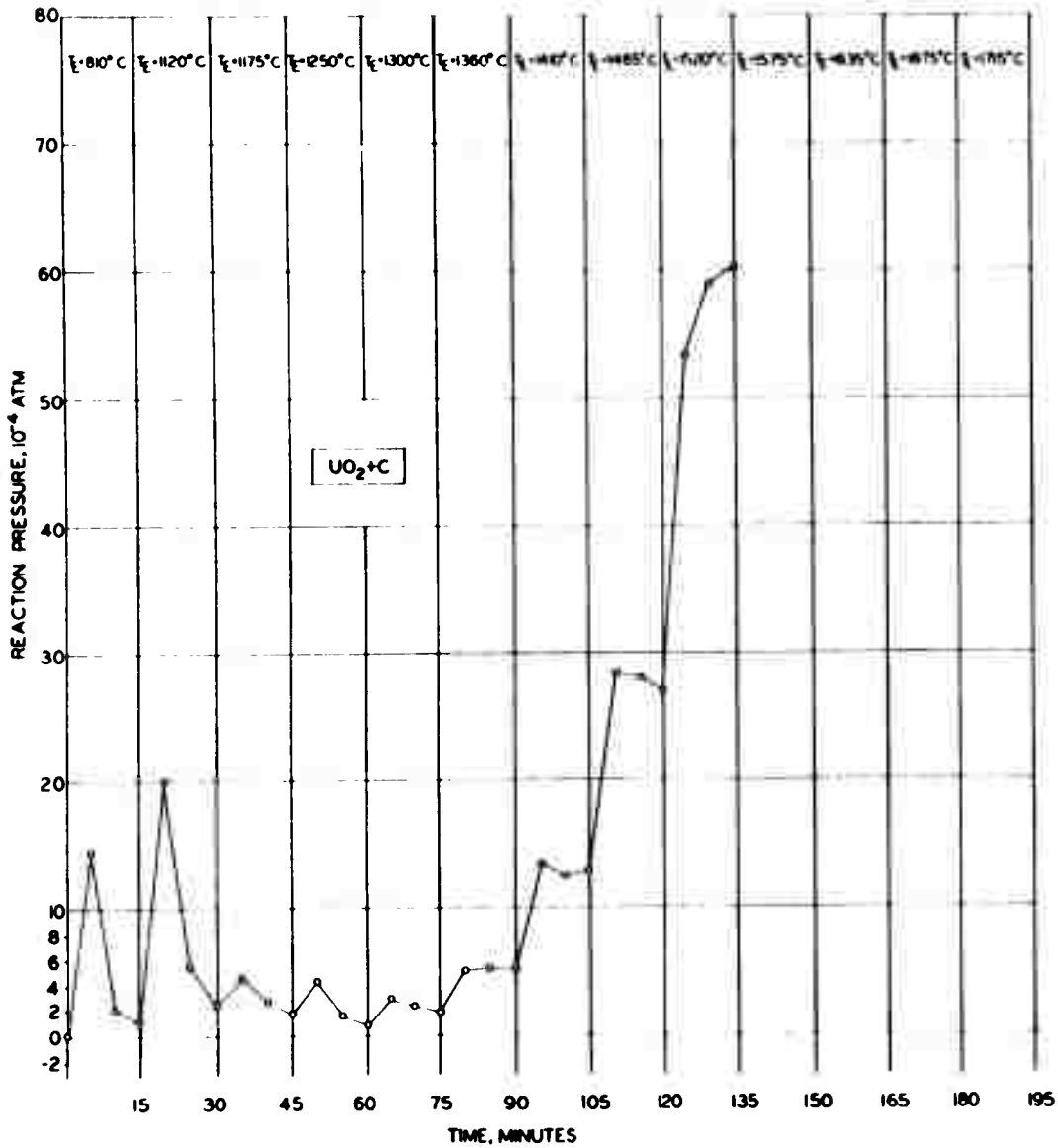

Figure 30. The Reaction of Graphite with Uranium Dioxide, Scanning Experiment L-893

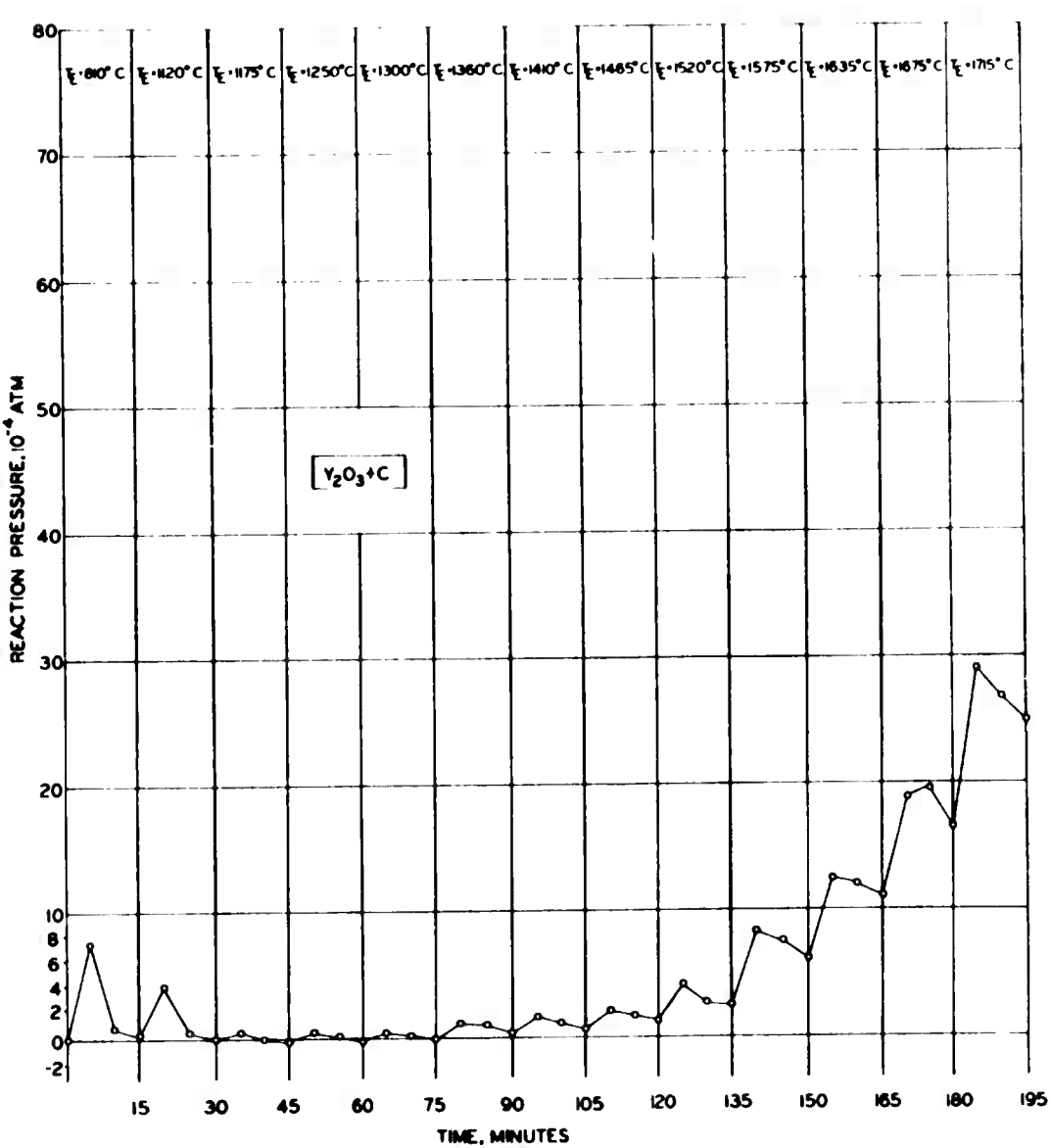

Figure 31. The Reaction of Graphite with Yttrium Sesquioxide, Scanning Experiment L-894

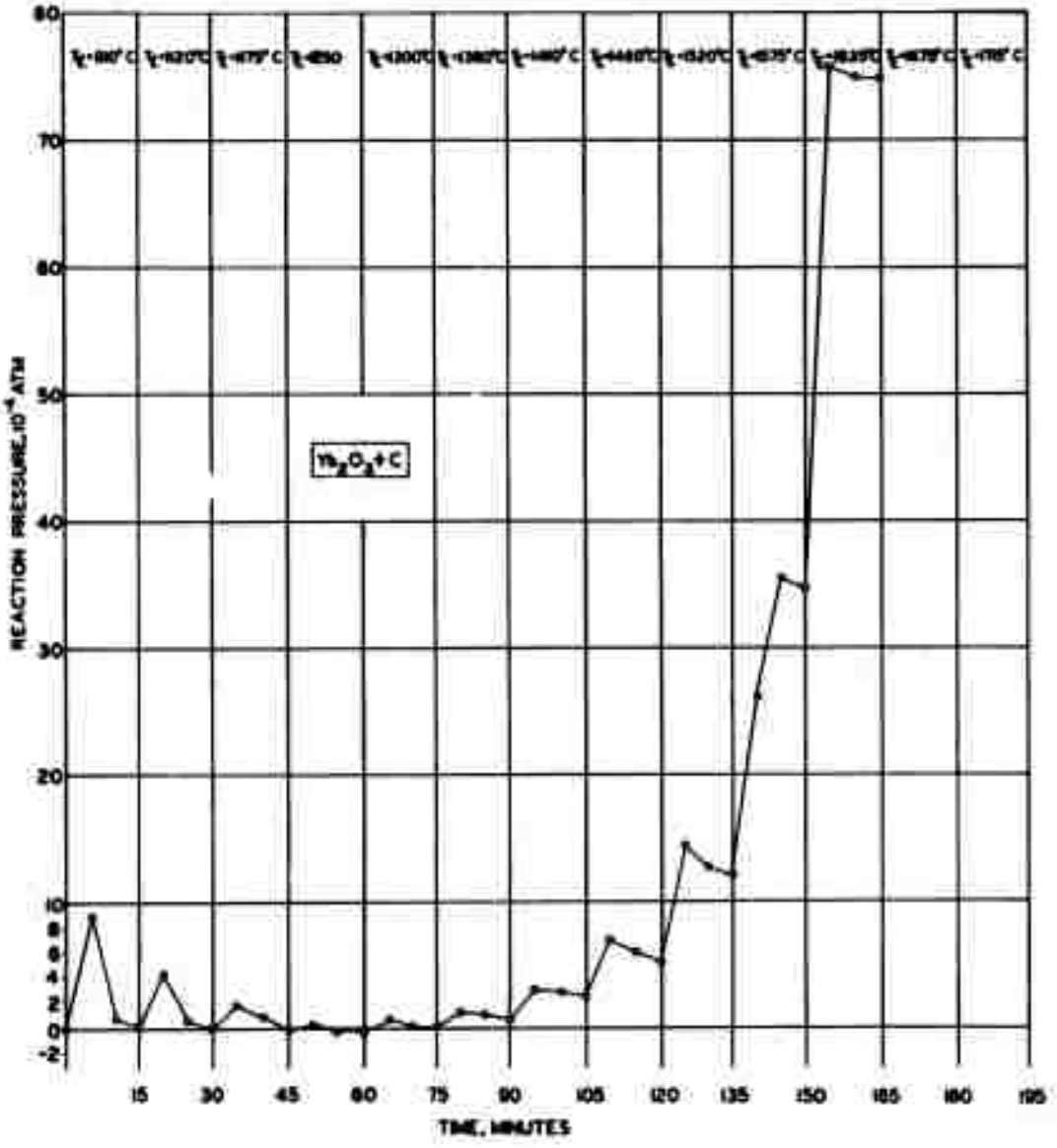

Figure 32. The Reaction of Graphite with Ytterbium Sesquioxide, Scanning Experiment L-895

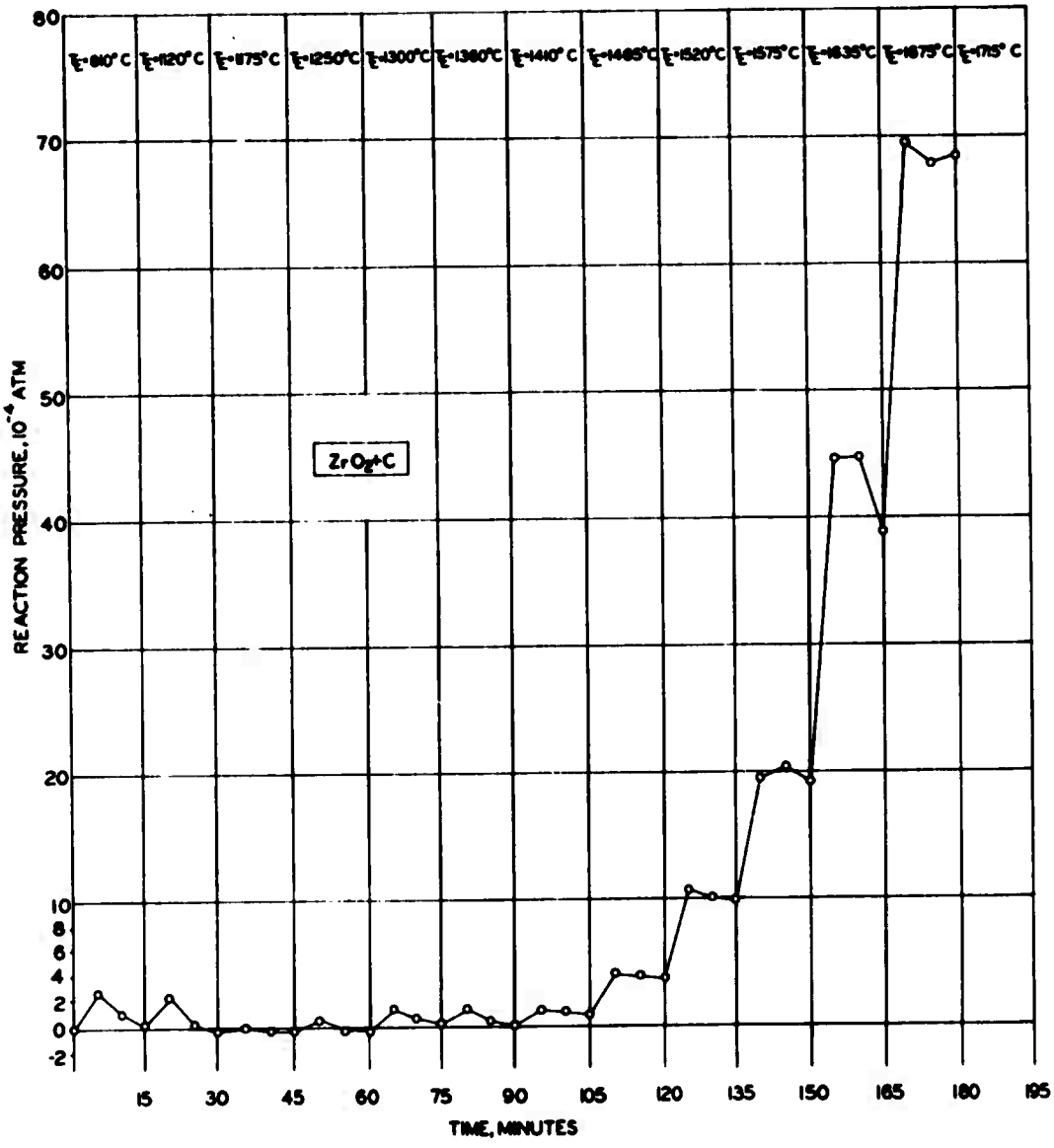

Figure 33. The Reaction of Graphite with Zirconium Dioxide, Scanning Experiment L-896

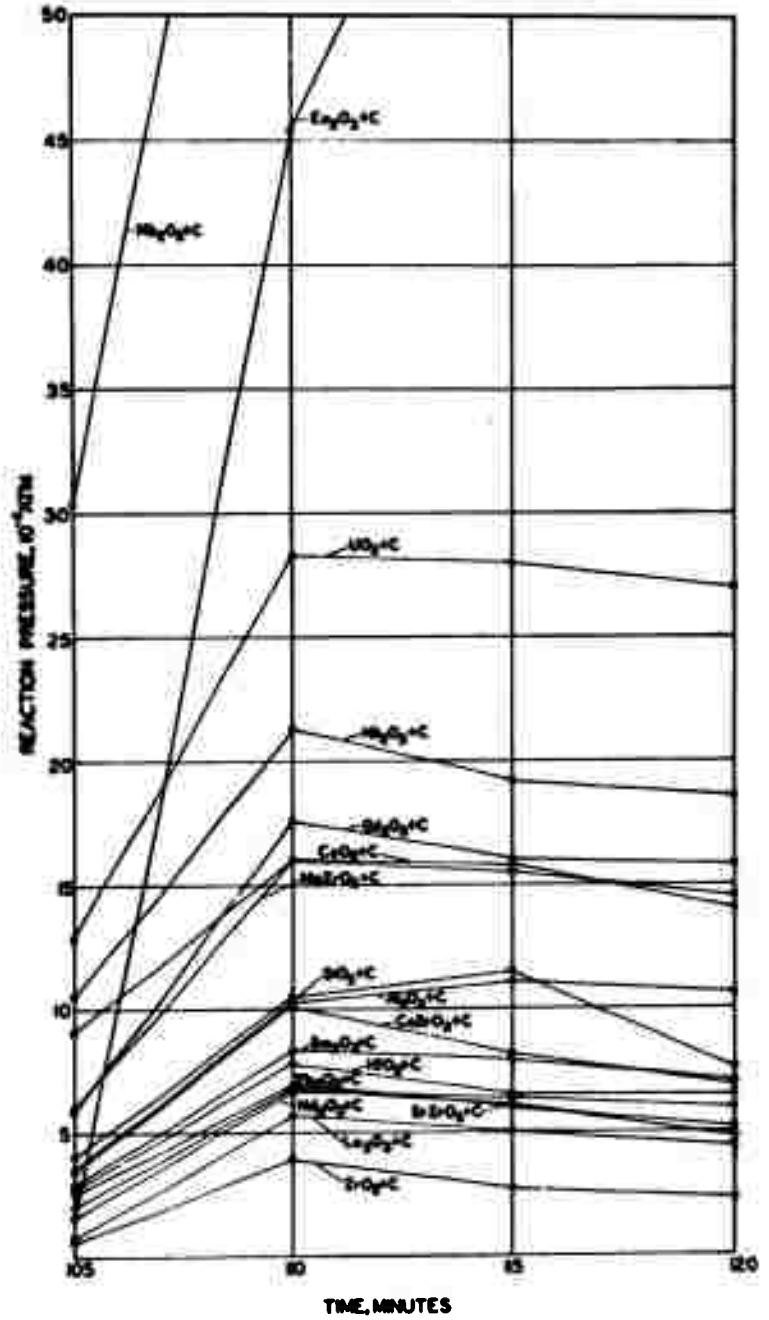

L-897

Figure 34. Reactions between Graphite and Refractory Oxides, Comparison of Scanning Experiments, Pressure Isotherms for an Equilibrium Temperature of 1465°C

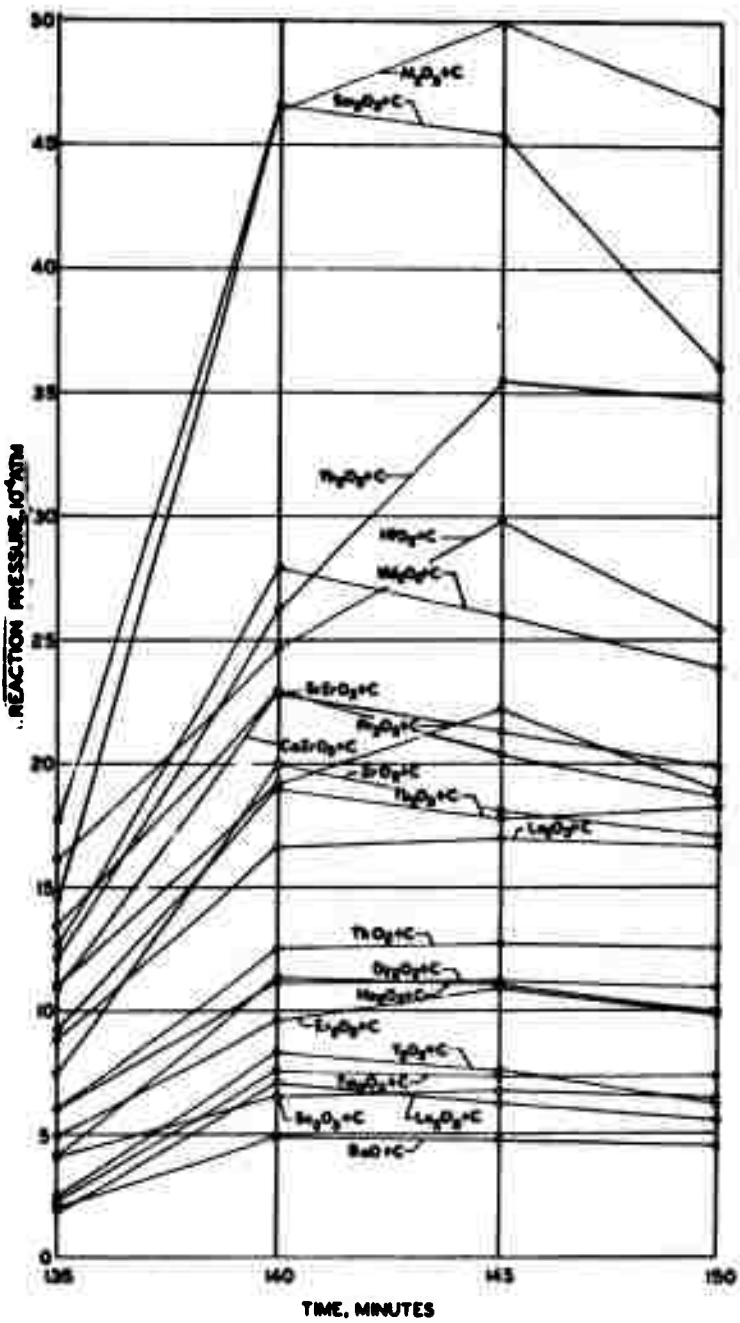

L-898

Figure 35. Reactions between Graphite and Refractory Oxides, Comparison of Scanning Experiments, Pressure Isotherms for an Equilibrium Temperature of 1575°C

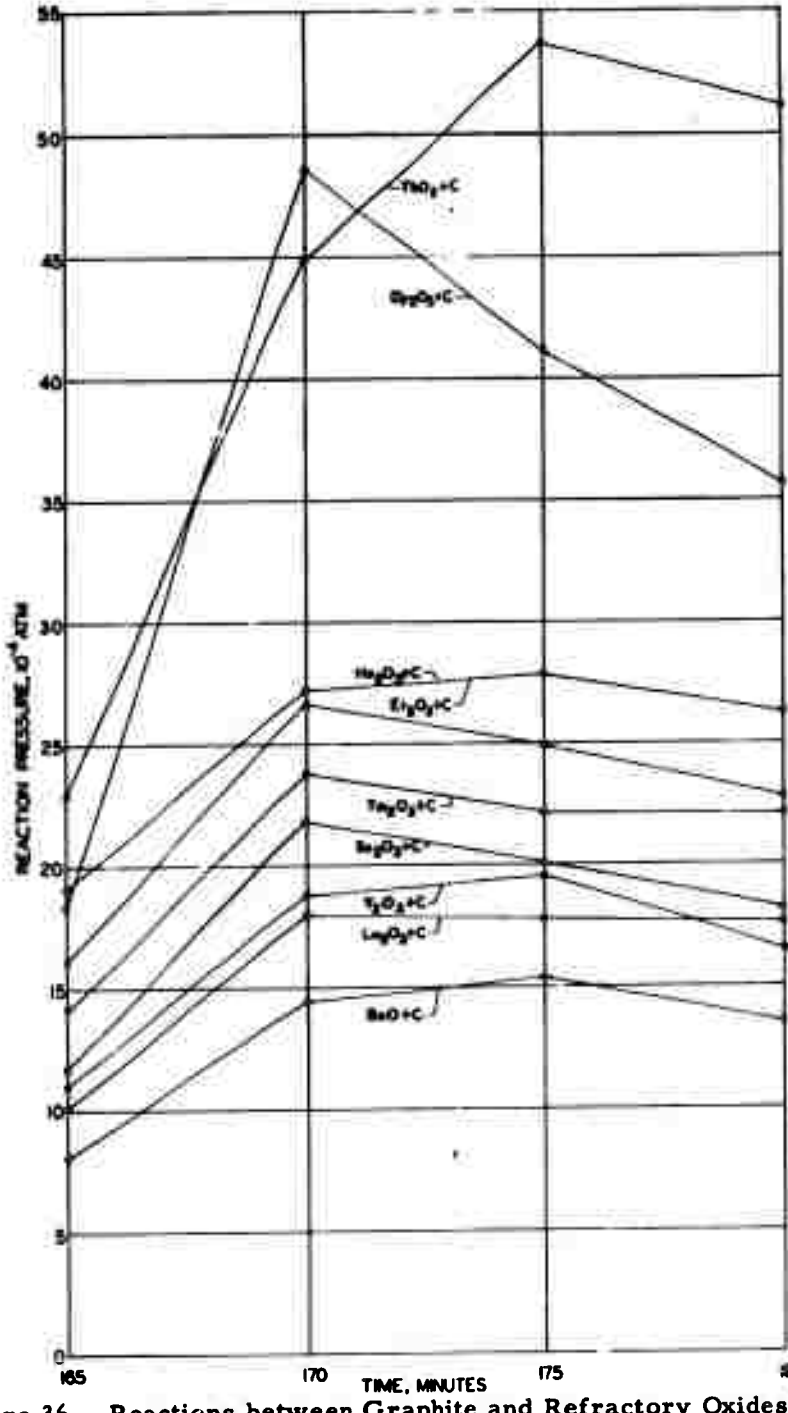

L-899

Figure 36. Reactions between Graphite and Refractory Oxides, Comparison of Scanning Experiments, Pressure Isotherms for an Equilibrium Temperature of 1675°C

3.2. Studies of Massive Graphite-Oxide Systems

Studies of the CO gas development in the previous section gave a measure of the reaction rates. In an actual situation, the composite will consist of massive oxide and graphite in contact. Reaction rates under these conditions are heavily influenced by the physical phenomena, such as barrier formation, diffusion, and surface tension, which control the contact among the reactants. Formation of a solid carbide at the interface may halt the progress of the reaction. Diffusion of the reactants in the matrix control the speed with which the protective oxide is formed and maintained. Surface tension plays an important role when the oxide is liquid at the operational temperatures. Depending on the effects to be studied, experiments were carried out with oxide spheres embedded in graphite or with oxide pellets on graphite pedestals. Careful examination of the components of the experiment after heating to temperature permit evaluation of the effects.

3.2.1. Oxide Spheres Embedded in Graphite

Reaction studies aimed at establishing the steps in heterogeneous reactions require careful planning to insure that good contact and uniform temperature are maintained at reaction interfaces. In case of reactants melting, the molten substances must be contained. To meet these requirements for graphite-oxide system studies, we developed the method of embedding oxide spheres in a consolidated graphite matrix.

3.2.1.1. Description of Apparatus and Experimental Procedure

This technique involves embedding a 1-inch diameter sphere of the oxide in a powdery blend consisting of graphite flour and pitch. The blend is pressed in a graphite mold as illustrated in Figure 37, heated rapidly to the desired temperature by induction, and held at that temperature for a specific period of time. During the early stages of heating, the mixture of graphite flour and pitch surrounding the oxide sphere consolidates into a matrix from coking-out of the pitch. In the temperature range of the reaction (usually above 1700°C for the oxides of interest), the graphite matrix exhibits a plasticity which insures that the pressure holds the graphite in intimate contact with the oxide sphere.

After the system has cooled to room temperature, the specimen is cut in such a way that a cross section of the sphere can be examined. The extent of the reaction, if any, is then measured and related to holding time and temperature. Examination of photographs of the cross sections, supplemented by qualitative X-ray analyses, facilitate a detailed study of the reaction system.

Investigations of this type are aimed at two objectives. First, to establish actual stability limits; i.e., the extreme conditions of temperature and time at which the oxide samples are structurally unaffected. Second, attention is given to the establishment of characteristics, kinetic and structural, which accompany any decay when the given stability limits are exceeded.

3.2.1.2. The Graphite-Alumina System

Cross sections of graphite-alumina systems after various exposures to high temperatures are illustrated in Figure 38. The results can be described as follows:

1800°C,	1 hour:	No indications of reaction.
1900°C,	1½ hours:	Discoloration (graying) of the oxide to a radial depth of 2 mm.
1950°C,	1 hour:	Discoloration prevailing throughout the entire cross section of the oxide sphere.

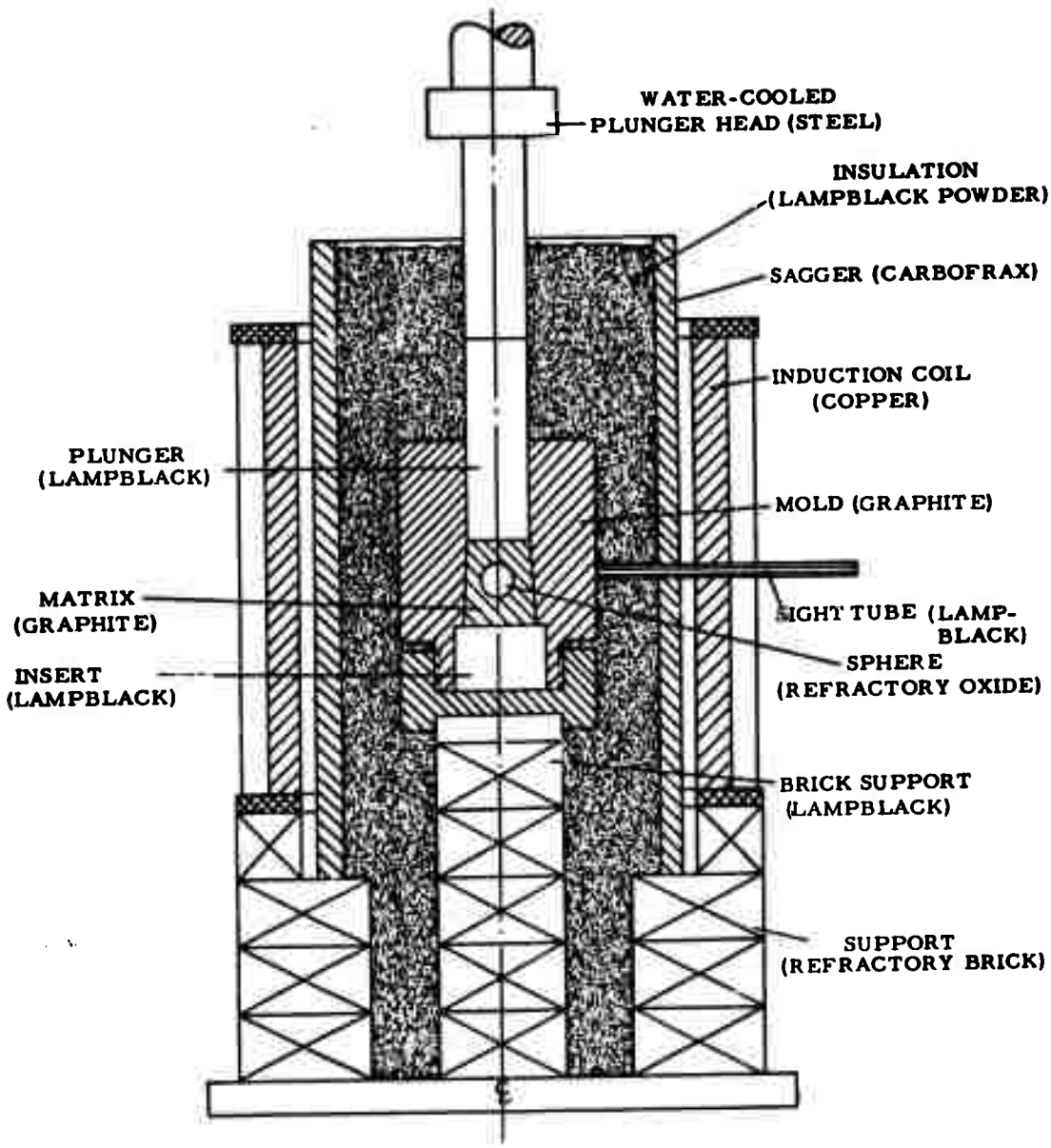

Figure 37. Apparatus for Stability Studies on Massive Graphite-Oxide Systems

L-174

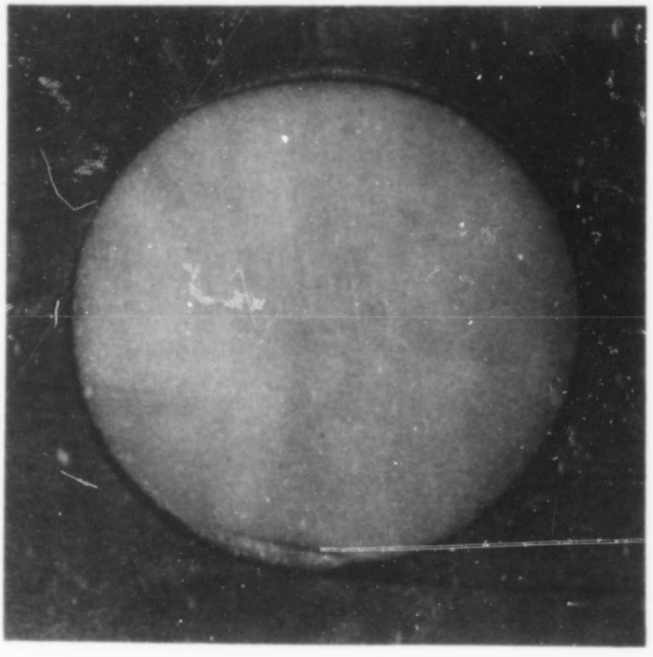

1800°C for 1 Hour

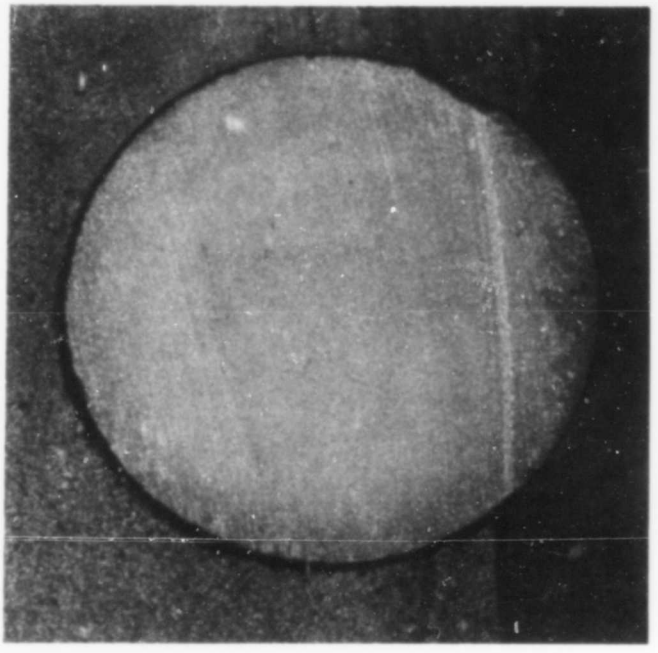

1900°C for 1½ Hours

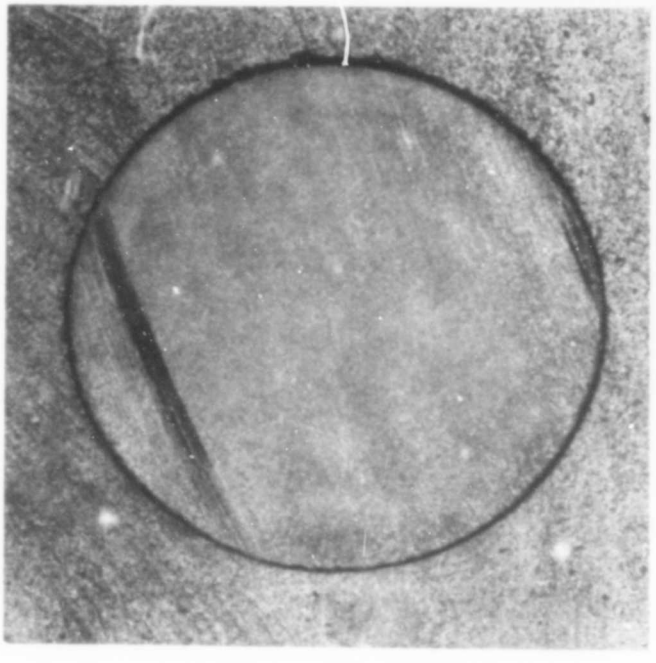

1950°C for 1 Hour

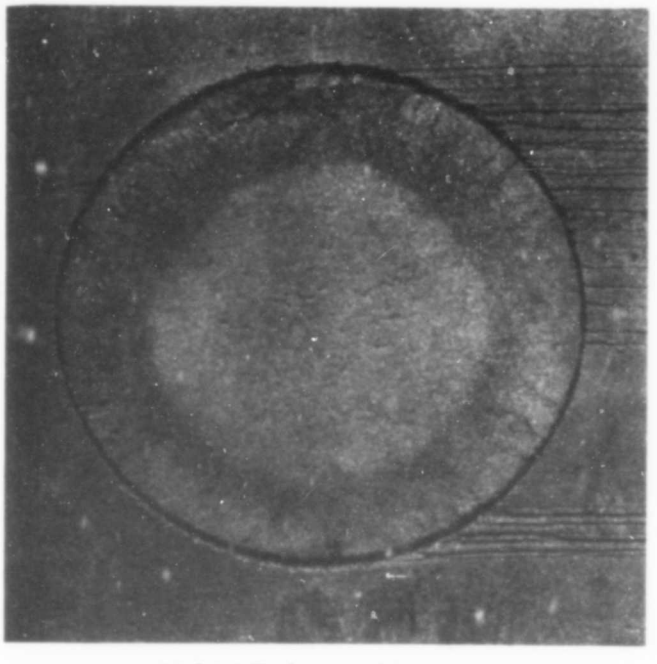

2000°C for 1 Hour

Figure 38. Graphite-Alumina Systems after Exposure to High Temperature

2000°C, 1 hour: Very distinct, though not catastrophic structural decay to a radial depth of approximately 5 mm.

Complete conversion of the oxide to the carbide was observed when the melting point (2045°C) was exceeded.

3.2.1.3. The Graphite-Beryllia System

Cross sections of graphite-beryllia systems after various exposures to high temperatures are illustrated in Figure 39. The results can be described as follows:

2150°C, 1 hour: Oxide unaffected except for a grain growth phenomenon which is inherent in BeO above 2000°C. [4]

2300°C, 1 hour: Discoloration of the oxide to a radial depth of approximately 10 mm. Grain growth is more pronounced. This shell of glossy material between oxide sphere and graphite matrix was analyzed by X-ray and found to be chiefly beryllium carbide with the balance being graphite.

2300°C, 2 hours: Oxide sphere completely consumed, leaving only blackish nodules in the bottom of the cavity. X-ray analysis showed the nodules to be an agglomeration of Be_2C, BeO, and graphite.

From this, the mechanism of the graphite-beryllia reaction evolves as follows:

1) The melting point of BeO is 2550°C. Any reaction below this temperature begins in the solid state by diffusion of carbon into the oxide. A "graying front" proceeds into the BeO, but no point in the oxide can reach a carbon concentration high enough for extensive carbide formation. In other words, the carbon-poor regions in the center of the sphere act as carbon sinks for the outer carbon-rich regions and prevent carbide from materializing in any significant quantity.

2) As more carbon diffuses into the oxide, the carbon concentration begins to increase in the outer regions of the sphere, leading to the formation of sizable amounts of carbide in the interface. Unfortunately, Be_2C has a melting point of 2127°C. Therefore, if the process described is taking place at 2300°C, a molten phase appears between the solid graphite matrix and the solid, carbon-enriched oxide sphere. As diffusion through liquids is much faster than through solids, the carbon transport to the oxide is greatly accelerated and leads to rapid conversion of the solid oxide to the liquid carbide.

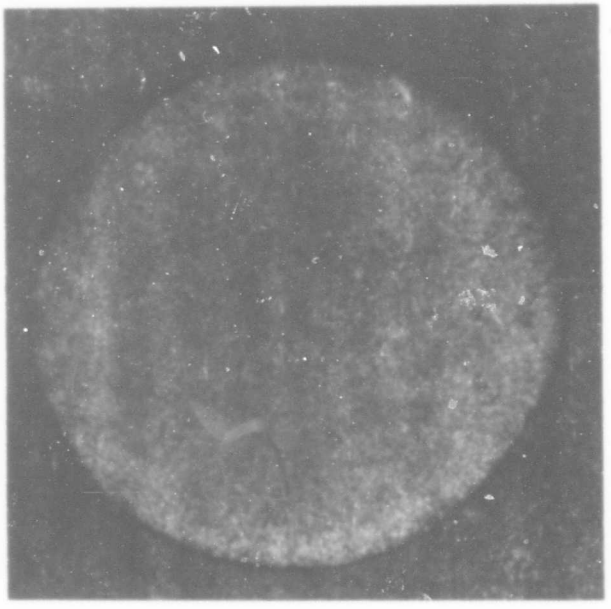

2150°C for 1 Hour

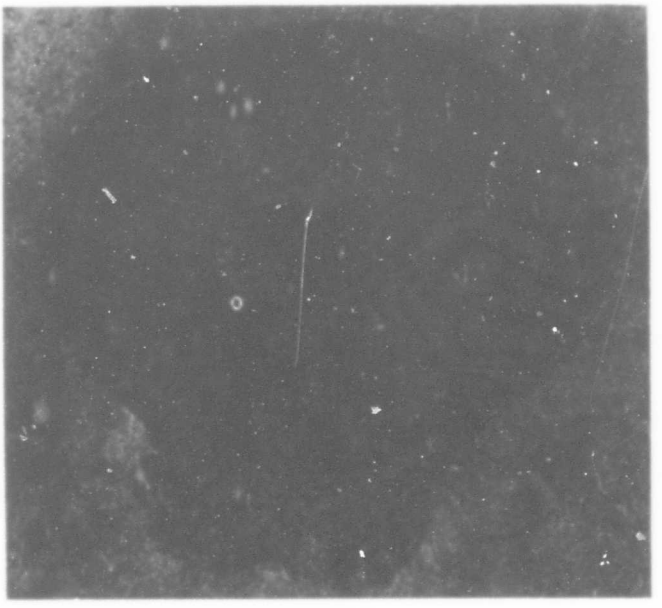

2300°C for 1 Hour

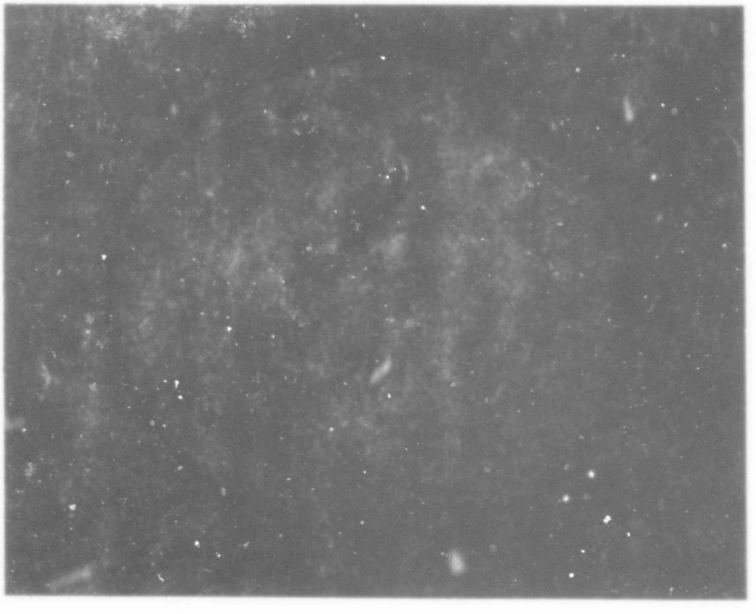

2300°C for 2 Hours

Figure 39. Graphite-Beryllia Systems after Exposure to High Temperature

BeO formed on graphite-base composites may be considered useful up to about 2100°C. Above this temperature BeO is no longer effective, since the carbide formed by the reduction process is a reaction accelerator rather than a reaction barrier.

3.2.1.4. The Graphite-Ceria System

Cross sections of graphite-ceria systems after various exposures to high temperatures are illustrated in Figure 40. The results can be described as follows:

1800°C, 1 hour: Formation of a thin shell on the oxide.

1800°C, 2 hours: Oxide coated with a shell of sizable thickness.

1900°C, ½ hour: Oxide was liquefied and one-third of it has been consumed by reaction.

1900°C, 1 hour: Oxide completely consumed.

The appearance of a liquid at 1900°C may be explained by a partial reduction. While ceria (CeO_2) has a melting point of 2730°C, the sesquioxide (Ce_2O_3) is reported to melt at 1690°C. Since no melting occurred at 1800°C, it is inferred that at this temperature the reduction does not proceed at a significant rate.

3.2.1.5. The Graphite-Hafnia System

Cross sections of graphite-hafnia systems after various exposures to high temperatures are illustrated in Figure 41. The results can be described as follows:

2300°C, 1 hour: Oxide unaffected.

2400°C, 1 hour: A thin shell of hafnium carbide has formed between oxide and graphite. Carbide is also apparent as lines in the core.

2500°C, 1 hour: Oxide was liquefied and one-third of it has been consumed by reduction.

The appearance of a liquid at 2500°C must be attributed to stabilizing agents since pure hafnia is reported to melt at 2777°C.

3.2.1.6. The Graphite-Strontium Zirconate System

Cross sections of graphite-strontium zirconate systems after various exposures to high temperatures are illustrated in Figure 42. The results can be described as follows:

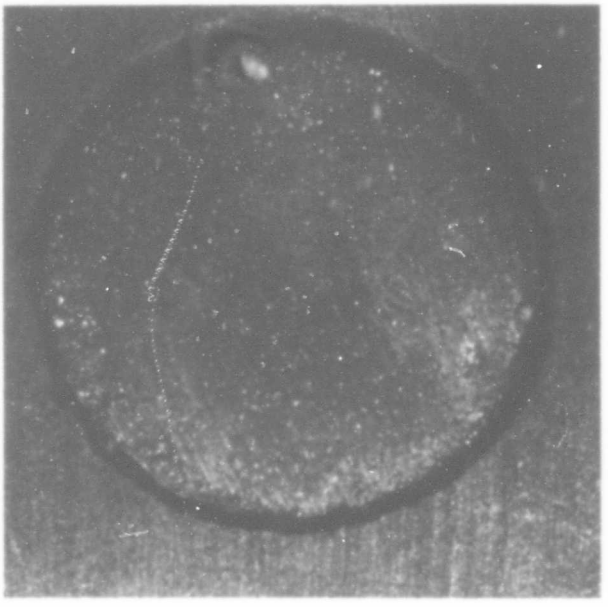

1800°C for 1 Hour

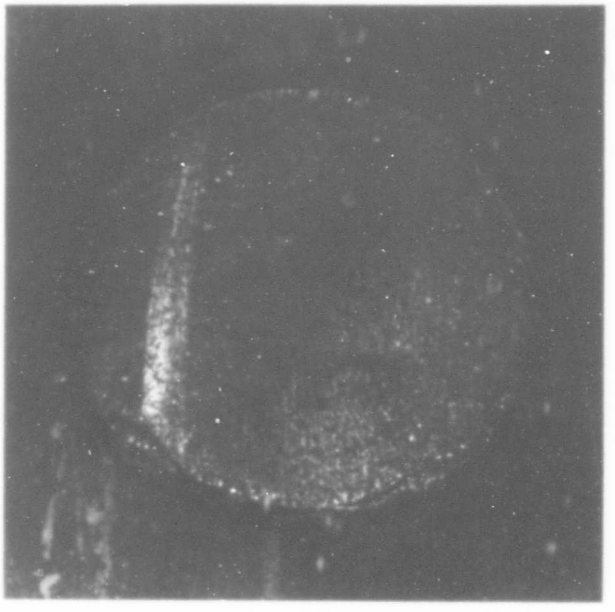

1800°C for 2 Hours

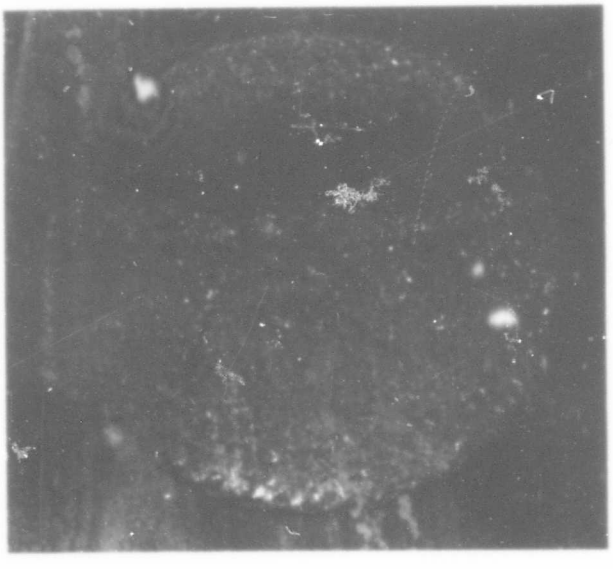

1900°C for $\frac{1}{2}$ Hour

1900°C for 1 Hour

Figure 40. Graphite-Ceria Systems after Exposure to High Temperature

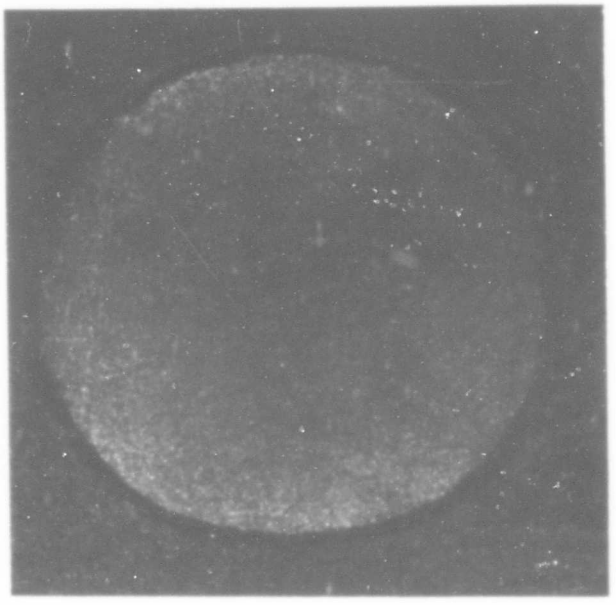

2300°C for 1 Hour

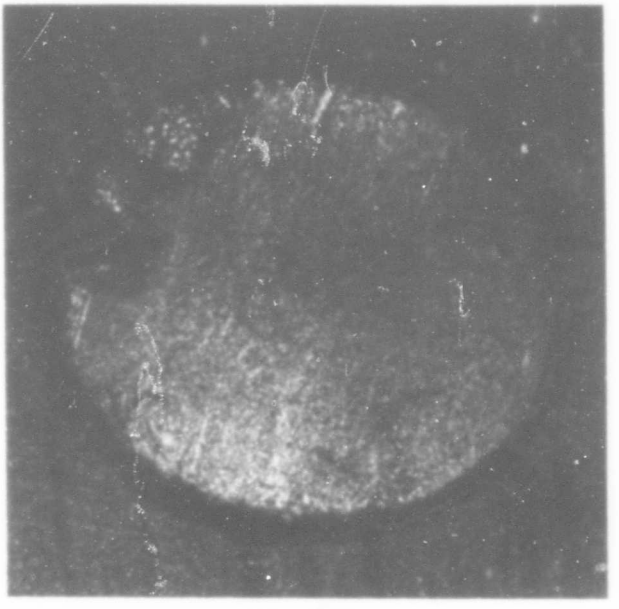

2400°C for 1 Hour

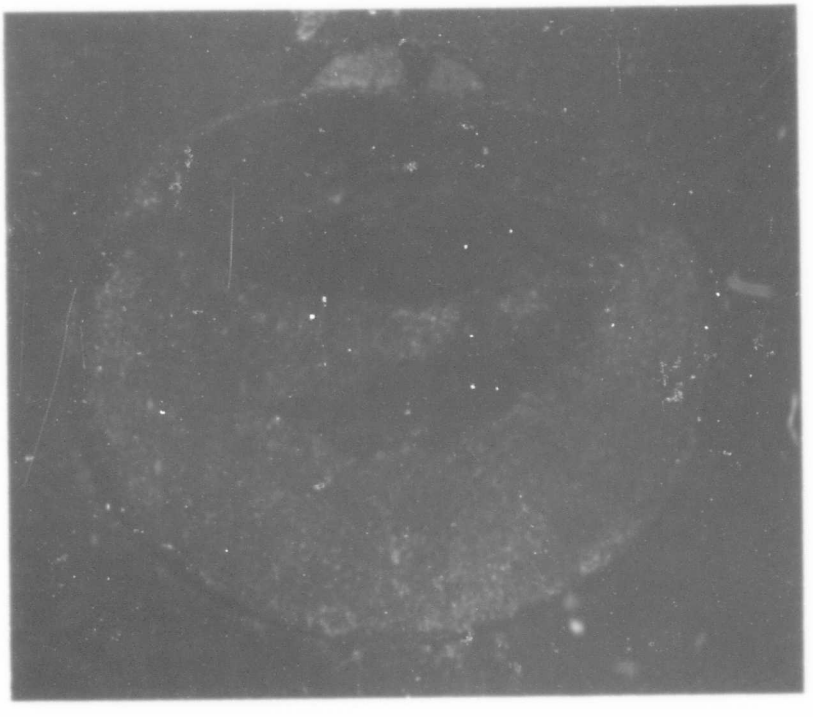

2500°C for 1 Hour

Figure 41. Graphite-Hafnia Systems after Exposure to High Temperature

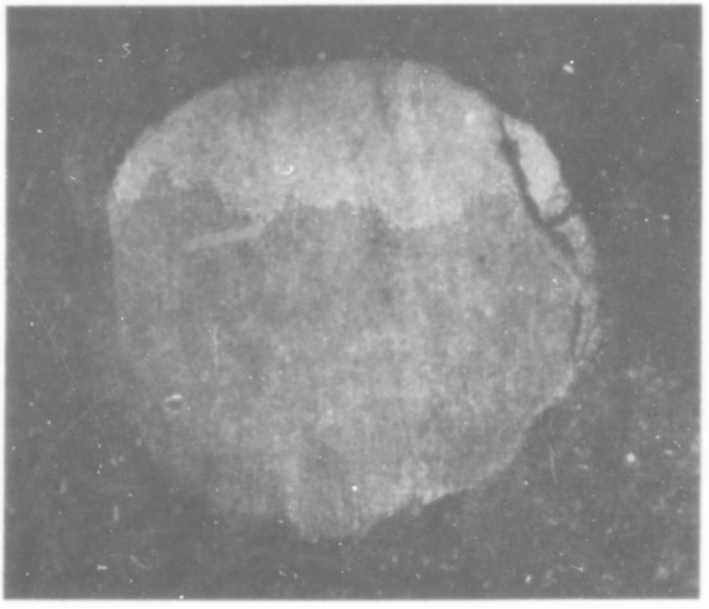

1900°C for 1 Hour

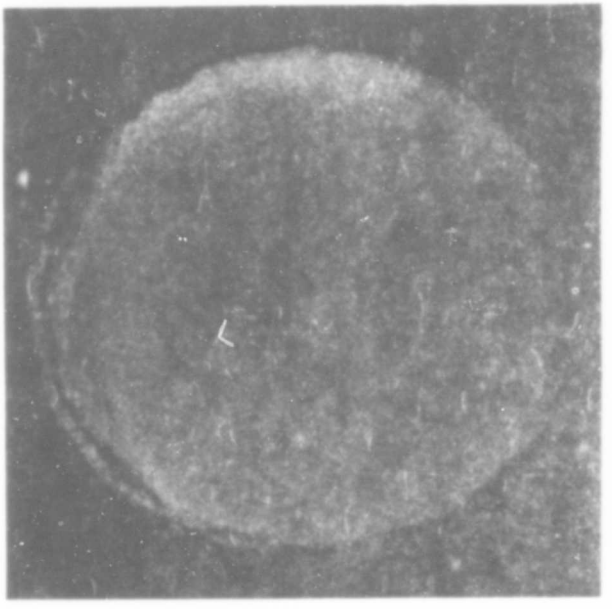

2100°C for 1 Hour

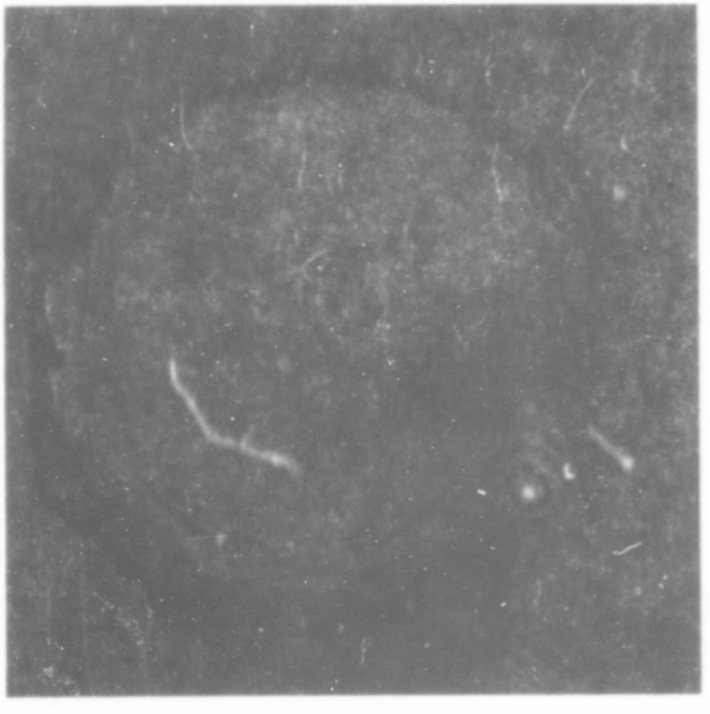

2300°C for 1 Hour

Figure 42. Graphite-Strontium Zirconate Systems after Exposure to High Temperature

1900°C, 1 hour: No signs of reaction.

2100°C, 1 hour: Some decrepitation of the oxide along the reaction interface. Grayed core surrounded by lighter shell. No indications of carbides by X-ray analysis.

2300°C, 1 hour: Oxide regions adjacent to the reaction interface greatly decrepitated. Loose pieces on the oxide sphere. X-ray anaylsis of the pieces showed high ZrC content and small quantities of $SrZrO_3$. SrC_2 may have escaped detection due to hydration. Evidence of grain boundary reactions in the core of the oxide.

3.2.1.7. The Graphite-Thoria System:

Cross sections of graphite-thoria systems after various exposures to high temperatures are illustrated in Figure 43. The results can be described as follows:

2100°C, 1 hour: Evidence of a thin carbide layer between oxide and graphite, providing an excellent bond. Structural failure believed to be due to this bond. Upon cooling, the oxide contracted more than the graphite and fractured in tension.

2300°C, 2 hours: Oxide greatly diminished in size. Matrix cavity coated and lower part of the matrix impregnated with a liquid. ThC_2 and ThC are known to melt at 2655 and 2625°C, respectively. It is assumed that the thorium-carbon system has a eutectic below 2300°C. This low-melting Th-C phase wets graphite readily.

2500°C, 2 hours: The matrix cavity was coated with a liquid phase, and the lower part of the matrix is seen to be strongly impregnated.

3.2.1.8. The Graphite-Yttria System

Cross sections of graphite-yttria systems after various exposures to high temperatures are illustrated in Figure 44. The results can be described as follows:

1800°C, 1 hour: Oxide unaffected.

1900°C, 1 hour: Formation of a thin layer of metallic material between oxide and graphite. Slight discoloration of the outer oxide regions.

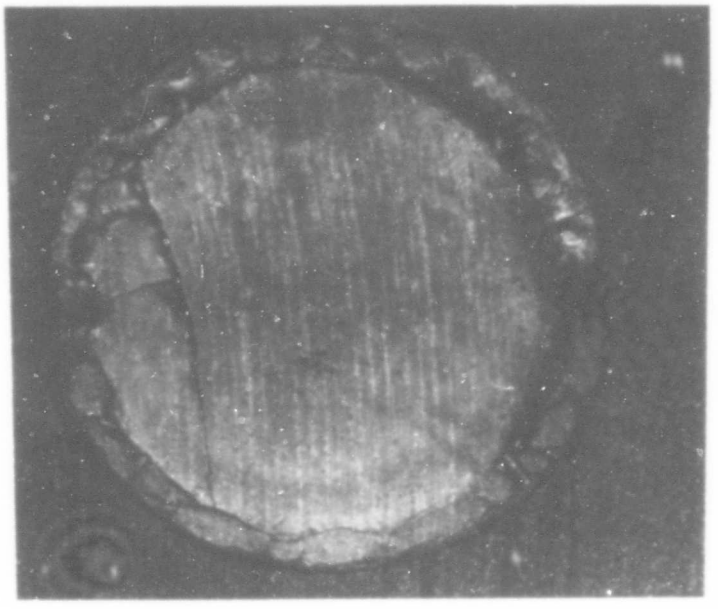

2100°C for 1 Hour

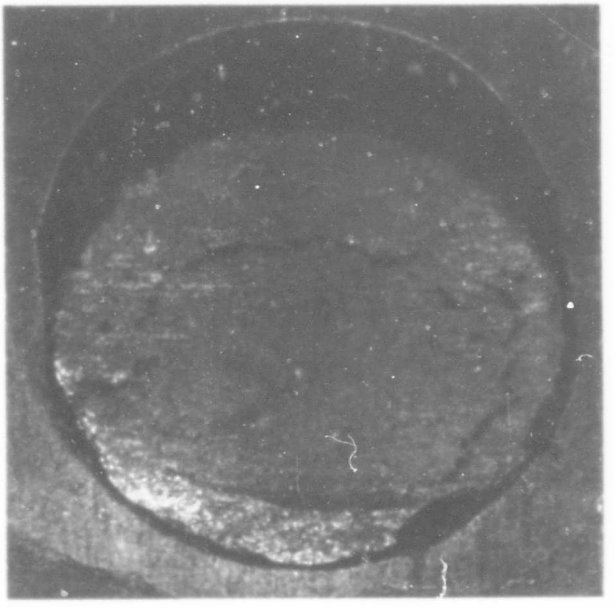

2300°C for 2 Hours

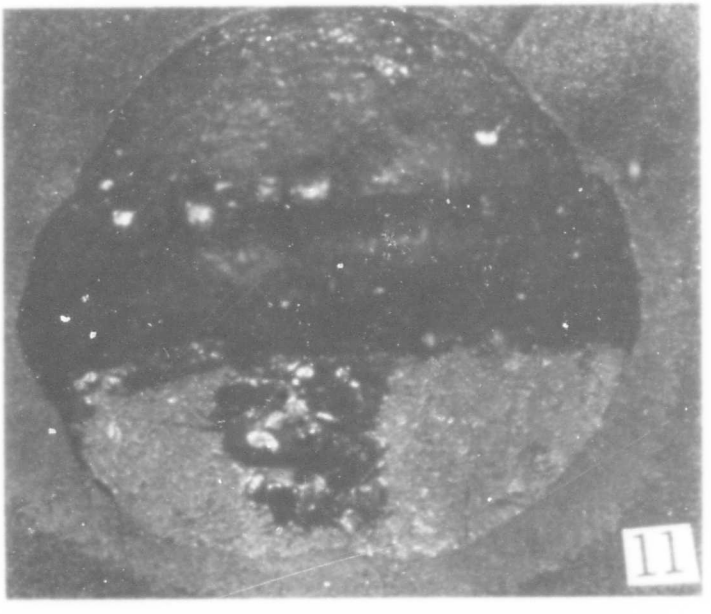

2500°C for 2 Hours

Figure 43. Graphite-Thoria Systems after Exposure to High Temperature

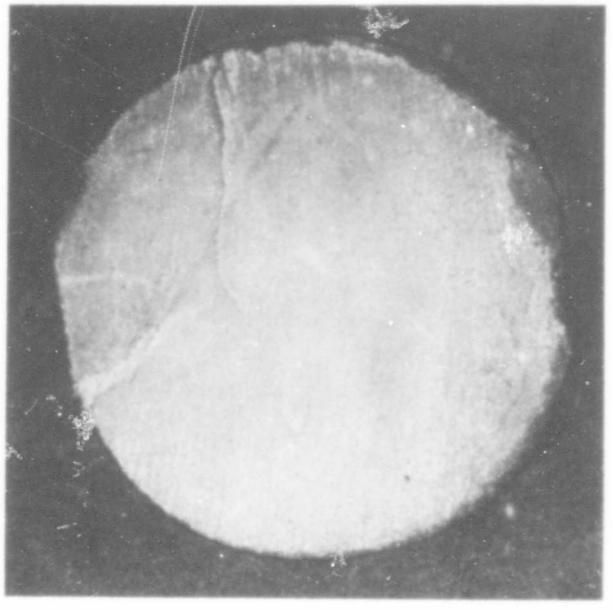

1800°C for 1 Hour

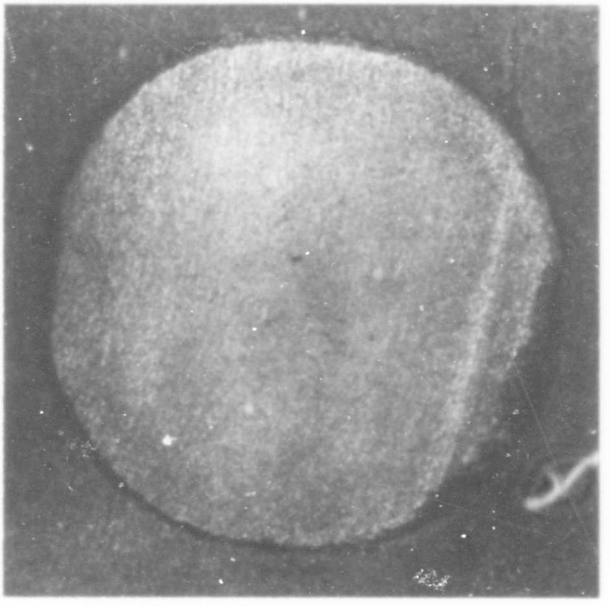

1900°C for 1 Hour

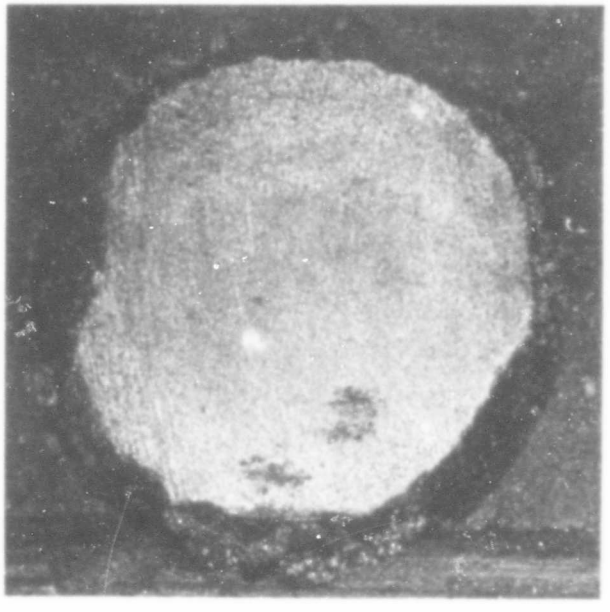

2000°C for 1 Hour

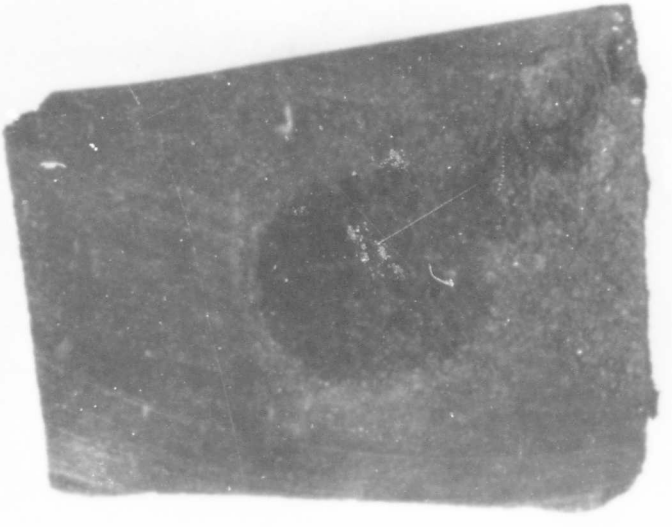

2100°C for 1 Hour

Figure 44. Graphite-Yttria Systems after Exposure to High Temperature

2000°C, 1 hour: Extensive reduction of the oxide.

2100°C, 1 hour: Oxide completely converted to the carbide. Wide-spread impregnation of the graphite occured. It is assumed that the yttrium-carbon system has a eutectic below 2100°C. The melting point of YC_2 lies above 2300°C.

3.2.1.9. The Graphite-Zirconia System

Cross sections of graphite-zirconia systems after various exposures to high temperatures are illustrated in Figure 45. The results can be described as follows:

1730°C, 1 hour: No indications of carbide formation, but oxide has assumed a dark gray color indicative of pronounced carbon diffusion. This effect was found at temperatures as low as 900°C.

2300°C, 1 hour: The gap between oxide and graphite is larger than what can be accounted for by differences in thermal contraction during cooling. The oxide developed a pronounced crust which was identified as ZrC.

2540°C, 1 hour: The oxide was liquefied, and one-half of it has been consumed by reduction.

A thin carbide diffusion barrier is separating the oxide melt from the graphite matrix.

The appearance of a liquid at 2540°C is attributed to stabilizing agents. Pure zirconia is reported to melt at 2687°C.

The experiment at 2300°C was considered unsatisfactory and a supplemental investigation was planned. ZrO_2 was placed in a graphite mold and pressed with graphite plungers to a pressure of 1000 lbs./in.^{2} to eliminate the shrinkage problem. The mold was heated to 2400°C and held for one hour. Figure 46 shows the upper surface of the oxide where it contacted the graphite plunger. A coherent carbide layer which halted further reaction was formed. The carbide formed on the oxide side of the interface. The bond between the carbide and the oxide was excellent. No bonding occurred between the carbide and the graphite. These observations indicate that the zirconium did not diffuse into the graphite.

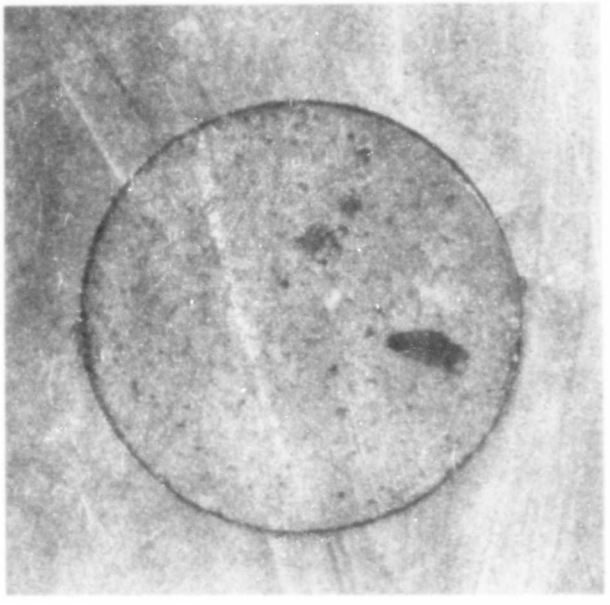

1730°C for 1 Hour

2300°C for 1 Hour

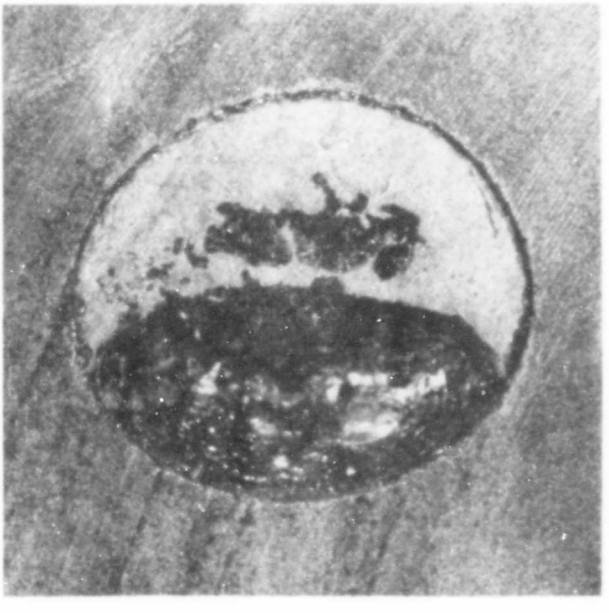

2540°C for 1 Hour

Figure 45. Graphite-Zirconia Systems after Exposure to High Temperature

Figure 46. ZrC Coating on ZrO_2, Produced by ZrO_2 in Contact with Massive Graphite at 2400°C for a Period of 1 Hour, Magnification: 7.75X

3.2.1.10. The Graphite-Zirconium Silicate System

Cross sections of graphite-zirconium silicate systems after various exposures to high temperatures are illustrated in Figure 47. The results can be described as follows:

1510°C, 1 hour: No signs of reaction.

1670°C, 1 hour: Slight crust formation on the oxide side of the reaction interface.

1800°C, 1 hour: Pronounced crust formation on the oxide side of the reaction interface. Distinct deterioration of the oxide core. It appears that the density of the core decreased in favor of increased crust density.

2000°C, 1 hour: Extensive void formation has decreased the density of the core. Pronounced densification of graphite matrix regions directly bordering the reaction interface.

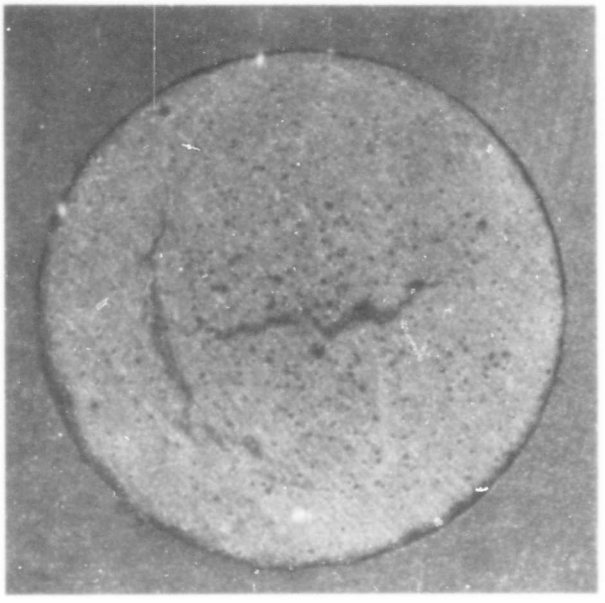

1510°C for 1 Hour

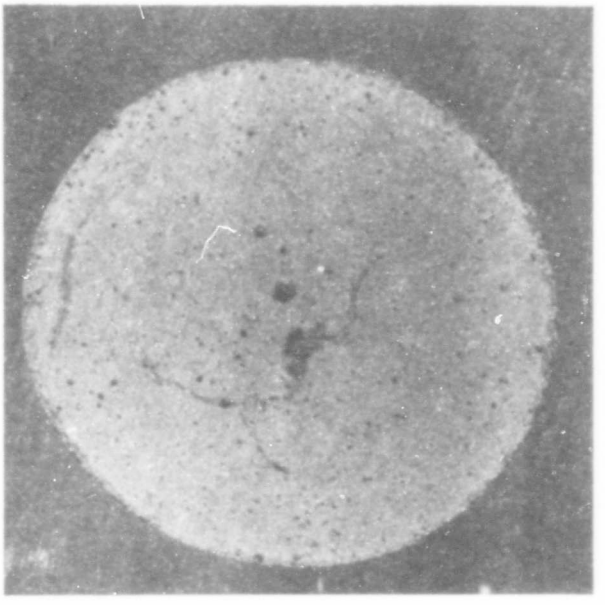

1670°C for 1 Hour

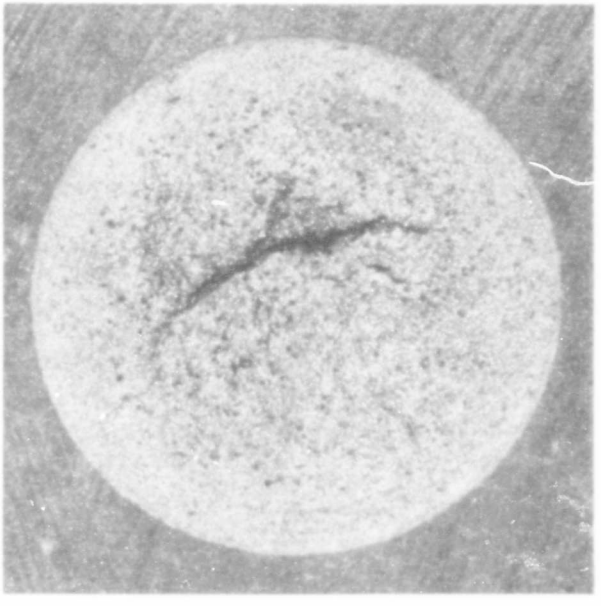

1800°C for 1 Hour

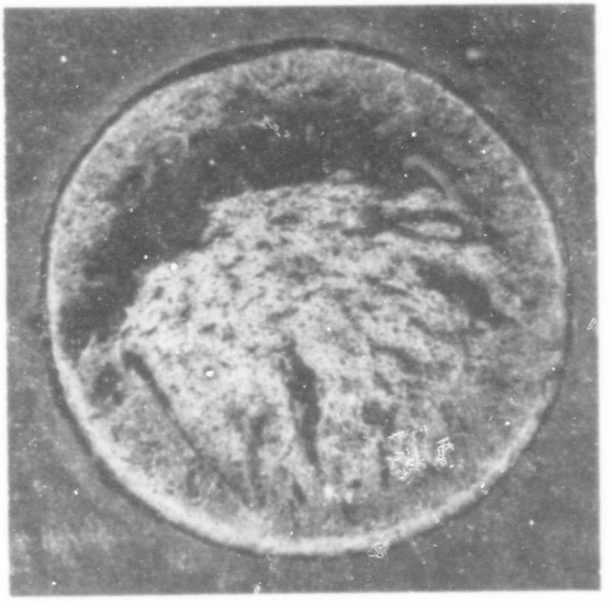

2000°C for 1 Hour

Figure 47. Graphite-Zirconium Silicate Systems after Exposure to High Temperature

The reaction sequence in this system is interpreted as follows:

At 1675°C, incongruent melting occurs in the oxide. A liquid phase appears which represents a binary solution consisting of SiO_2 with a small amount of ZrO_2. At the graphite-oxide interface, Si from the liquid phase diffuses into the graphite matrix to form SiC while solid ZrO_2 precipitates to build up an oxide crust..

From the experiment conducted at 2000°C, X-ray analysis showed the oxide shell to be ZrO_2. Significant amounts of SiC were present in the bordering graphite matrix.

3.2.1.11. Synopsis of Results

Based on the results obtained from these experiments, the practical stability of the systems investigated; i.e., the stability of massive graphite-oxide composites, as opposed to finely divided powders, can be arranged in the following order:

Refractory Oxide	Practical Limit of Stability, °C
$ZrSiO_4$	1675
CeO_2	1800
Y_2O_3	1900
Al_2O_3	1950
BeO	2100
$SrZrO_3$	2100
ThO_2	2100
HfO_2	2300
ZrO_2	2400

Apart from this classification, the results suggest the following:

1) At low temperatures, significant amounts of carbon can diffuse through oxides without reacting to form a carbide.

2) In case of ZrO_2, the formation of a carbide at the interface at high temperatures can diminish carbon diffusion. The same applies to HfO_2.

3) The occurrence of a liquid phase, be it oxide, carbide or a eutectic, terminates lasting stability, since a liquid is a more favorable transport medium than a solid. This means that practical stability may depend more strongly on melting points and minimum liquidus characteristics than on chemical reactivity.

4) At 2100°C, a strong bond forms between graphite and thoria.

5) The thorium-carbon system has a eutectic below 2300°C. The liquid phase wets graphite readily.

6) Silicon in zirconium silicate penetrates graphite without forming a liquid carbide.

3.2.2. Oxide Pellets on Graphite Pedestals

In order to study unpressurized gas-oxide-carbon systems, preformed pellets of the oxide were heated by radiation while resting on a graphite pedestal in an argon atmosphere.

Studies included contact angle, diffusion of carbon and metal oxide and adhesion of the oxide on the graphite.

3.2.2.1. Description of Apparatus and Experimental Procedure

The apparatus is shown in Figure 48. A pendent graphite pedestal is supported on a boron-nitride funnel. The pedestal is heated with an induction coil and flushed with fast-flowing argon. For effective cooling, the funnel and induction coil are submerged in water. The boron-nitride funnel has a silicone coating to prevent decrepitation by the water. A two-color pyrometer sighted through the quartz window measures the temperature of the pellet.

The oxide pellet is placed on the graphite pedestal and heated to the desired temperature for 15 minutes. Evaluation of the results is carried out after cooling.

3.2.2.2. Results

Among the liquid phases of primary interest for graphite-refractory composites is molten SiO_2. Due to its good performance in protection of a composite, there have been speculations that it might wet graphite. This, however, is not the case as shown in Figure 49.

Three other observations were made:

1) Carbon does not diffuse into molten or solid SiO_2 to any significant extent. Therefore, there is no carbide formation within the oxide.

2) The interface between molten SiO_2 and graphite recedes into the graphite, with carbide formation on the graphite side of the interface. In the case of solid SiO_2, no such process was detected.

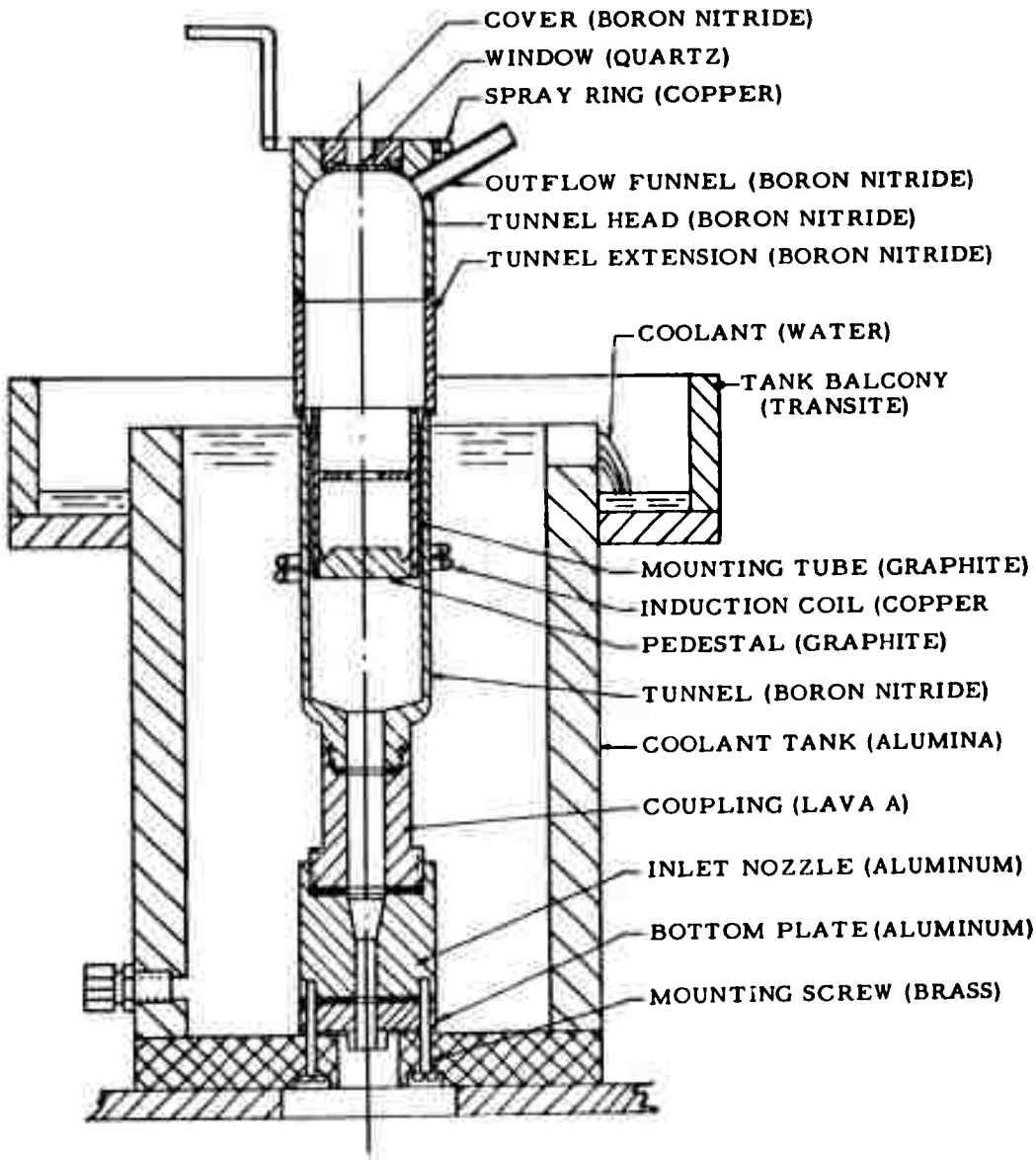

Figure 48. Apparatus for Heating Oxide Pellets on a Graphite Pedestal L-900

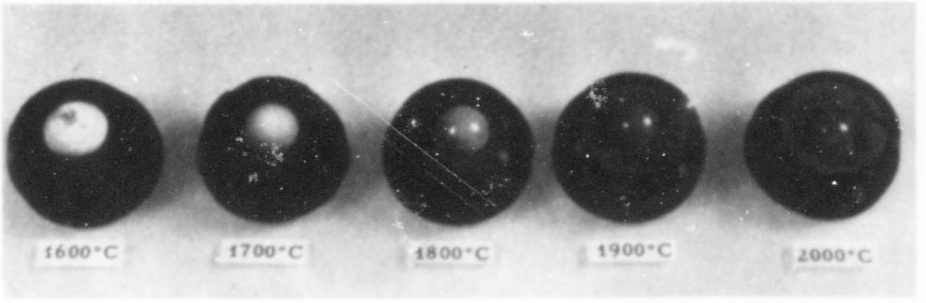

Figure 49. SiO_2 Pellets After Being Heated on Graphite to Various Temperatures

3) After the experiment conducted at 2000°C, the pedestal surface beneath the oxide specimen was found to have droplets of silicon on a layer of SiC. Presumably, they were formed by the reaction

$$SiC + SiO_2 \rightarrow Si + SiO + CO.$$

Other oxides behave quite differently. Figures 50 and 51 illustrate what happens with Y_2O_3 and Dy_2O_3. Carbon diffuses readily into the oxide at temperatures as low as 1800°C. Carbide formation takes place within the oxide and not within the graphite. Complete wetting of the graphite occurs when Dy_2O_3, and Y_2O_3 are heated to 1900 and 2000°C. As neither the oxides nor the carbides melt at this temperature, a carbide-carbon eutectic must be formed. The same behavior was found with Sc_2O_3.

Figure 50. Y_2O_3 Pellets After Being Heated on Graphite to Various Temperatures

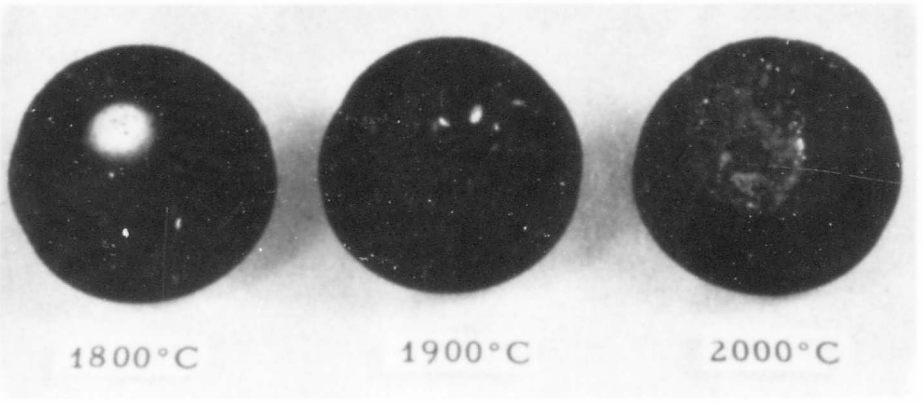

Figure 51. Dy_2O_3 Pellets After Being Heated on Graphite to Various Temperatures

Studies of this type indicate that stability of an oxide on graphite at high temperatures depends on diffusion phenomena.

3.3. Conclusions

The protection of the graphite-refractory composite in high-temperature air is based on the formation of a stable oxide coating on the exposed surface of the composite. This stability of the coating may be expressed in terms of three fundamental requirements.

1) High-temperature refractory and barrier properties of the carbide reaction product (3.2) - ZrO_2 and HfO_2.

2) Resistance to carbon diffusion (3.2) - indicated by reaction on the graphite side of the graphite-oxide interface - SiO_2.

3) Least reactive in terms of reaction with the graphite base - as shown in the gas development studies (3.1) - BeO, Lu_2O_3 and Y_2O_3.

Design of the graphite-refractory composite involves the selection of the ingredients to fulfill specific roles in the coating. There are essentially two roles. One is that of the predominant oxide which is to provide the bulk of the coating, and the other is that of an auxiliary agent to counter any deficiencies of the bulk oxide.

For high-temperature applications, the bulk of the coating will almost certainly be ZrO_2 or HfO_2. The deficiencies of these oxides lie in poor adherance of their carbides to graphite. As an auxiliary agent to counteract this, SiO_2 is the best material studied so far. It reacts with the graphite to establish a bond with the parent material, and it reacts with ZrO_2 and HfO_2 to form silicates. The fact that SiO_2 does not

wet graphite may be of little significance as long as it wets the bulk oxide.

Another approach would be to employ ThO_2 as the bulk coating material. While this oxide was shown to lack the temperature potential of ZrO_2 and HfO_2, it was found to exhibit bonding to graphite. Although thorium oxides tend to hydrate, alloying with graphite and other refractory materials seems to eliminate this problem. Stable composites of this type have been prepared. [3]

A third approach to high-temperature composites containing graphite could be based on reactivity alone. Instead of incorporating materials which convert to suitable oxides upon high-temperature exposure in air, the oxides themselves could be added. Such a procedure would permit the formation of firm graphite-carbide-oxide bonds under controlled processing conditions. Complete conversion of the oxide to carbide during the processing would be the limitation on processing. Likewise, only oxides of low reactivity with carbon would be useful. Other than BeO, Y_2O_3, Sc_2O_3, and some of the rare-earth oxides that form easily hydrated carbides, the next best possibilities for oxide additions to graphite are ThO_2 and ZrO_2.

4. COMPOSITIONAL STUDIES ON GRAPHITE-BASE REFRACTORY COMPOSITES

The development of graphite-base refractory composites by an empirical approach of selective modification has been continued. JTA has been used as a reference base in evaluating these new composites. Studies have been performed to establish the contribution of individual additives as well as replacement constituents to the oxidation resistance of the composite. Table 1 introduces the experimental grade numbers assigned to each of these materials and summarizes, by composition, the various composites investigated.

4.1. Fabrication

The fabrication techniques for processing new composites were the same as those employed for JTA.[3] The raw materials are hot pressed in an inductively heated graphite mold.

4.2. Preliminary Screening for Oxidation Resistance

Preliminary screening tests for oxidation resistance of new composites were performed on easily prepared rectangular-bar samples, $\frac{1}{4}$ by $\frac{1}{4}$ by 2 inches (± 0.001 inch) in size. The tests were carried out in a simple apparatus in which heating is accomplished by passing a current directly through the sample held by water-cooled copper terminals. The resulting hot zone between the terminals is approximately 1 inch long. Its temperature is monitored by a two-color pyrometer. The sample is exposed to the air throughout the test.

In the early development work conducted under this contract, a screening temperature of 1700°C was selected. Samples from each of the new compositions were tested at 1700°C for intervals of 5, 10, 20, and 30 minutes with a new specimen being used for each interval. A warming period of 60 seconds was not counted as part of the oxidation time. To provide a comparison, samples of JTA were tested in the same fashion along with the new compositions.

When composites are tested that have little low-temperature oxidation protection, weight losses determined by the resistance method were found to be meaningless. The cold ends of the sample oxidized much faster than the hot zone, eliminating any reasonable relation between total weight loss and hot zone temperature. Therefore, examinations of the overall coating appearance and hot zone cross sections have become very significant for the evaluation of coating performance. Similar samples were exposed for 10 minutes at 1700, 1800, 1900, and 2000°C. As in the earlier tests, a new specimen was used at each temperature level. Oxidation rate determinations have been left to more sophisticated testing which will be described later.

Table 1. Summary of Compositions Investigated

Experimental Grade Number	Approximate Elementary Analysis in Per Cent by Weight											
	C	Zr	B	Si	Nb	Ce	La	Hf	Y	Sr	Dy	O*
JTA	48	35	8	9	0	0	0	0	0	0	0	0
JT-0950	48	35	8	9	0	0	0	0	0	0	0	0
JT-0951	48	37	6	9	0	0	0	0	0	0	0	0
JT-0952	48	39	4	9	0	0	0	0	0	0	0	0
JT-0953	48	41	2	9	0	0	0	0	0	0	0	0
JT-0954	48	43	0	9	0	0	0	0	0	0	0	0
JT-0961	48	35	8	7	2	0	0	0	0	0	0	0
JT-0962	48	35	8	4.5	4.5	0	0	0	0	0	0	0
JT-0963	48	35	8	2	7	0	0	0	0	0	0	0
JT-0964	48	35	8	0	9	0	0	0	0	0	0	0
JT-0965	48	43	0	7	2	0	0	0	0	0	0	0
JT-0966	48	43	0	4.5	4.5	0	0	0	0	0	0	0
JT-0967	48	43	0	2	7	0	0	0	0	0	0	0
JT-0968	48	43	0	0	9	0	0	0	0	0	0	0
JT-0969	48	35	8	0	0	9	0	0	0	0	0	0
JT-0974	48	35	8	7	0	2	0	0	0	0	0	0
JT-0975	48	35	8	7	0	0	2	0	0	0	0	0
JT-0976	48	35	8	0	0	9	0	0	0	0	0	0
JT-0977	48	43	0	0	0	0	9	0	0	0	0	0
JT-0979	48	35	0	9	8	0	0	0	0	0	0	0
JT-0980	48	35	2	15	0	0	0	0	0	0	0	0
JT-0981	48	35	0	17	0	0	0	0	0	0	0	0
JT-0982	48	52	0	0	0	0	0	0	0	0	0	0
JT-0983	48	47	0	5	0	0	0	0	0	0	0	0
JT-0984	48	27	0	25	0	0	0	0	0	0	0	0
JT-0985	48	17	0	35	0	0	0	0	0	0	0	0
JT-0990	48	49	0	3	0	0	0	0	0	0	0	0
JT-0991	36	0	0	13	0	0	0	51	0	0	0	0
JT-0992	33	0	0	12	0	0	0	55	0	0	0	0
JT-0993	48	0	0	17	0	0	0	35	0	0	0	0
JT-0001	48	0	0	10	0	0	0	0	33	0	0	9
JT-0002	46	0	5	5	0	0	0	0	34	0	0	9
JT-0003	38	0	5	5	0	0	0	0	41	0	0	11
JT-0004	48	0	1.5	8.5	0	0	0	0	33	0	0	9
JT-0005	48	0	0	15.5	0	0	0	0	29	0	0	7.5
JT-0007	48	0	0	11	5	0	0	0	29	0	0	7
JT-0008	48	0	0	0	0	0	0	0	41	0	0	11
JT-0009	48	0	0	26	0	0	0	0	20.5	0	0	5.5
JT-0010	48	0	0	5	0	0	0	0	37	0	0	10
JT-0011	48	0	0	21	0	0	0	0	24.5	0	0	6.5
JT-0030	48	25	0	18.5	0	0	0	0	0	0	0	8.5
JT-0040	48	13.5	0	18.5	0	0	0	0	0	13	0	7
JT-0052	48	0	0	18.5	0	0	0	0	0	0	29	4.5
JT-0060	48	0	0	34.5	0	0	0	0	0	0	0	17.5
JT-0070	48	0	0	18.5	0	0	0	0	0	28.5	0	5
JT-0080	48	0	0	18.5	0	0	0	28.5	0	0	0	5

* Added as the metal oxide, amount in composite may vary.

4.3. Results

The program of composite development involved compositional modifications of JTA. JTA is made from graphite, pitch, zirconium diboride, and silicon. Since the ZrB_2 component does not permit variation of the zirconium and boron content independently, the ZrB_2 was replaced with a mixture of boron and ZrC. The resulting composite, with the same final composition as JTA, was designated JT-0950 and served as the basis for all modifications. Performance comparisons were referred to JTA, exclusively.

A comparison of JTA with JT-0950 is shown in Figure 52. Hot zone cross sections after tests at 1700, 1800, and 1900°C for 10 minutes are compared. Within the scope of screening experiments, the two materials are equivalent. Direct comparisons between JTA and composites derived from JT-0950 should not be misleading.

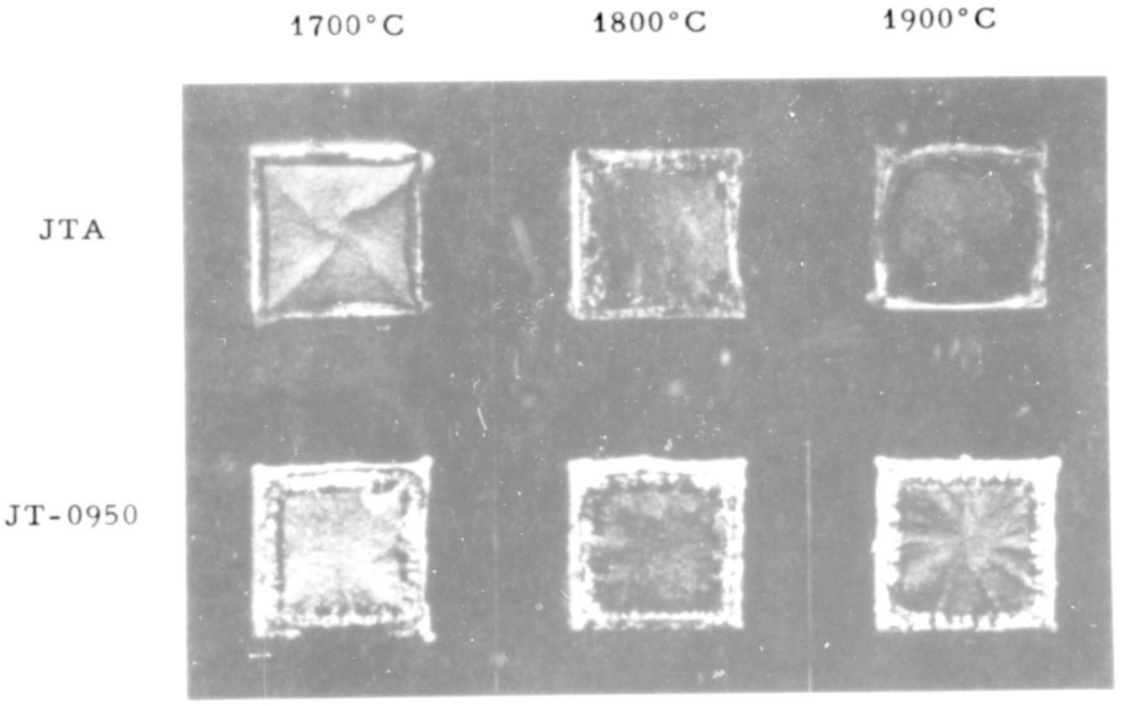

Figure 52. Cross Sections of JTA and JT-0950 Test Samples After 10-Minute Exposures, Actual Size of Each Cross Section, $\frac{1}{4}$ Inch by $\frac{1}{4}$ Inch

4.3.1. Effect of Replacing Boron in JTA

Boron plays an important role in providing low-temperature oxidation protection for graphite-refractory composites.[3] Its oxide, B_2O_3, has a very low melting point (450°C) but excellent chemical stability with respect to carbon. As illustrated in Figure 1, the reaction between liquid B_2O_3 and graphite does not reach a CO equilibrium pressure of 1 atm. until a temperature of 1595°C is reached. Of all the oxides, for which thermochemical data are available, only B_2O_3 reacts with carbon and attains a CO equilibrium pressure below 1 atm. while in the liquid state. At temperatures above 1500°C, B_2O_3 assumes a considerable vapor pressure which causes its rapid loss from any composite surface it might be protecting. To achieve lasting high-temperature protection, boron in JTA would have to be replaced by some other material capable of forming a less volatile oxide.

4.3.1.1. Replacement of Boron by Zirconium

Four composites were prepared, JT-0951, JT-0952, JT-0953, and JT-0954 which represented 25, 50, 75, and 100 per cent boron replacements by zirconium. Hot zone cross sections of the materials are illustrated in Figure 53. Substitution of zirconium for boron gives significant improvements in protection at 1700°C. More moderate but still impressive benefits are evident at the higher temperatures, particularly with the boron-free material, JT-0954.

4.3.1.2. Replacement of Boron by Silicon

Two composites were prepared in which silicon was substituted for 75 and 100 per cent of the boron. The grade designations are JT-0980 and JT-0981, respectively. Figure 54 shows the performance of these materials at 1700, 1800, 1900 and 2000°C. The reduction of parent material is very much smaller than with JTA. A porous but sound buffer layer of carbides bonds the coating to the parent material.

4.3.1.3. Replacement of Boron by Niobium

Niobium was considered the most promising boron substitute not contained already in the JTA system. It forms four oxides, Nb_2O_5, Nb_2O_3, NbO_2, and NbO, which have melting points below 1800°C, and are not reported as being volatile. The first two oxides exhibit a high reactivity with graphite. The large number of suboxides is likely to increase oxygen transport. Conceivable advantages were seen in adherence and that the Nb_2O_3 is capable of extensive alloying with ZrO_2.[4]

The boron in JTA was replaced by niobium in JT-0979. As Figure 55 shows, substitution of niobium for boron eliminated the gap below the coating, but there is no significant improvement as far as cross-section reduction of the parent material is concerned.

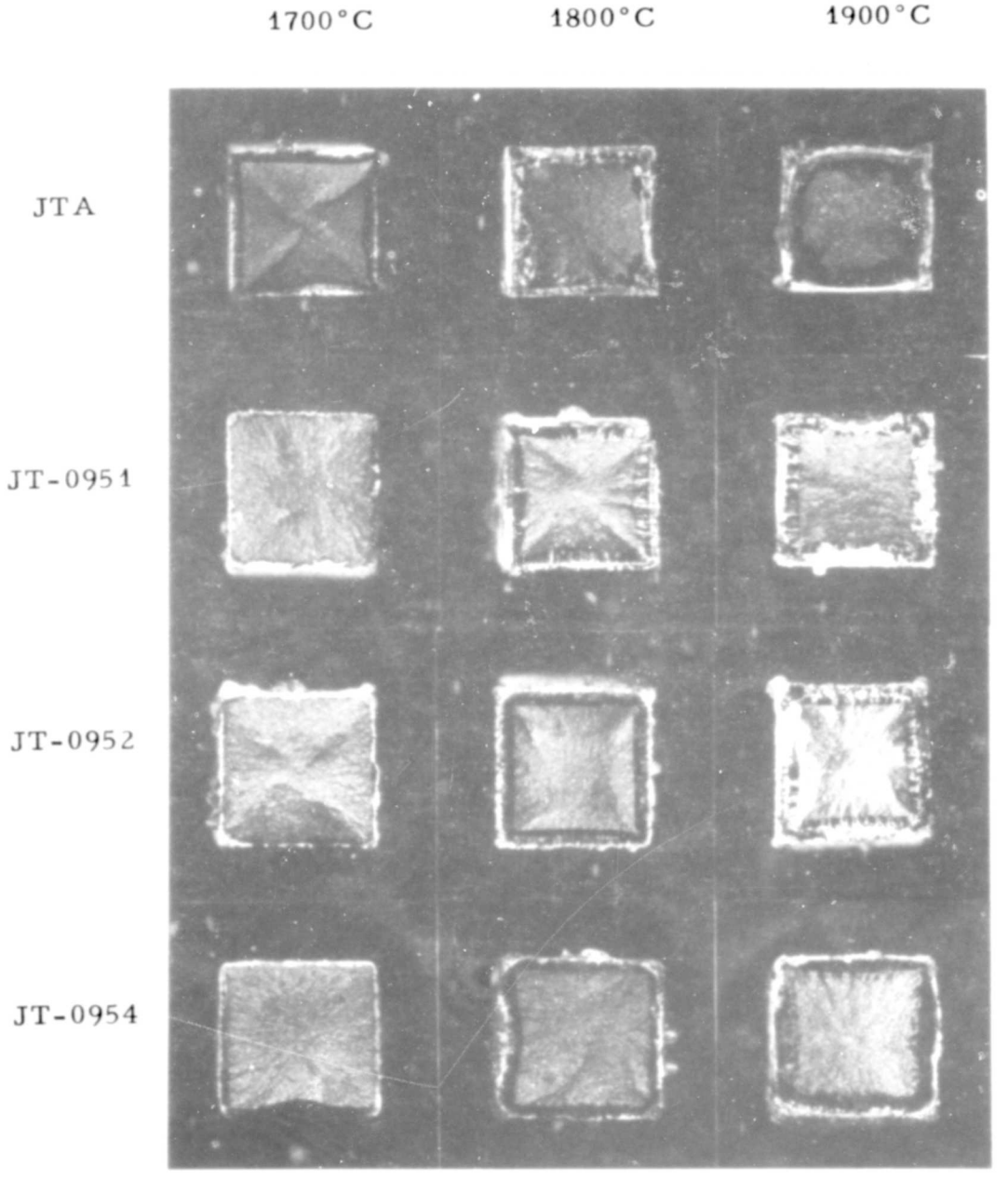

Figure 53. The Effect of Replacing Boron by Zirconium in JTA on the Cross Section of Test Samples Exposed for 10 Minutes, Actual Size of Cross Section, $\frac{1}{4}$ Inch by $\frac{1}{4}$ Inch

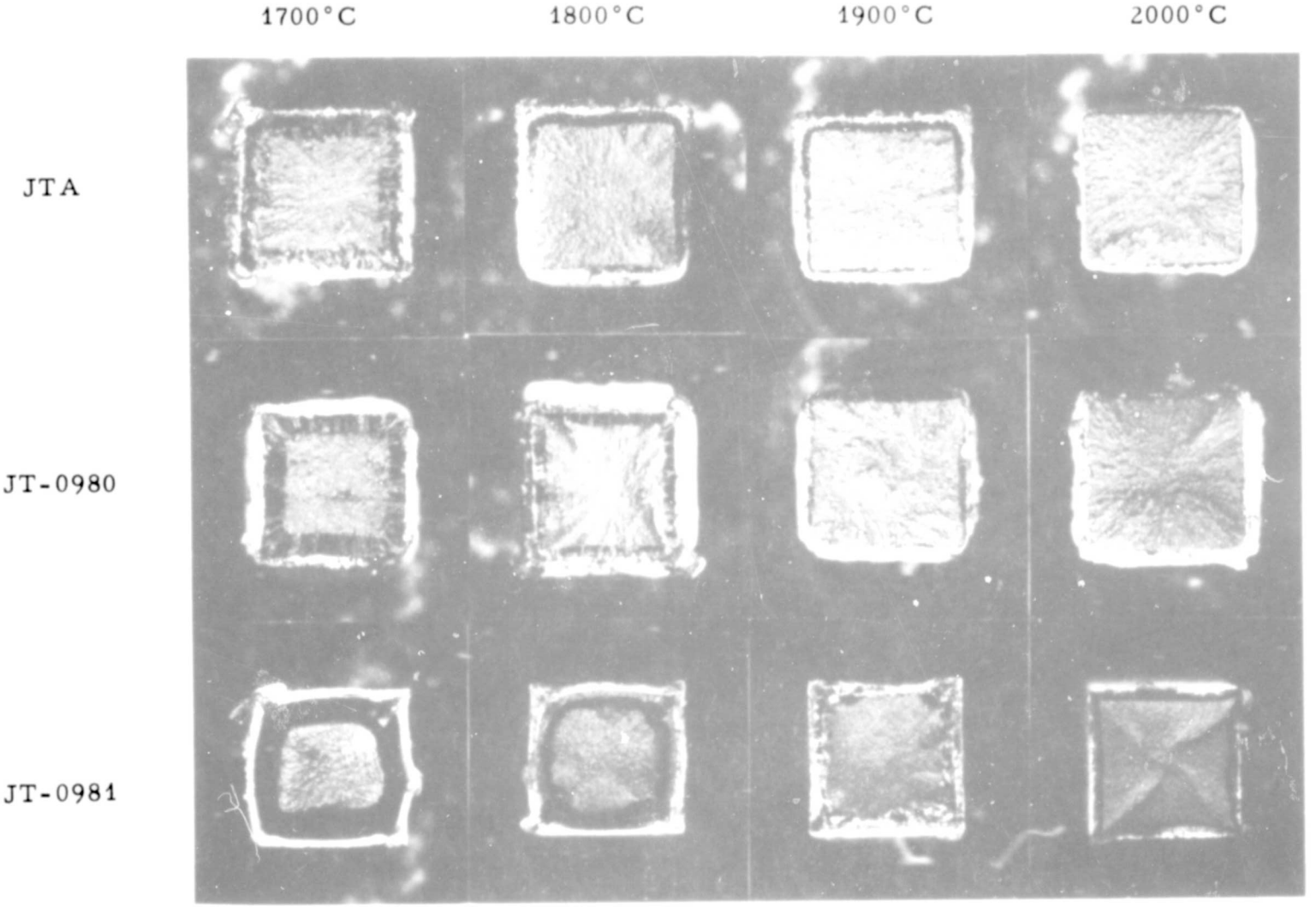

Figure 54. The Effect of Replacing Boron by Silicon in JTA on the Cross Section of Test Samples Exposed for 10 Minutes, Actual Size of Cross Section, $\frac{1}{4}$ Inch by $\frac{1}{4}$ Inch

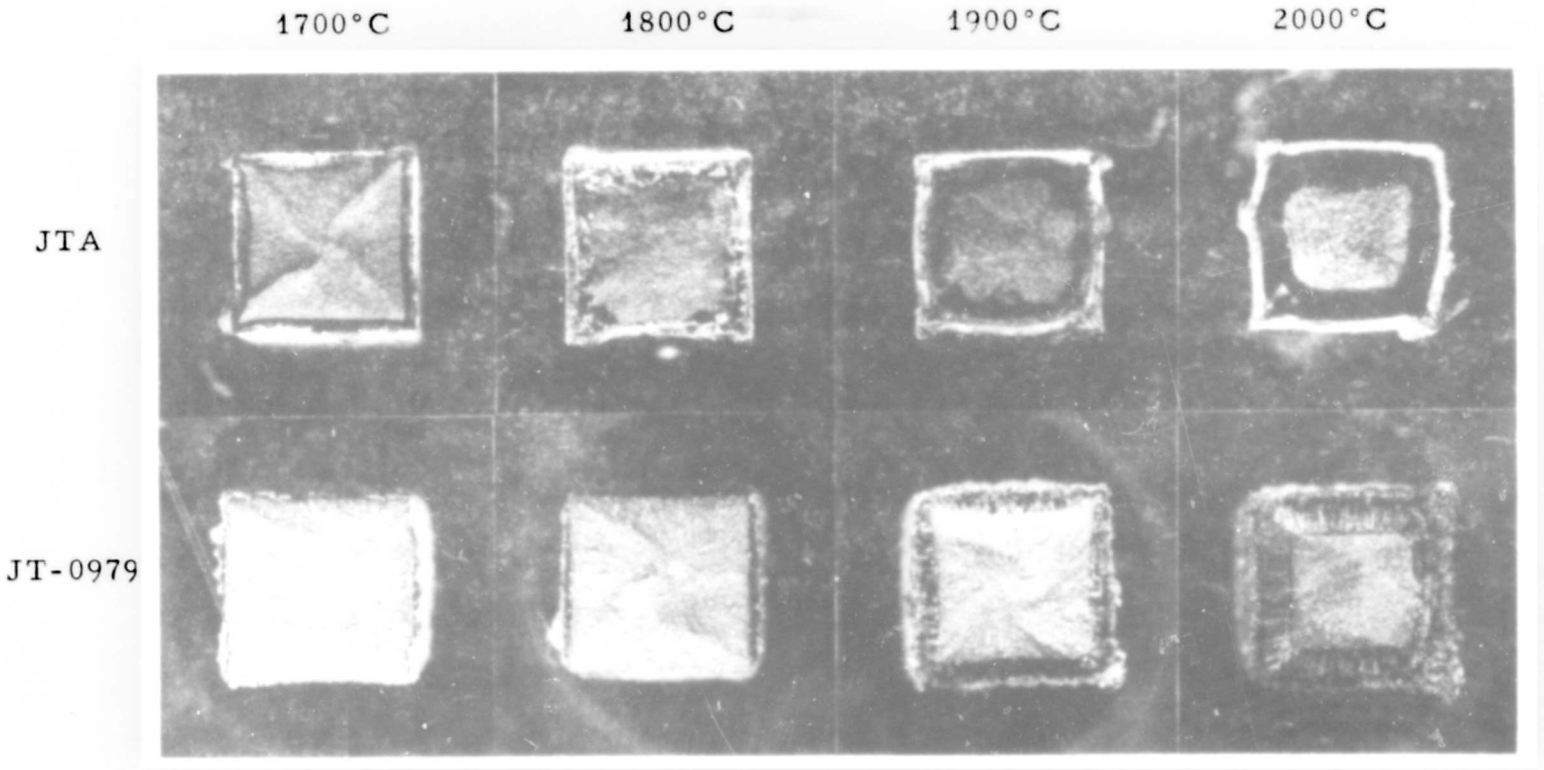

Figure 55. The Effect of Replacing Boron by Niobium in JTA on the Cross Section of Test Samples Exposed for 10 Minutes, Actual Size of Cross Section, $\frac{1}{4}$ Inch by $\frac{1}{4}$ Inch

4.3.2. Effect of Replacing Silicon in JTA

In the coatings on JTA, SiO_2 is thought of as a high-temperature bonding agent for ZrO_2, the main coating constituent. Desirable qualities of replacements for silicon are a moderately low melting point, low volatility, low chemical reactivity with respect to carbon, formation of a highly refractory carbide, and a capability to alloy with ZrO_2.

4.3.2.1. Replacement of Silicon by Niobium

Replacement of silicon in JTA by niobium resulted in JT-0961, JT-0962, JT-0963, and JT-0964. Results are shown in Figure 56.

In the hot zone cross sections, it is interesting to note the many complex stratifications which arise from niobium additions. Presumably they are a consequence of the fact that niobium is capable of forming a number of suboxides. Some composites exhibit very impressive coatings, particularly at 1900°C where the coatings have grown to remarkable thickness without developing the large gap between coating and parent material as in the case of JTA.

4.3.2.2. Replacement of Silicon by Lanthanum

Lanthanum was considered another promising substitute for silicon. Its oxide, La_2O_3, exhibits a lower reactivity with respect to graphite than SiO_2, and it forms wide ranges of solid solutions with ZrO_2.[5] Although it has a relatively high melting point (2250°C) and a relatively high eutectic with ZrO_2 (2100°C), the presence of B_2O_3 was expected to yield liquefaction well below 2000°C.

Composites were prepared in which lanthanum was substituted for 25 and 100 per cent of the JTA silicon content. The grade designations are JT-0975 and JT-0976, respectively.

After oxidation at 1700, 1800, 1900, and 2000°C, neither of the materials formed a coherent coating because of an apparent inability of the ensuing oxides to wet the parent material, Figure 57.

4.3.2.3. Replacement of Silicon by Cerium

The second rare earth selected for evaluation in JT composites was cerium. Composites were prepared in which the cerium was substituted for 25 and 100 per cent of the JTA silicon content. The grade designations are JT-0969 and JT-0974, respectively.

The overall appearance of oxidized samples of these two materials is illustrated in Figure 58. The coatings formed on JT-0969 did not wet the parent material, similar to coatings containing lanthanum.

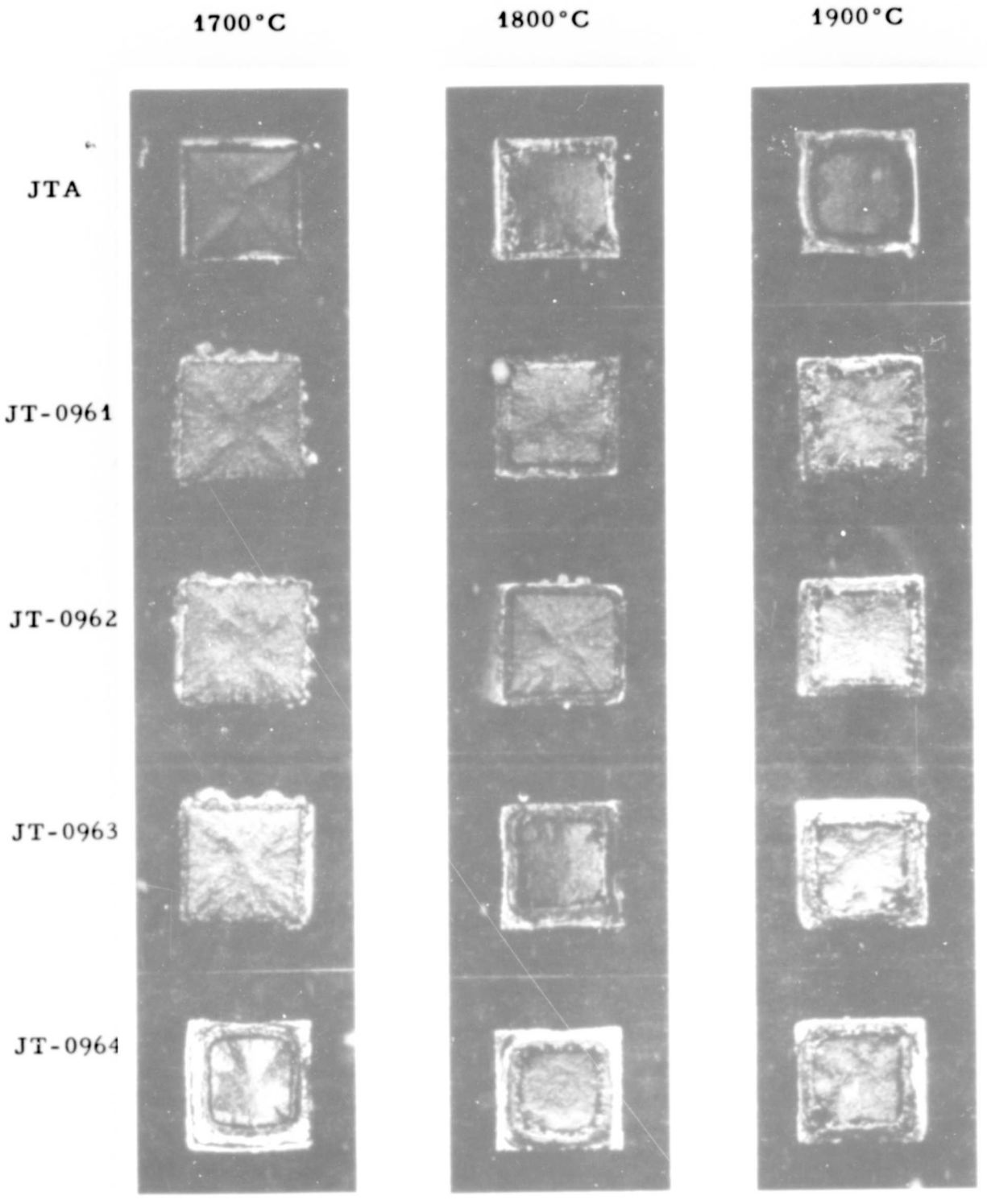

Figure 56. The Effect of Replacing Silicon by Niobium in JTA on the Cross Section of Test Samples Exposed for 10 Minutes, Actual Size of Cross Section, $\frac{1}{4}$ Inch by $\frac{1}{2}$ Inch

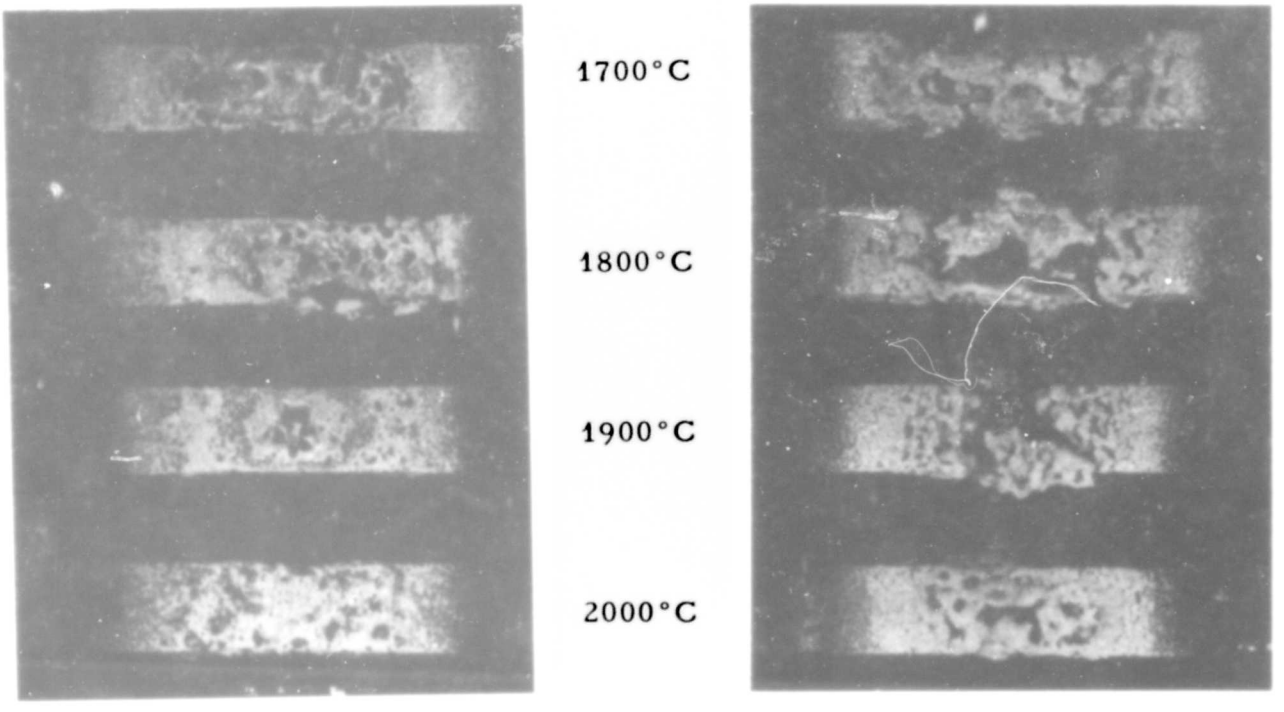

Figure 57. The Effect of Replacing Silicon by Lanthanum in JTA, Appearance of Samples after 10-Minute Exposures

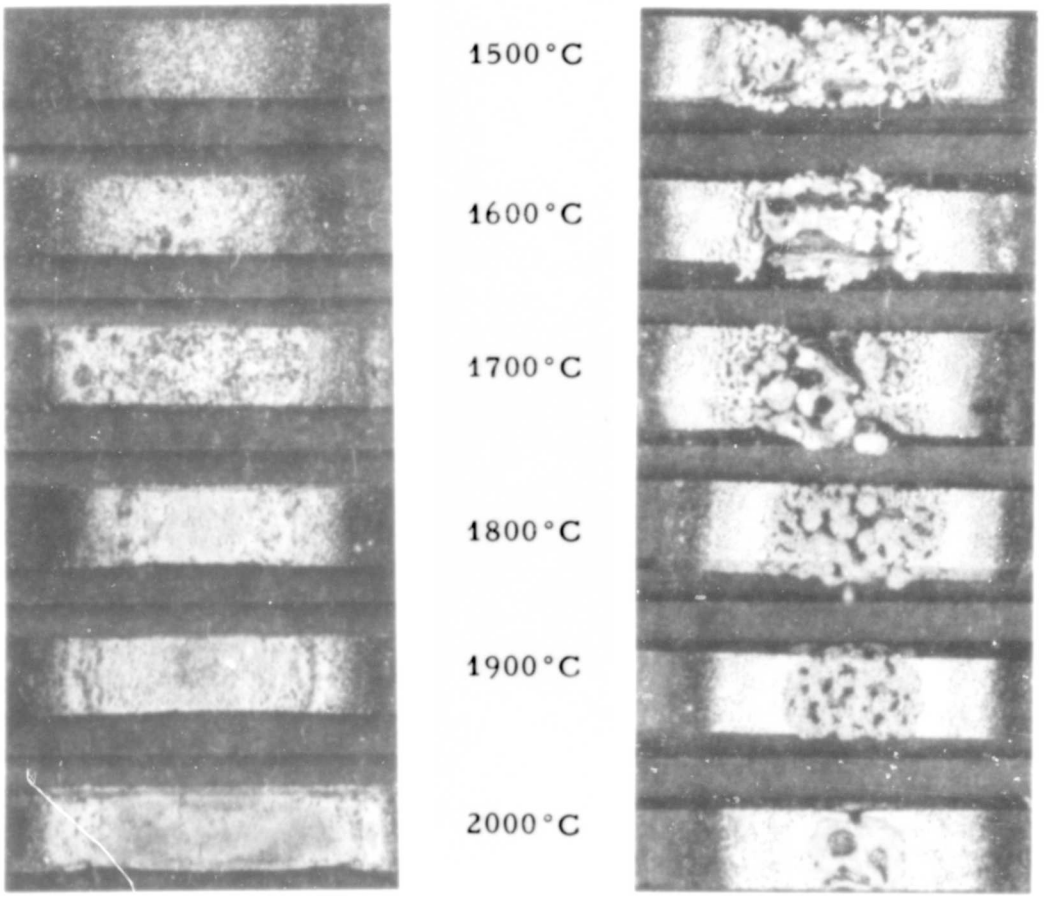

Figure 58. The Effect of Replacing Silicon by Cerium in JTA, Appearance of Samples after 10-Minute Exposures

The coatings on JT-0974 appear to be smooth and continuous; however, an examination of the cross section illustrated in Figure 59 revealed these coatings to be badly undermined at temperatures above 1700°C.

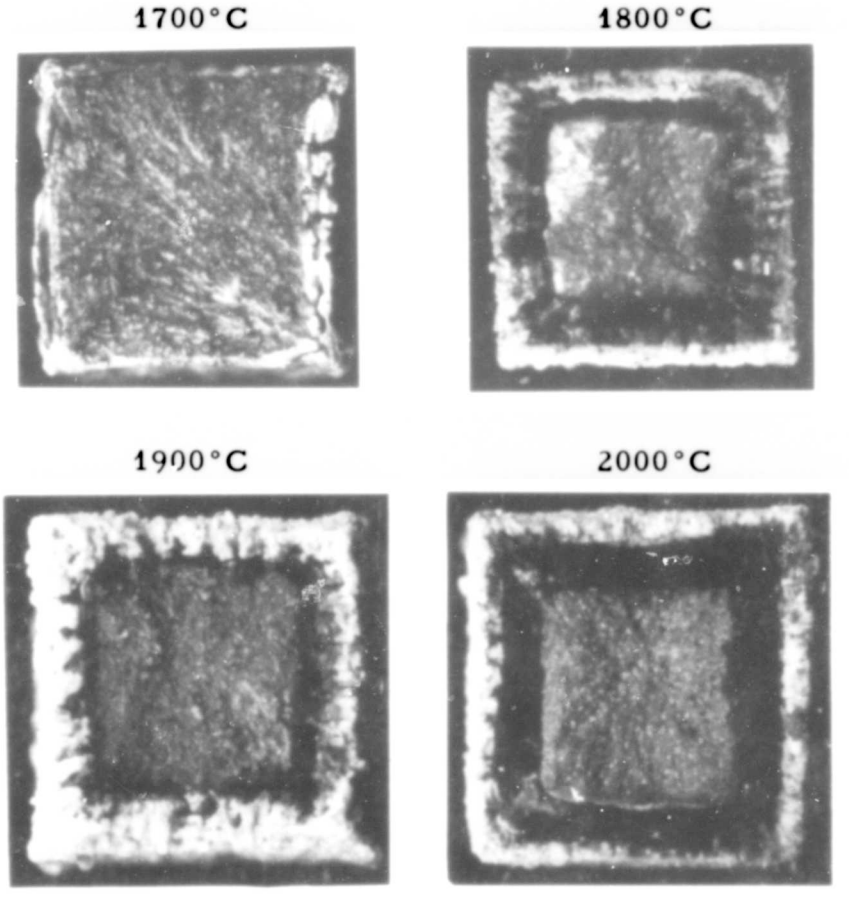

Figure 59. Cross Sections of JT-0974 After 10-Minute Exposures, Actual Size of Cross Section, $\frac{1}{4}$ Inch by $\frac{1}{4}$ Inch

4.3.3. Effect of Multiple Replacements in JTA

In an effort to optimize the zirconium-silicon ratio of JT-0981, grades JT-0982, JT-0983, JT-0984, and JT-0985 were prepared. A comparison of the hot zone cross sections of JT-0981 to these composites as well as JT-0954 are shown in Figure 60. The figure indicates that the silicon-zirconium ratio of JT-0981 is very near the optimum for this particular composite.

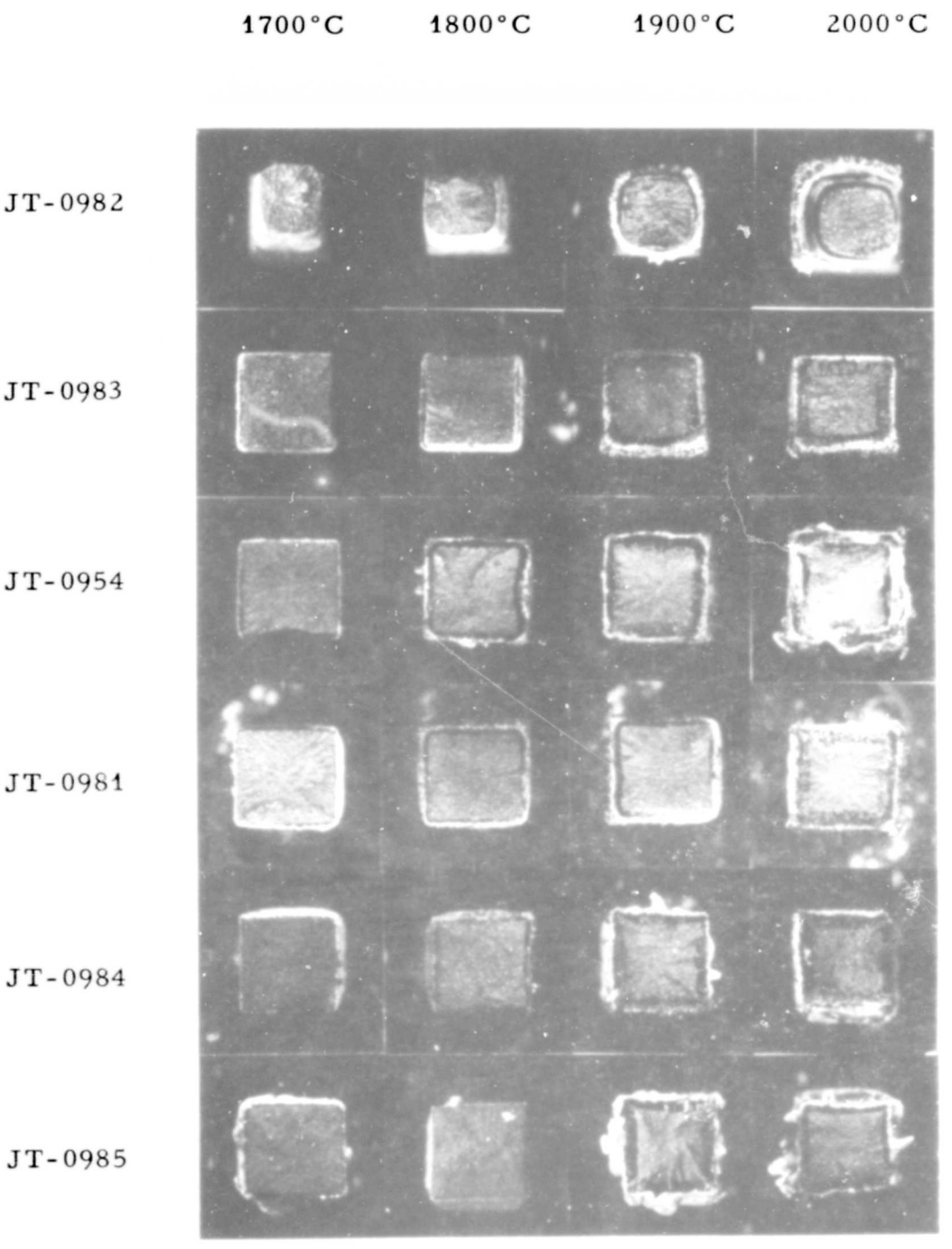

Figure 60. The Effect of Varying the Ratio of Silicon to Zirconium in C/Zr/Si Composites With a Carbon Content of 48 Per Cent on the Cross Section of Test Samples Exposed for 10 Minutes, Actual Size of Cross Section, $\frac{1}{4}$ Inch by $\frac{1}{4}$ Inch

In order to learn about the effect of niobium in the absence of boron, we prepared a composite in which niobium was substituted for 25 per cent of the silicon content of JT-0954, a boron-free grade. The resulting material was designated JT-0965. In Figure 61, the respective hot zone cross sections are compared with those of JTA. While JTA exhibits increasing parent material reduction with rising temperature, JT-0965 shows a reversal of this trend. It was the first grade to do so, and may thus be considered a promising candidate for applications at 1900°C and above. Its lack of good protection at 1700 and 1800°C is apparently due to the fact that in this particular coating system no liquid phases materialize below 1900°C.

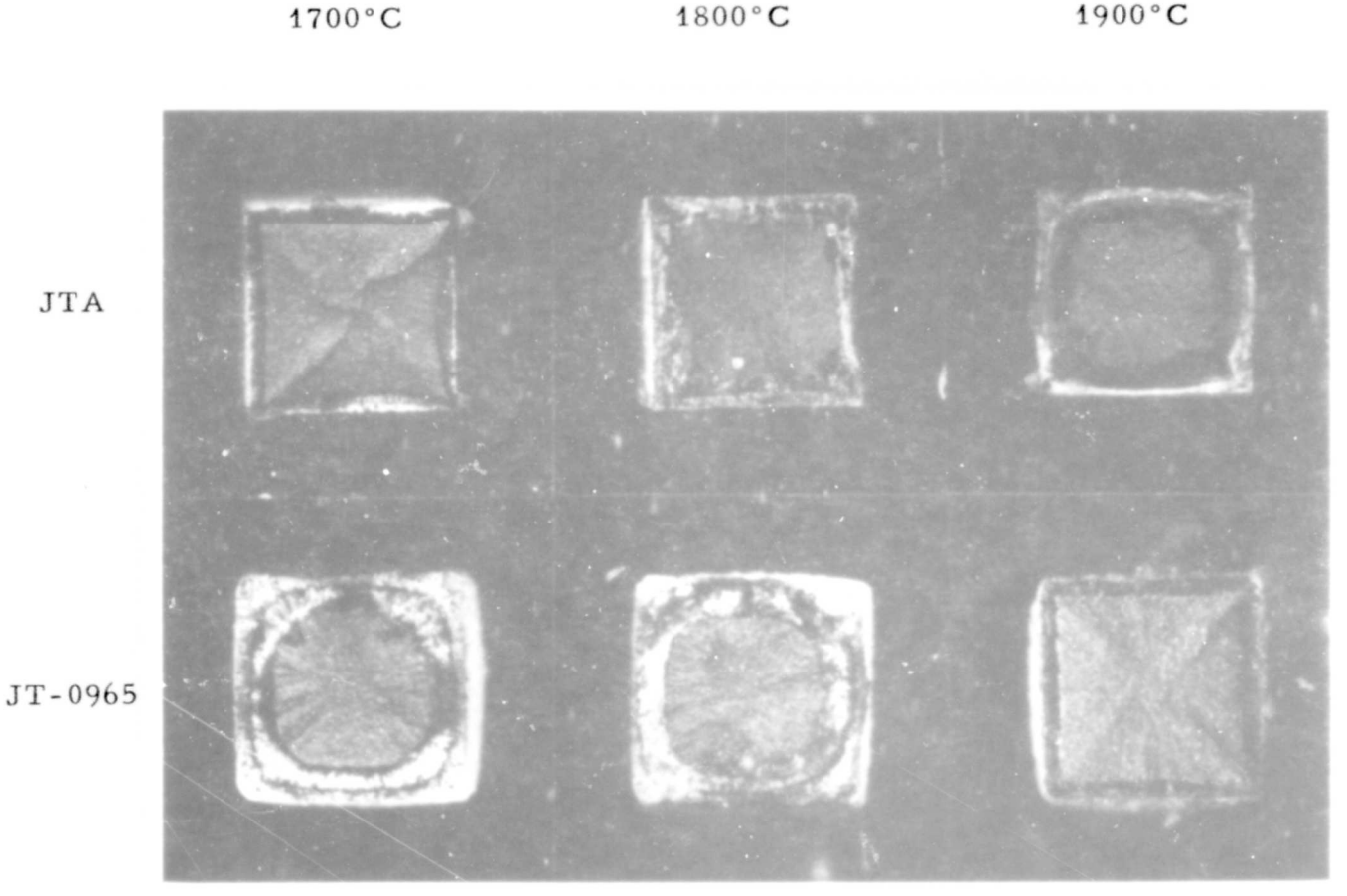

Figure 61. Cross Sections of JTA and JT-0965 After 10-Minute Exposures, Actual Size of Cross Section, $\frac{1}{4}$ Inch by $\frac{1}{4}$ Inch

An attempt was made to scan the potential of hafnium by using it as a replacement for zirconium in JT-0981. Limitations in time prevented full evaluation of the composite (JT-0993), but oxidation rates were determined. (See section 5.1.1.7.)

4.3.4. Effect of Increasing the Carbon Content of JTA

It was considered a matter of interest to investigate to what extent, if any, the oxidation behavior of JTA would suffer by an increase in its carbon content. The carbon content has a significant bearing on machinability and thermal shock. Three compositions were prepared in which the total free carbon content of JTA was increased by 5, 10, and 20 per cent by weight. Testing was carried out at 1400°C since JTA performs very well at this temperature. The results compiled in Table 2 indicate that an increase in carbon content increases only the initial weight loss, but does not prevent the attainment of steady-state conditions. At 1700°C, the behavior was similar, but the weight loss was about doubled.

Table 2. Oxidation Results for Increases in Carbon Content of Grade JTA

Experimental Grade Number	Approximate Elementary Analysis in Per Cent by Weight				Per Cent Weight Loss on Exposure to Air at 1400°C at Time Shown in Minutes			
	C	Zr	B	Si	5	10	20	30
JTA	48	35	8	9	0.8	1.0	1.0	1.5
JT-0958	50	33	8	9	1.5	2.0	2.5	3.0
JT-0959	54	31	7	8	2.5	5.5	4.5	4.5
JT-0960	58	28	6	7	2.5	3.5	5.0	5.0

4.3.5. Graphite-Oxide-Silicon Composites

Torsional effusion experiments have produced results which indicate that there are a few refractory oxides, notably beryllium monoxide, erbium sesquioxide, dysprosium sesquioxide, thorium dioxide, and yttrium sesquioxide, which require very high temperatures to effect their reduction by carbon. These observations were interpreted to mean that it should be feasible to prepare refractory graphite-oxide composites with such materials.

In order to test this concept, we decided to try yttrium oxide in combination with graphite and silicon. The silicon was expected to be useful in the formation of a bonded coating.

Perhaps the most direct approach to producing an effective graphite-oxide composite; i.e., one which is capable of forming an impervious

oxide coating, is to optimize the silicon level. A number of pieces were fabricated in order to determine the effect of silicon content on the oxidation resistance of the composite. The results are shown in Table 3. In $C/Y_2O_3/Si$ systems with a carbon content of 48 per cent (equal to that of JTA), an optimum silicon level is observed at approximately 20 per cent.

Table 3. Oxidation Characteristics of $C/Y_2O_3/Si$ Composites, Performance as a Function of the Silicon Content at a Constant Carbon Level of 48 Per Cent

Experimental Grade Number	Silicon Content Per Cent by Weight	Weight Loss After 10 Minutes of Exposure*, Per Cent by Weight			
		1500°C	1600°C	1700°C	1800°C
JT-0008	0	12.35	12.60	16.09	16.02
JT-0010	5	12.94	15.79	13.94	17.38
JT-0001	10	9.32	9.31	9.37	11.35
JT-0005	15.5	3.04	7.80	6.92	8.14
JT-0011	21	-	6.80	5.61	7.86
JT-0009	26	5.81	4.65	6.16	10.32

* Test Conditions:

Sample Size: $\frac{1}{4}$ x $\frac{1}{4}$ x 2 Inches
Axes of all Samples Perpendicular to the Grain
Resistance Heating
Free Length of Sample Between Terminals: $1\frac{1}{2}$ Inches
Heating Time 60 Seconds (Not Counted as Oxidation Time)
Surface Temperature in Hot Zone Kept Constant
Natural Convection of Non-Dry Air
Weight Loss Referred to Total Sample

Hot zone cross sections for JT-0001 and JT-0005 are shown in Figure 62. Up to 1700°C, the coatings formed on these composites are of impressive integrity and their effect as barriers against oxygen attack is highly satisfactory. At 1800°C, however, oxidation proceeded rapidly.

Since the presence of boron or niobium had enhanced the oxidation resistance of conventional JT-composites, these same materials might also improve the performance of the graphite-yttria composites. JT-0002, JT-0003, and JT-0004 were fabricated to include varying amounts of boron, while JT-0007 contained niobium. Oxidation tests demonstrated that these composites performed poorly.

The addition of boron or niobium fluxes the components of the coating system as intended. Pronounced bubbling caused the molten material to be spalled from the surface of the sample. The net result is a drastic weight loss.

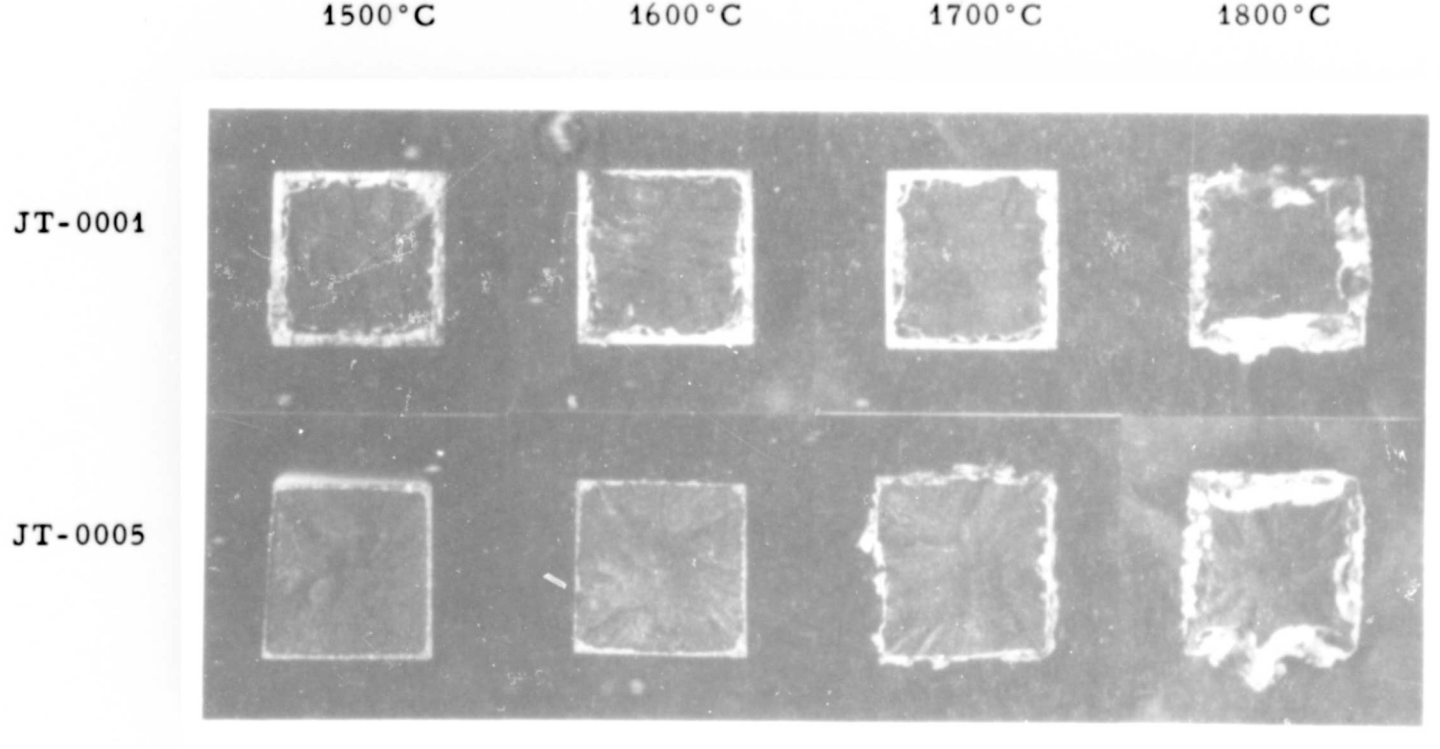

Figure 62. Hot Zone Cross Sections of JT-0001 and JT-0005 After 10-Minute Exposures

Further work was aimed at briefly scanning the potential of oxides other than Y_2O_3. All composites for this study consisted of 48 per cent carbon, 18.5 per cent silicon, and 33.5 per cent of the oxide to be evaluated. The tests on these materials is summarized in Table 4. At low temperatures, strontium zirconate appears to be an effective additive. The best performance at high temperatures is obtained with ZrO_2 and HfO_2.

Table 4. Oxidation Characteristics of Various Graphite-Oxide-Silicon Composites, Carbon Content - 48 Per Cent, Silicon Content - 18.5 Per Cent

Experimental Grade Number	Refractory Oxide (33.5 % by Wt.)	Weight Loss After 10 Minutes of Exposure*, Per Cent by Weight				
		1400°C	1500°C	1600°C	1700°C	1800°C
JT-0030	SrO_2	8.36	6.60	5.44	5.08	5.31
JT-0040	$SrZrO_3$	4.39	4.03	4.61	5.70	11.98
JT-0052	Dy_2O_3	8.08	6.18	5.63	6.31	9.50
JT-0060	SiO_2	Power source would not heat samples				
JT-0070	SrO	Samples Crumbled after exposure to air				
JT-0080	HfO_2	6.66	6.75	5.98	5.44	6.15

* Test Conditions:

Sample Size: $\frac{1}{4} \times \frac{1}{4} \times 2$ Inches
Axes of all Samples Perpendicular to the Grain
Resistance Heating
Free Length of Sample Between Terminals: $1\frac{1}{2}$ Inches
Heating Time 60 Seconds (Not Counted as Oxidation Time)
Surface Temperature in Hot Zone Kept Constant
Natural Convection of Non-Dry Air
Weight Loss Referred to Total Sample

Hot zone cross sections for JT-0030, JT-0040, and JT-0080 are shown in Figure 63. Composites containing ZrO_2 and HfO_2 improve in performance with rising temperature.

The findings on graphite-oxide-silicon composites indicate that in the high-temperature range the oxidation characteristics of JT-0030 and JT-0080 are superior to those of JTA. Under the standard test conditions JTA lost 7.0 per cent by weight in a 10-minute exposure while JT-0030 and JT-0080 lost 5.3 and 6.1 per cent, respectively. For this reason, we feel that further work on graphite-oxide composites is certainly warranted.

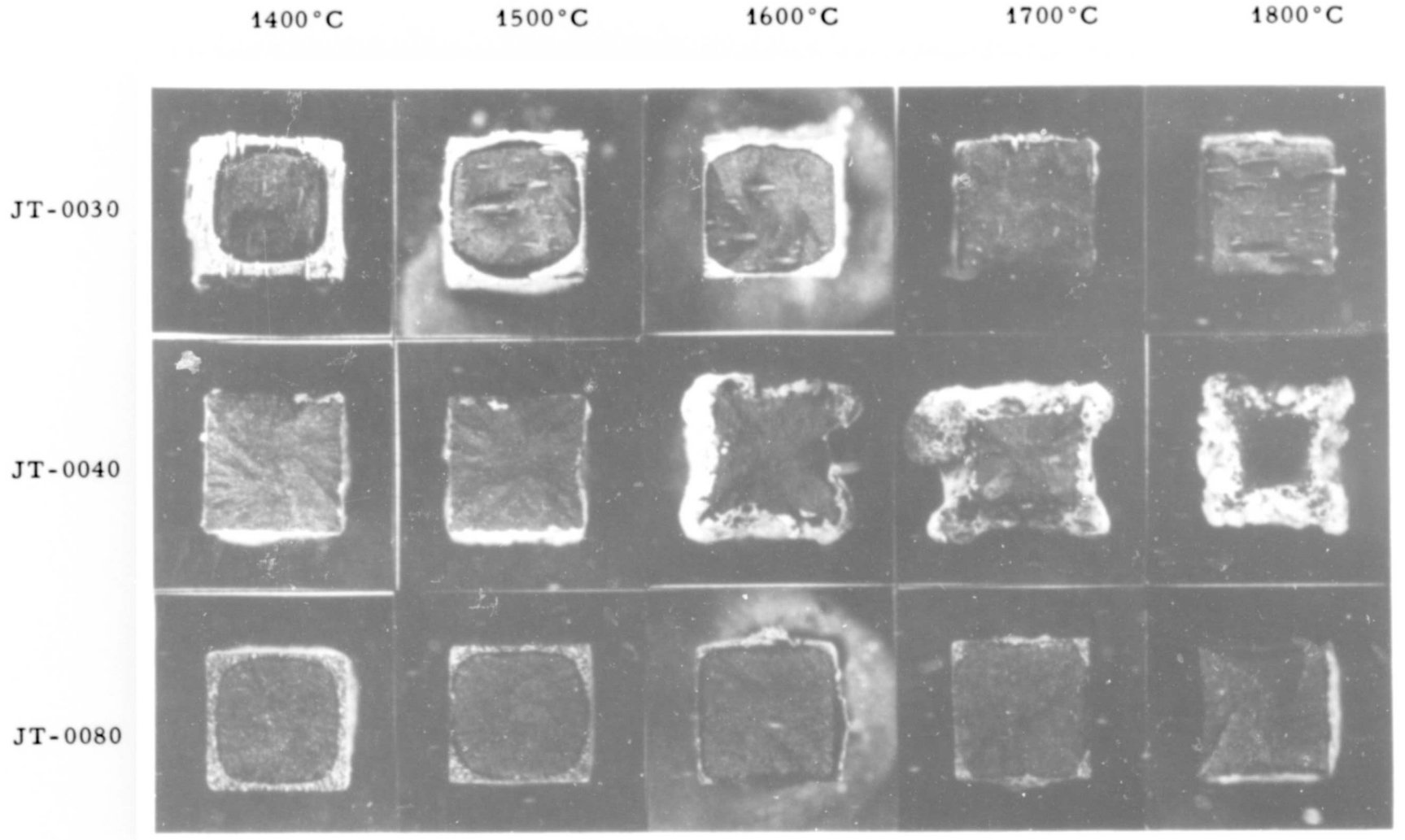

Figure 63. Hot Zone Cross Sections of JT-0030, JT-0040, and JT-0080 After 10-Minute Exposures

5. CHARACTERIZATION OF SELECTED MATERIALS

Oxidation behavior of the composites in a newly-developed test apparatus was used to evaluate the progress of the work.

Selected composites were characterized further to facilitate the proper application of the JT-materials. Both oxidation behavior and mechanical properties are presented.

Since only a cursory examination of the materials was possible under this program, the results presented should be used only for preliminary guidance. JT-materials form their protective coating by reaction with the environment; thus, for any particular application careful consideration of the actual conditions of operation are necessary to determine the applicability of the composite.

5.1. Oxidation Resistance

A series of oxidation tests were carried out with the composites to evaluate their value as oxidation-resistant materials. The tests were also used to guide the further work.

The results of all testing procedures must be carefully considered in light of the actual conditions of the test and the number of samples evaluated. We feel, in general, that the results given are obtained under more severe temperature condition than indicated.

5.1.1. Testing at Atmospheric Pressure

The oxidation units existing at the beginning of this contract were somewhat limited in scope. A radiation apparatus[3] employs suspension of the test sample on a platinum wire connected to a recording balance. The platinum wire limits applicability of this apparatus to approximately 1650°C. Attempts to attain higher temperatures by replacing the platinum wire with rhodium wire or beryllia rods were unsuccessful because both materials alloyed with the test specimen and disintegrated rapidly. Oxidation tests based on direct resistance heating of the sample in air overcome the temperature limitation of the radiation equipment; however, there are certain inherent disadvantages. Large temperature gradients between the electrical contacts result in nonuniform sample temperature, and rule out the chance to obtain weight change data of sufficient accuracy to be useful.

5.1.1.1. Development of a High-Temperature Oxidation Apparatus Employing Aerodynamic Levitation

Because of the limitations of the existing test equipment, a high-temperature oxidation apparatus was constructed which uses electromagnetic levitation. A spherical sample was suspended by forces associated with induction heating. The same coil was used for levitation and heating. Independent control of temperature and suspension was not possible.

A modified design circumvented some of the problems associated with electromagnetic levitation. A spherical sample was suspended aerodynamically above the opening of a vertical pipe having a diameter only slightly larger than the sample. Heating was again by induction. The independent control of suspension and temperature inherent in this system was recognized as a substantial improvement. The open-pipe suspension tube greatly limited the exposure time, and as the volume of the sample diminished to a critical size due to oxidation, levitation could no longer be maintained because of the reduced aerodynamic lift. This problem was resolved by replacing the open-pipe system with a carrier nozzle, similar to a gas bearing. The carrier nozzle was machined with a recess having a hemispherical contour slightly larger than the test sample. The overall design is illustrated in Figure 64.

This type of suspension permits exposure until the sample diameter has been reduced from $1\frac{1}{2}$ inches to $\frac{3}{4}$ inch. Uniformity of temperature and oxidation is enforced by rotating the sample electromagnetically with a tilted induction coil, as illustrated in Figure 65. Boron nitride has been used exclusively for all enclosure parts exposed to both heat and the electromagnetic field of the induction coil. The boron nitride is easily machinable and capable of withstanding the extreme thermal shock inherent in the test. Effective cooling of the nozzle walls is necessary, and almost the entire enclosure is submerged in water. The apparatus has been successfully operated at temperatures up to 2000°C.

The surface temperature of the sample is monitored with a two-color pyrometer which is previously calibrated with a standard optical pyrometer. The upstream pressure of the gas stream is controlled with a pressure regulator. It can be varied from 20 to 60 lbs./in^2 gauge, which corresponds to a mass flow rate of 525 and 975 lbs./hr., respectively. A general view of the apparatus and its auxiliary equipment is shown in Figure 66.

5.1.1.2. Description of Test Procedure

The weighed $1\frac{1}{2}$-inch diameter sphere was suspended on argon during the heating cycle. Once the sample reached the testing temperature, the argon supply was switched off and the air supply was switched on to support the sample. After oxidizing for a predetermined period, the transition from air to argon was reversed. The oxidation time is obtained from a recorder energized by the switch which operates the air inlet valve.

The experimental results are reduced to oxidation data by converting the weight change to a weight loss in per cent as well as to a mean oxidation rate. The weight loss is calculated from the initial and final weight of the sample. Because of the uniform oxidation effected by rotation of the sample, the mean oxidation rate can be related to the density, weight change, and oxidation time by the following equation:

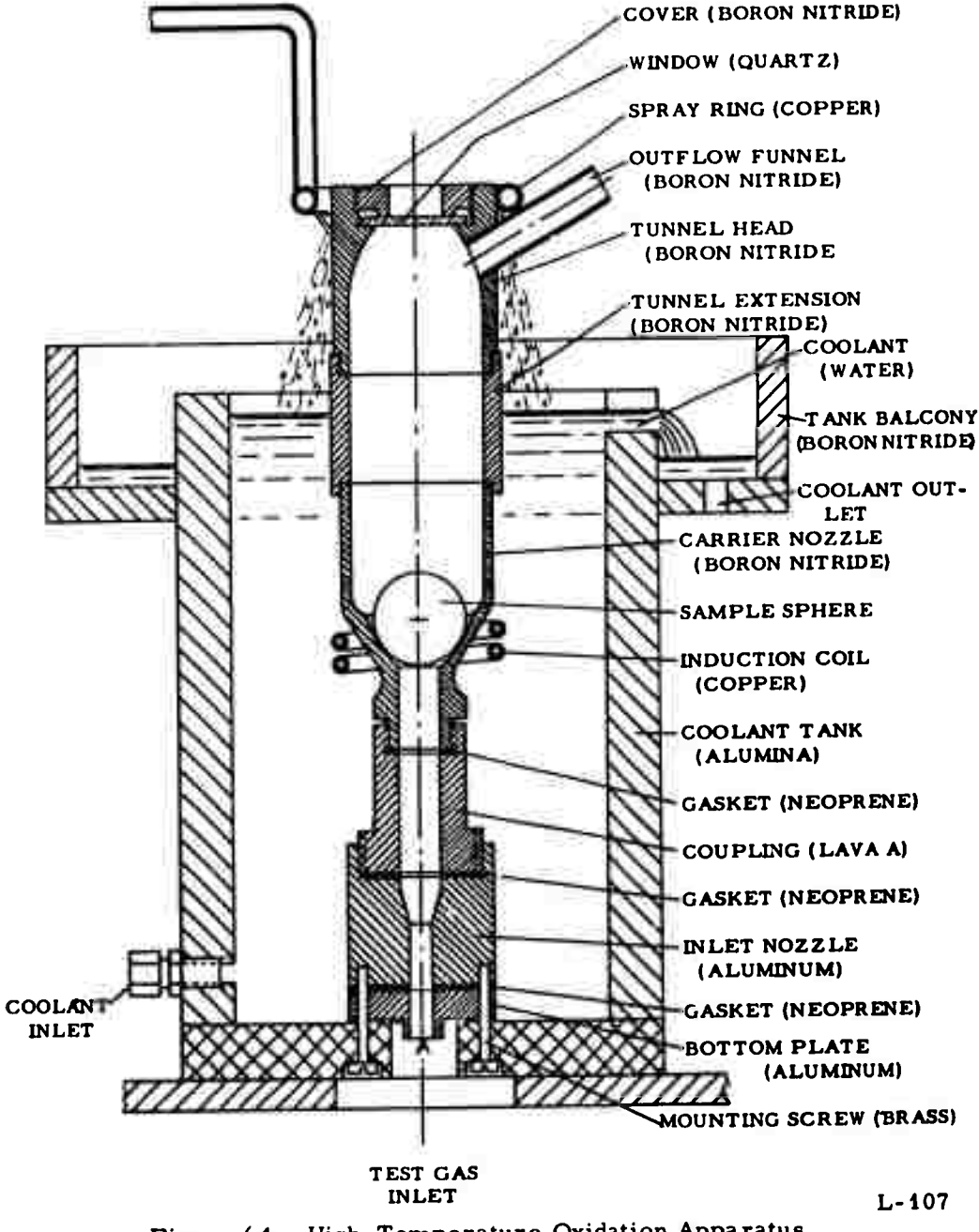

Figure 64. High-Temperature Oxidation Apparatus, Cross Section

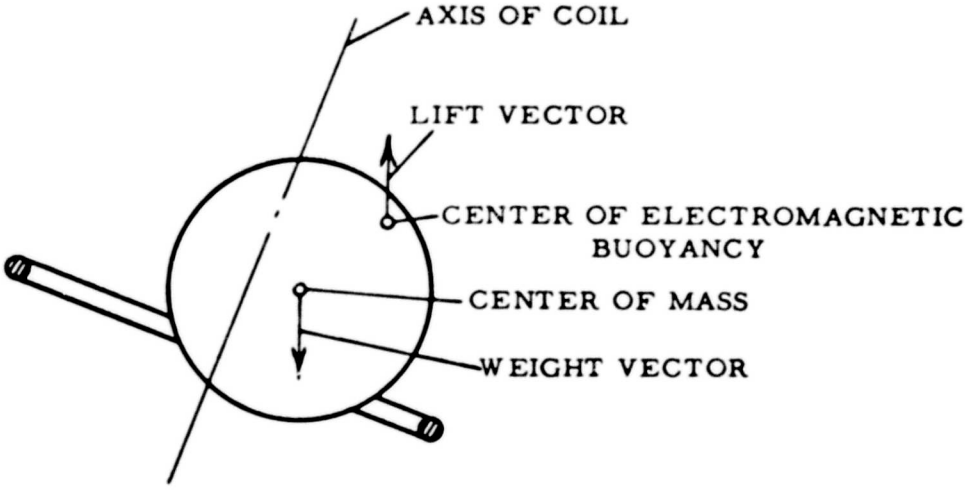

L-156

Figure 65. Electromagnetic Rotation of Sample Sphere

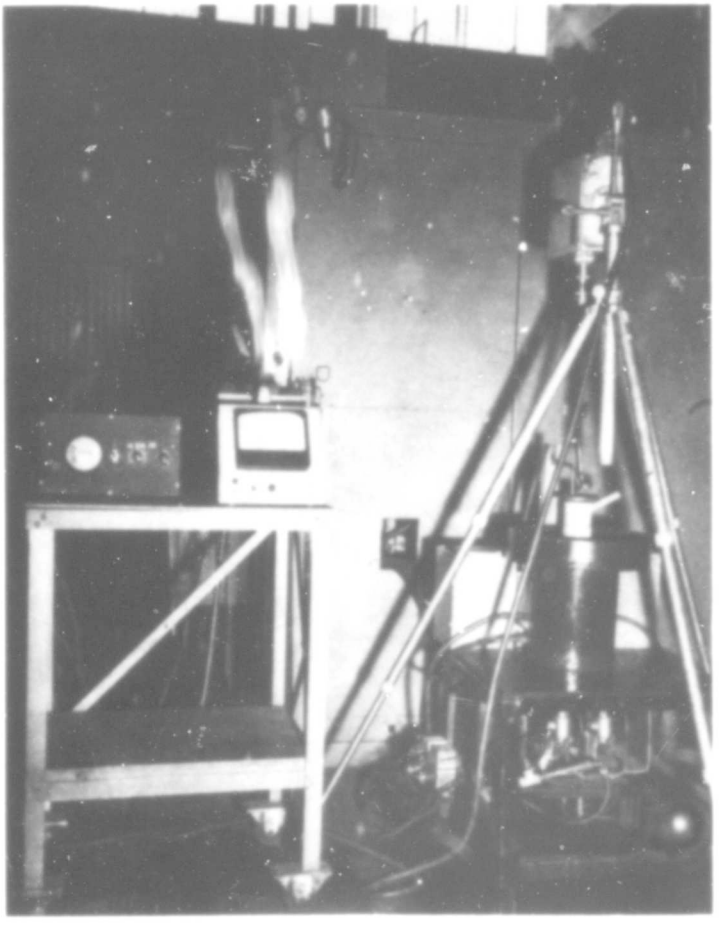

Figure 66. High-Temperature Oxidation Apparatus

$$\kappa\Big|_{t_1}^{t_2}(T) = \frac{3\rho}{4\pi(t_2 - t_1)}^{\frac{2}{3}} (W_1^{\frac{1}{3}} - W_2^{\frac{1}{3}});$$

where t_i = Time of exposure,

$\kappa\Big|_{t_1}^{t_2}(T)$ = Mean oxidation rate for a time interval from t_1 to t_2 at the temperature T,

ρ = Sample density,

W_1 = Weight of sample before oxidation,

W_2 = Weight of sample after oxidation.

Oxidation rates calculated from this equation for JT materials will not be so direct as for certain other materials since only some of the oxides formed are volatile and immediately removed. The weight change will be a combination of weight loss from oxidation and disintegration and weight gain from oxide formation.

5.1.1.3. Evaluation of ATJ Graphite

The high-temperature oxidation characteristics of ATJ graphite were determined to obtain a base line for comparisons with composites.

The test series was aimed at determining relative weight loss and mean oxidation rate over the temperature range of 1400 to 2000°C using an exposure time of 1 minute. Results from two runs are shown in Table 5. From these data it is concluded that the mean oxidation rate of ATJ increases with temperature up to 1600 or 1700°C then decreases with increasing temperature. Apparently, the oxygen diffusion rate thru the boundary layer limits the oxidation rate in the high-temperature tests.

Table 5. Oxidation Characteristics of ATJ Graphite

Temperature, °C	Oxidation Time, t Seconds		Per Cent Weight Loss of 1½" Diameter Sphere		$\kappa\Big\|_{o}^{t}$, mg/cm^{-2} hr^{-1}	
	Series No. 1	Series No. 2	Series No. 1	Series No. 2	Series No. 1	Series No. 2
1400	-	60.4	-	6.49	-	4370
1500	-	60.4	-	7.00	-	4702
1600	60.8	60.3	7.72	7.44	5117	4991
1700	60.7	60.4	7.28	7.49	4944	5119
1800	60.5	60.4	7.14	7.44	4880	5065
1900	60.6	60.4	7.04	6.80	4723	4634
2000	60.4	60.3	6.05	6.47	4113	4409
Upstream Pressure: 20 lbs./in.^{2} gauge						

5.1.1.4. Evaluation of SiC-Coated RVC Graphite

To permit further comparisons with composites, another test series was devoted to samples of SiC-coated RVC. Because of the good oxidation resistance expected, successive 5-minute exposure periods were used on each specimen with a weighing between each cycle. Two specimens were thus tested at 1600°C. Both exhibited no weight loss until an opening in the SiC coating exposed the RVC substrate. In one case, this happened after 5 cycles (25 minutes of total exposure), and in the other case after 4 cycles (20 minutes of total exposure). At 1700°C, obvious coating failure occurred after 2 minutes of exposure. The appearance of the 1700°C specimen as compared with an unoxidized one is illustrated in Figure 67. Extended use of SiC-coated graphite in air at one atmosphere pressure is limited to a maximum of 1600°C.

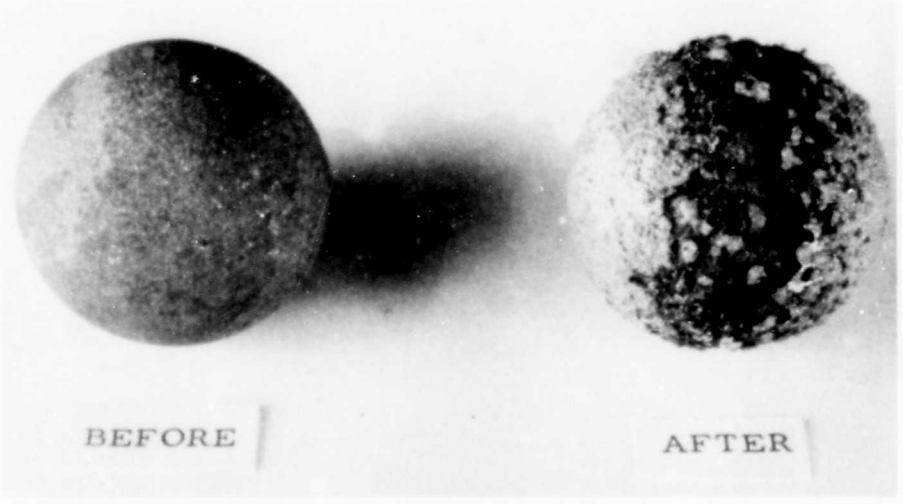

Figure 67. SiC-Coated RVC Graphite Before and After Oxidation at 1700°C

5.1.1.5. Evaluation of JTA

5.1.1.5.1. Cyclic Exposure

Samples of JTA were subjected to 12 consecutive 5-minute exposures at 1600, 1700, or 1800°C after which a single 30-minute exposure concluded the test. After 9 exposures of 5 minutes each at 1900°C, the size was critically reduced and the test temperature could no longer be reached due to diminshed coupling. One sample was run at each temperature.

After each cycle any loose coating was removed before weighing. This procedure was necessary to prevent rotation problems and errors in temperature measurement during the subsequent cycle, and to

see if "scaling' would lead to any change in oxidation characteristics. The data were not meant to establish a mean oxidation rate over oxidation times greater than one cycle.

Several observations were made of the behavior of JTA in the tests. The samples tested at 1600, 1700, and 1800°C exhibited a release of vapors during the initial 20 to 40 seconds of each cycle. The cessation of this vapor release is attributed to the formation of a stable coating. The specimen tested at 1900°C continued to release vapor throughout theoxidation period, indicating that at this temperature a completely stable coating is not formed under the conditions of this test.

Another observation of interest is the occasional appearance of small bubbles on the surface of oxidizing JTA. Figure 68 shows an example of such bubbles on a specimen of JTA after 5 minutes of oxidation at 1700°C. The phenomenon is a characteristic of the oxidation of JTA at low air velocities. At higher velocities, the external gas pressure is higher than the internal pressure preventing formation of bubbles. Even during oxidation at low velocities, however, bubbles do not always appear. For example, the specimen shown in Figure 69 was oxidized for a total time of 20 minutes (4 cycles) at 1700°C. The resulting coating was uniform, bubble free and tenaciously bonded to the sphere. An additional 5-minute cycle showed no adverse effect on the coating and no weight loss was experienced. The coating finally scaled off after the sixth cycle.

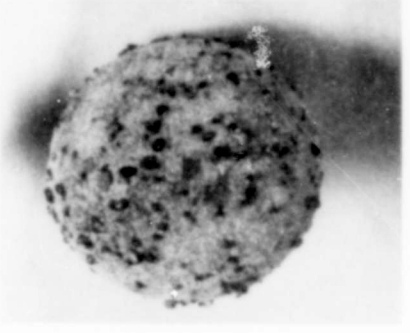

Figure 68. JTA Sample After 5 Minutes of Oxidation at 1700°C

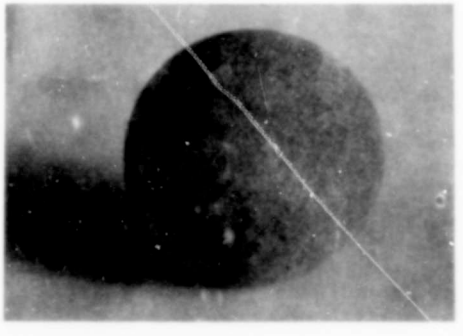

Figure 69. JTA Sample Demonstrating Uniform Coating After 20 Minutes (4 Cycles) Oxidation at 1700°C

The results compiled in Table 6 indicate that between 1600 and 1900°C, the mean oxidation rate of JTA as referred to a 5-minute exposure is essentially independent of the prior history of the sample. On the other hand, the ratio of mean oxidation rates for 5 and 10 minutes of exposure is shown to greatly differ from unity in all cases, thus pointing to the necessity of characterizing the oxidation behavior of composites as a function of exposure time.

Table 6. Mean Oxidation Rates of Grade JTA Using Cyclic Exposure

Cycle No. n	Oxidation Rate, $\kappa \Big\vert_{(n-1)\times 5\ \text{Min.}}^{n\times 5\ \text{Min.}}$ mg cm^{-2} hr.$^{-1}$			
	1600°C	1700°C	1800°C	1900°C
1	311	909	1089	2497
2	160	1027	1062	1975
3	271	1035	1060	1740
4	269	874	1045	1513
5	220	699	1044	1421
6	185	717	1053	1364
7	225	700	1041	1304
8	246	617	995	1284
9	319	553	1029	1245
10	317	611	1017	-
11	289	593	1021	-
12	270	624	1018	-
$\kappa \Big\vert_{60}^{90\ \text{Min.}}$	1600°C	1700°C	1800°C	
	183.6	50.40	165.6	
Upstream Pressure - 20 lbs./in.^{2} gauge Sample Size: 1½-Inch Diameter Sphere				

An attempt to obtain oxidation data at 2000°C was unsuccessful. After 80 seconds at 2000°C, rotation of the sample ceased and an intumescent mass appeared on the downstream side of the specimen as illustrated in Figure 70. The surface receiving direct air impingement appeared normal.

5.1.1.5.2. Continuous Exposure (Upstream Pressure - 20 lbs./in.^{2} gauge)

Oxidation characteristics of JTA as a function of time were obtained over the temperature range of 1400 to 1800°C using continuous exposures of 5, 15, 30, and 60 minutes. The results are shown in Figure 71. Each point represents data from a single sample. For comparison,

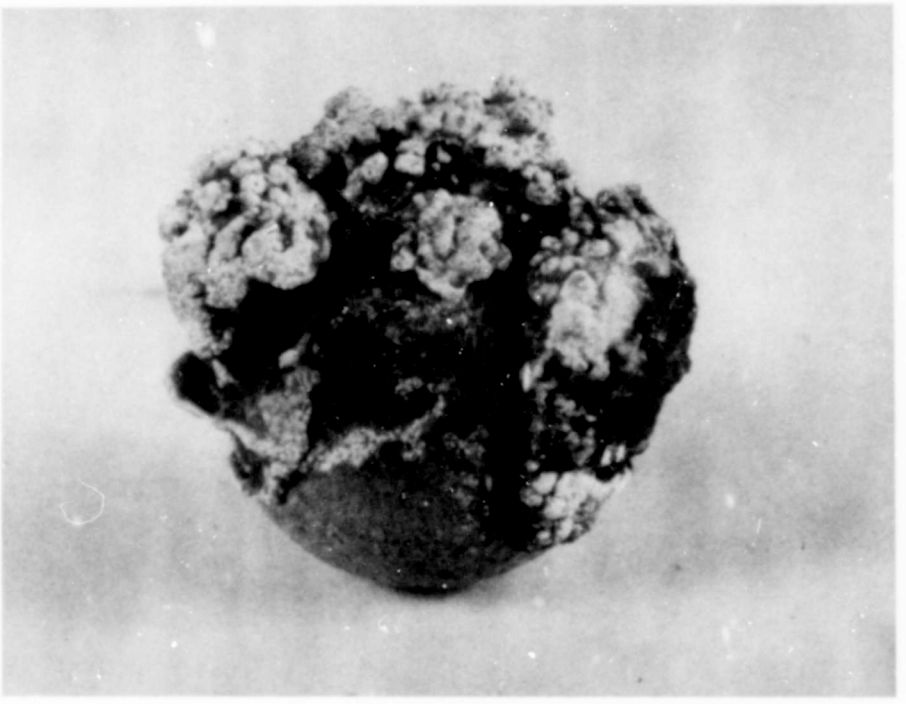

Figure 70. Surface of JTA Sample Opposite Air Impingement After 80 Seconds at 2000°C

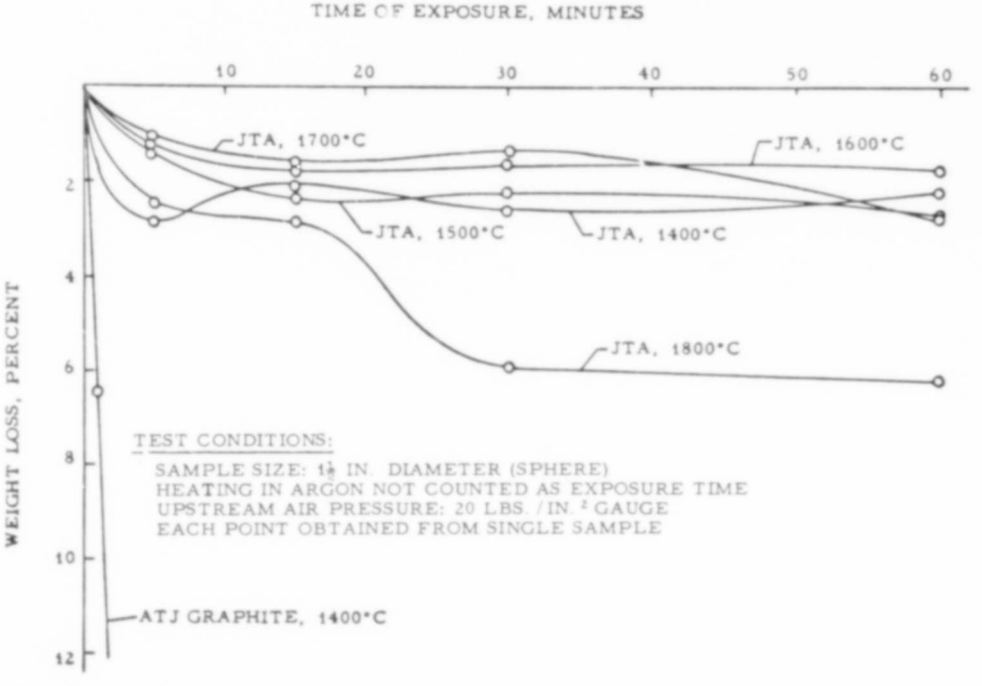

Figure 71. Weight Loss Versus Exposure Time of JTA Between 1400 and 1800°C L-268

the performance of ATJ graphite at 1400°C is included. As can be seen, JTA exhibits excellent oxidation resistance up to 1700°C and somewhat diminished but still impressive stability at 1800°C.

The appearance of the samples after testing is illustrated in Figure 72. Evidently, after extended exposure at 1600°C, bubbles began to form, and they eventually stopped the rotation of the sample.

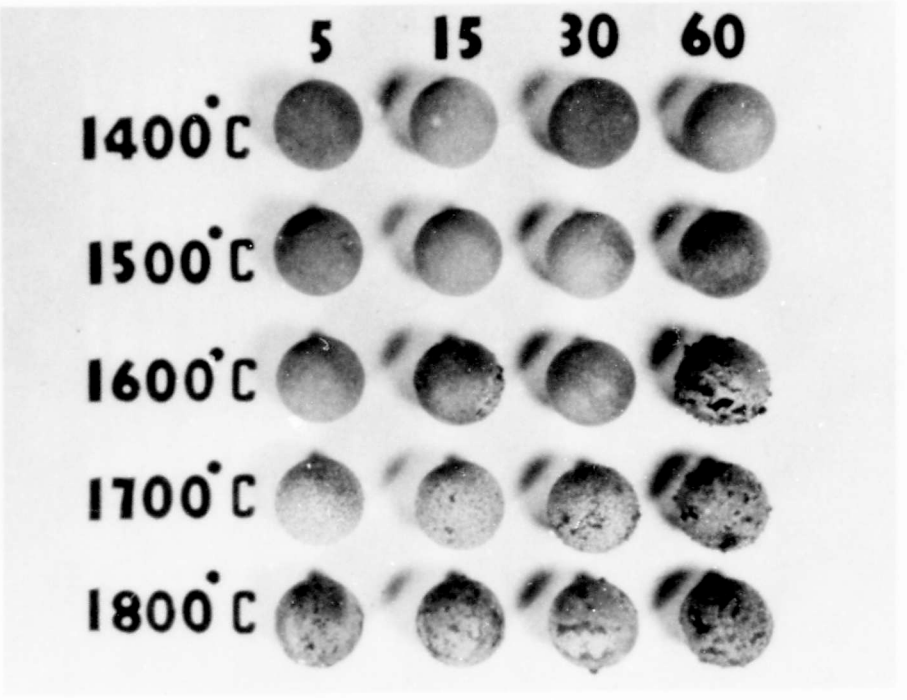

Figure 72. Appearance of JTA Samples After Testing, Upper Numbers Indicating Time of Exposure in Minutes

The mean oxidation rate versus time of exposure is shown in Figure 73, and demonstrates that short-time testing of JT composites does not reveal their full potential.

Attempts to obtain data for 1900°C were unsuccessful since after 11 minutes of exposure the sample ruptured and discharged molten material. The result is illustrated in Figure 74. Sample failure at 1900°C appears to be caused by internal melting of the additives. The internal temperature of the spherical sample is necessarily higher than the surface temperature because of the radiation to the surroundings, and appears to be much greater than expected since the minimum eutectic of JTA is known to lie above 2100°C. The experiment indicates that when the surface temperature is 1900°C, the internal temperature is at least 200°C higher. This effect can be reproduced in argon. This situation is not desirable but it demonstrates the severity of the test.

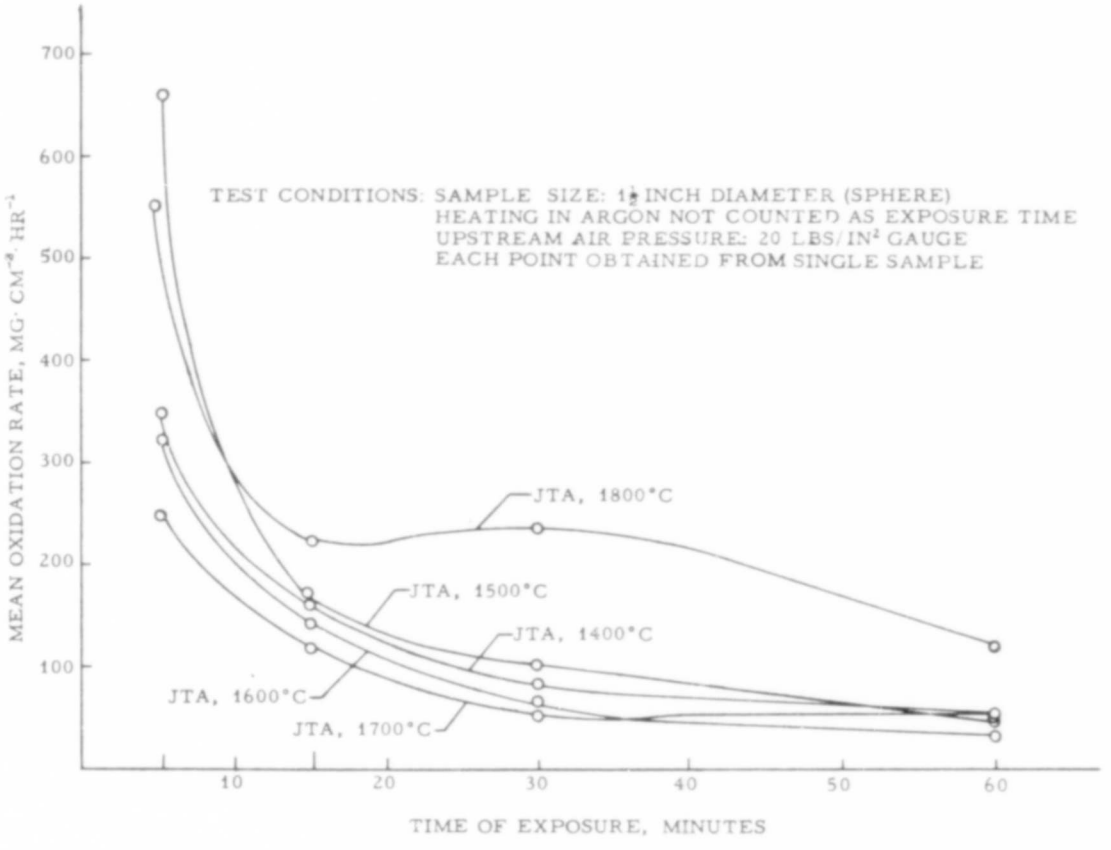

Figure 73. Mean Oxidation Rate Versus Exposure Time for Grade JTA L-290

Figure 74. Appearance of JTA Sample After Being Tested for 11 Minutes at 1900°C

5.1.1.5.3. Effect of Upstream Pressure on Oxidation Characteristics

Further tests with JTA were aimed at determining the effect of upstream pressure on the oxidation characteristics. The results of these experiments performed at 1800°C using 15-minute exposures over an upstream pressure range of 20 to 60 lbs./in.^{2} gauge are presented in Table 7.

Table 7. Effect of Upstream Pressure on the Oxidation Characteristics of JTA at 1800°C

Upstream Pressure, lbs./in.^{2} gauge	Oxidation Characteristics	
	Weight Loss, per cent	Mean Oxidation Rate mg cm^{-2} hr.$^{-1}$ $\kappa\Big|_0^{15}$ (1800)
20	2.816	219.6
40	1.930	202.0
50	1.535	134.3
60	1.891	194.8

Generally, the oxidation rate decreases with increased upstream pressure up to 50 lbs./in.^{2} gauge. The increased air velocity at the higher upstream pressures also improves continuity of sample rotation.

5.1.1.5.4. Continuous Exposure (Upstream Pressure - 50 lbs./in.^{2} gauge)

Figure 75 illustrates relative weight losses resulting from continuous exposures over 5, 15, 30, and 60 minutes. Each point represents data from a single sample. For comparison, reference is made to the behavior of ATJ graphite at 1400°C. Oxidation rates of JTA are presented in Figure 76. The appearance of the samples of this series after testing is shown in Figure 77.

5.1.1.6. Screening of New Composites

To appraise the high-temperature oxidation resistance of selected new composites, a testing time of 15 minutes was chosen. This exposure time permits the coating to form and gives an indication of its effectiveness after formation.

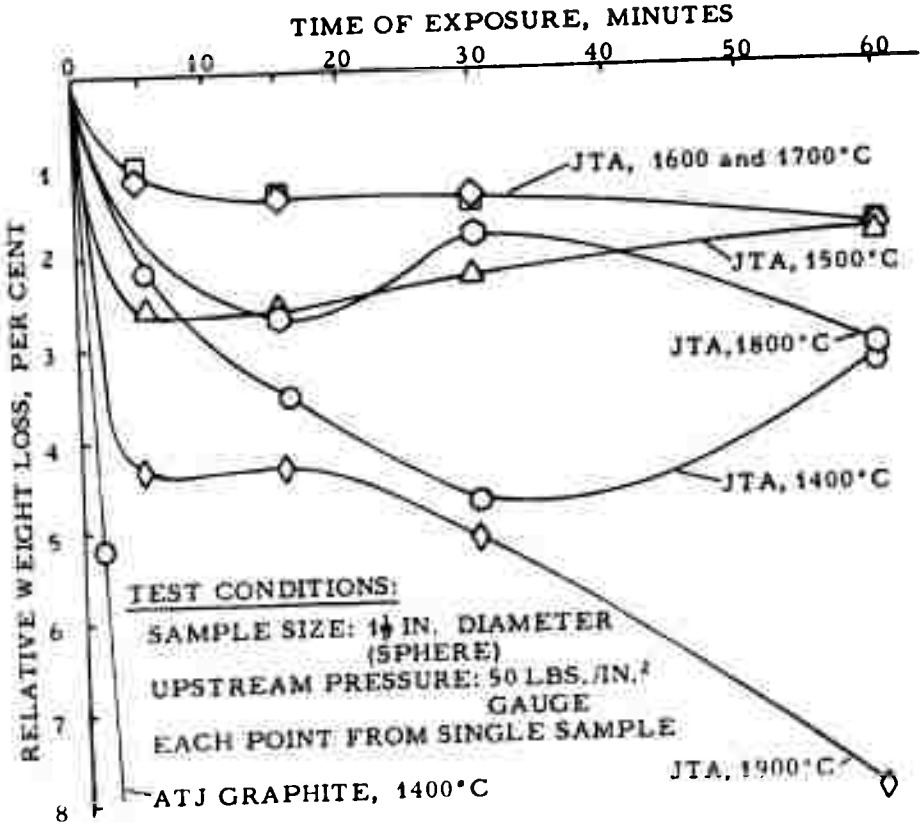

L-901

Figure 75. Oxidation Characteristics of JTA Between 1400 and 1900°C, Relative Weight Loss Versus Time of Exposure

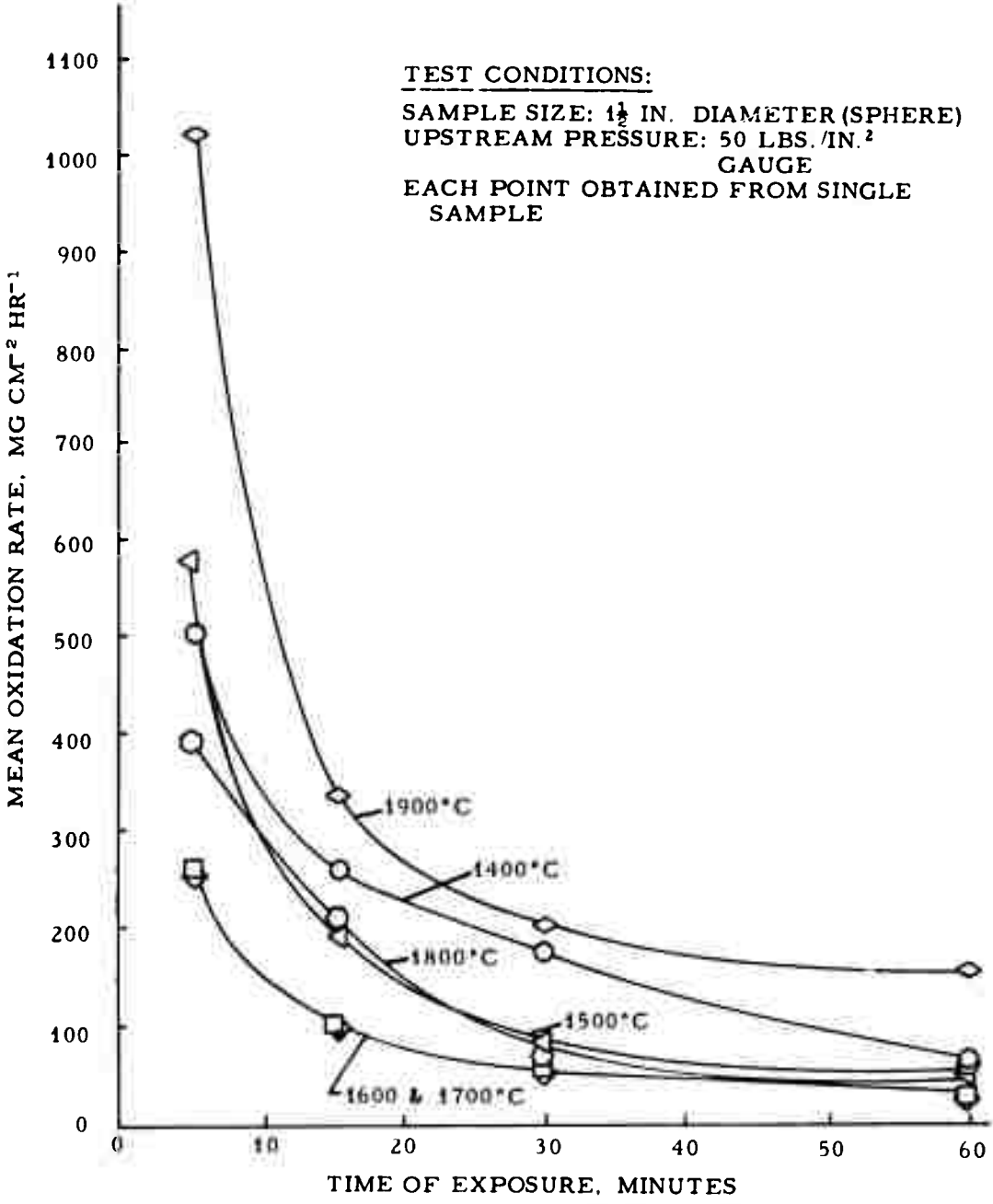

Figure 76. Oxidation Characteristics of JTA Between 1400 and 1900°C, Mean Oxidation Rate Versus Time of Exposure L-902

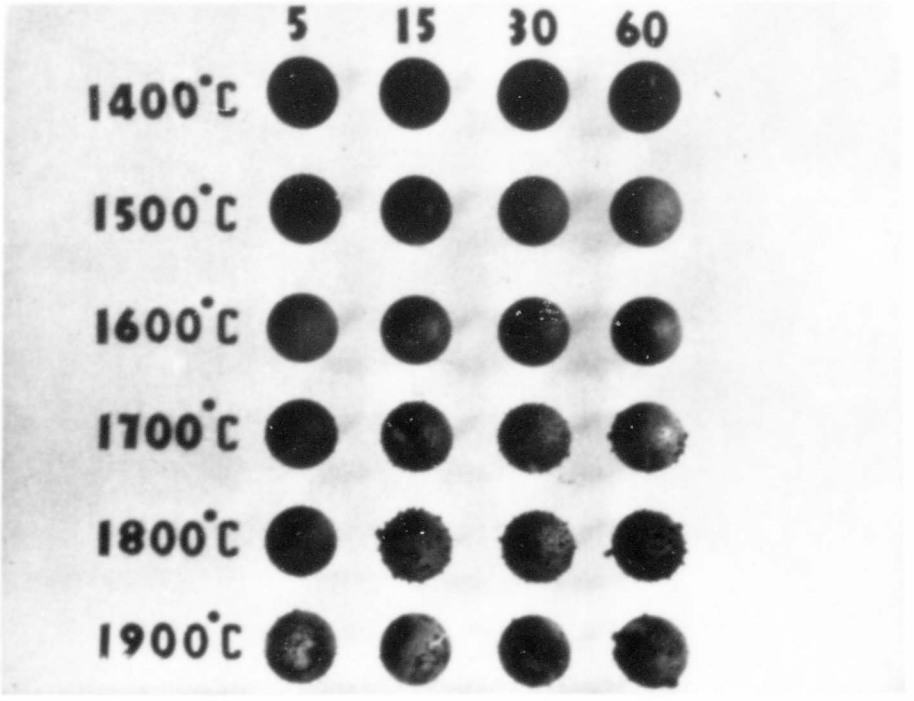

Figure 77. Appearance of JTA Samples After Testing, Upper Numbers Indicating Time of Exposure in Minutes

The results are presented in Table 8. Based on these data, the following conclusions can be drawn:

1) For high-temperature oxidation resistance, the replacement of boron in the JTA system is advantageous. In the C/Zr/Si system, the oxidation behavior depends on the silicon level. For a constant carbon content of 48 per cent and a test temperature of 1800°C, the effect of varying the silicon and zirconium content is shown in Figure 78. JT-0981, with a silicon content of 17 per cent appears to be the best composition in this series. (It was selected for a more complete characterization.)

2) Replacement of silicon with niobium in JTA is, in general, not advantageous. JT-0961 with 2 per cent niobium content does appear useful at 1800°C where the coating appeared to have excellent integrity and to be well-bonded to the substrate as shown in Figure 79.

Table 8. Oxidation Characteristics of Selected New Composites

Experimental Grade Number	Approximate Elementary Analysis Per Cent by Weight								Upstream Pressure, lbs./in.^{2} gauge	Oxidation Characteristics					
										Per Cent Relative Weight Loss of 1½-Inch Diameter Sphere After 15 Minutes of Exposure at Temperature T			Mean Oxidation Rate $\kappa \int_0^{15} (T)$ mg cm^{-2} hr.$^{-1}$		
	C	Zr	B	Si	Nb	La	Ce	Hf		T=1700°C	T=1800°C	T=1900°C	T=1700°C	T=1800°C	T=1900°C
JTA	48	35	8	9	0	0	0	0	20 50	1.592 1.315	2.816 2.672	4.324	116.7 100.3	219.6 211.3	344.4
JT-0950	48	35	8	9	0	0	0	0	20 50	1.844	2.238 1.287		138.5	169.8 97.8	
JT-0951	48	37	6	9	0	0	0	0	20 50	1.192	5.372 1.037		94.5	427.1 73.2	
JT-0952	48	39	4	9	0	0	0	0	20 50	1.260	2.043 0.976		100.0	160.6 73.0	
JT-0954	48	43	0	9	0	0	0	0	50		0.711			55.9	
JT-0961	48	35	8	7	2	0	0	0	20 50	2.411	1.174 2.205	7.032	185.8	90.3 170.3	568.8
JT-0962	48	35	8	4.5	4.5	0	0	0	20		7.990			615.6	
JT-0963	48	35	8	2	7	0	0	0	20		14.49			1498	
JT-0964	48	35	8	0	9	0	0	0	20		20.63			1837	
JT 0965	48	43	0	7	2	0	0	0	20 50		1.239 0.828	9.067		98.6 66.2	715.0
JT-0966	48	43	0	4.5	4.5	0	0	0	20		8.814			707.0	
JT-0974	48	35	8	7	0	0	2	0	20		6.313			500.4	
JT-0975	48	35	8	7	0	2	0	0	20		9.312			741.6	
JT-0980	48	35	2	15	0	0	0	0	20 50	1.011	0.992 1.101	4.684	78.3	78.7 85.6	690.8
JT-0981	48	35	0	17	0	0	0	0	20 50	0.533 0.536	0.805 0.470	2.381 2.618	39.5 39.3	62.0 35.9	181.9 194.3
JT-0983	48	47	0	5	0	0	0	0	50		1.036			83.5	
JT-0984	48	27	0	25	0	0	0	0	50		0.618			46.5	
JT-0990	48	49	0	3	0	0	0	0	50		2.110			181.8	
JT-0991	36	0	0	13	0	0	0	51	50		0.675			67.6	
JT-0992	33	0	0	12	0	0	0	55	50		0.232			25.7	
JT-0993	48	0	0	17	0	0	0	35	50		0.519			41.9	

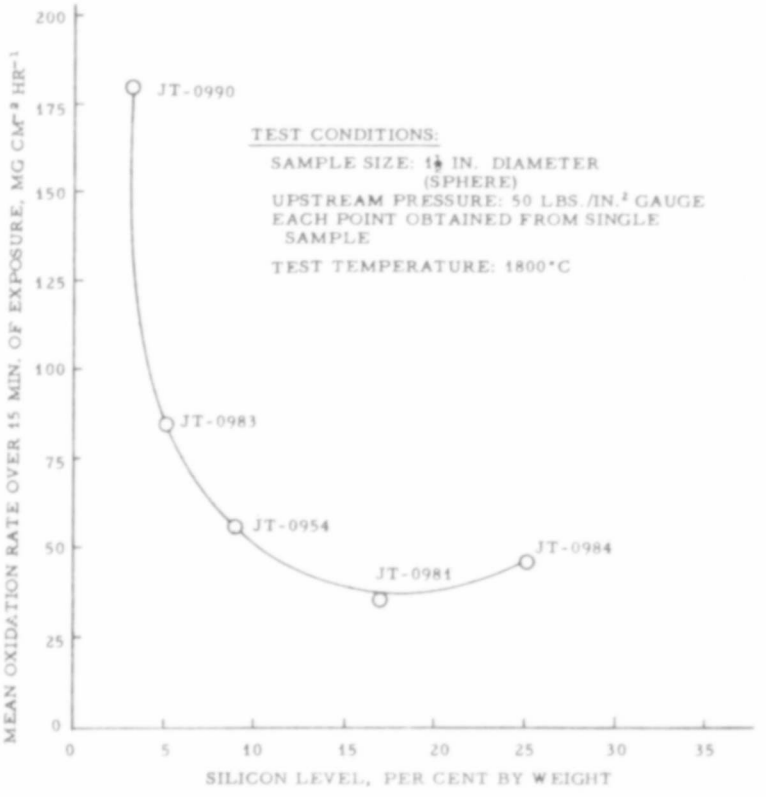

Figure 78. Effect of the Silicon Level on the Oxidation Behavior of C/Zr/Si Composites With a Carbon Content of 48 Per Cent L-903

Figure 79. Appearance of JT-0961 After 15 Minutes of Oxidation at 1800°C

3) Substitution of cerium or lanthanum for 25 per cent of the silicon in JTA, as represented by JT-0974 and JT-0975, yields poor oxidation resistance. No coherent coating was formed since the liquid-oxide phases appearing on the surface did not wet the parent material.

4) Replacements of zirconium by hafnium in JT-0981 as carried out on molar, volume, and weight bases, are JT-0991, JT-0992, and JT-0993, respectively. Substitutions on bases other than weight were introduced here for the first time because of the density difference between hafnium and zirconium (13.3 versus 6.4 g/cc). All three bases of substitution led to materials with extremely low oxidation rates, and the quality of the coatings was found to be superior to both JTA and JT-0981 coatings, Figure 80. The coatings of the composites containing hafnium are free of bubbles and tenaceously bonded to the parent material.

Further study of these materials is recommended.

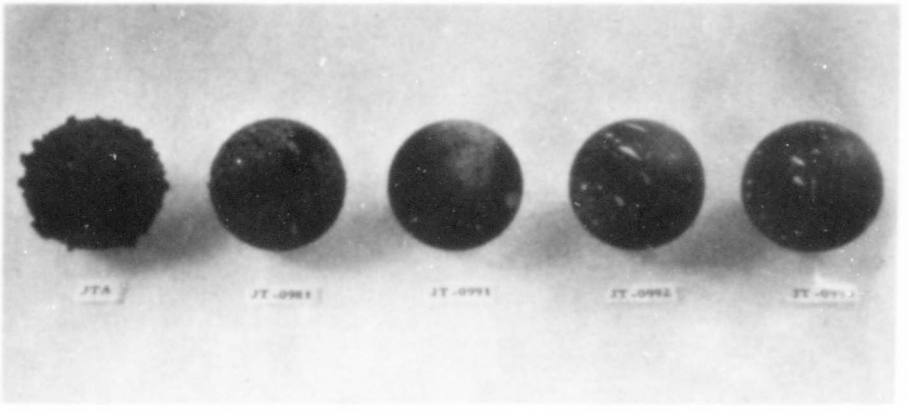

Figure 80. Coating Appearance of C/Hf/Si Composites as Compared with JTA and JT-0981 After 15 Minutes of Oxidation at 1800°C

5.1.1.7. Evaluation of JT-0981

JT-0981 was selected for more characterization. Prior to testing the composites containing hafnium, it was the most promising new material.

Relative weight losses and mean oxidation rates versus time of exposure are shown in Figures 81 and 82. The samples after testing are shown in Figure 83. JT-0981 appears stable up to 2000°C. A 30-minute continuous test at 2000°C resulted in a weight loss of about 5 per cent. Data for the 60-minute test is lacking because the sample exploded after 57 minutes and ejected the greater part of the core in the molten state. This again illustrates the temperature gradients existing in the samples during the testing.

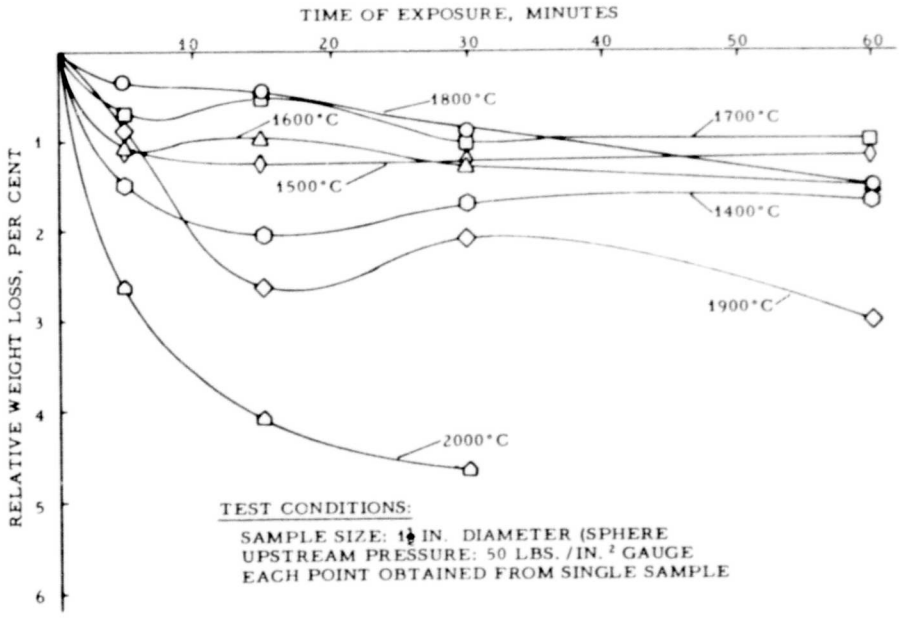

Figure 81. Oxidation Characteristics of JT-0981 Between 1400 and 2000°C, Relative Weight Loss Versus Time of Exposure

L-904

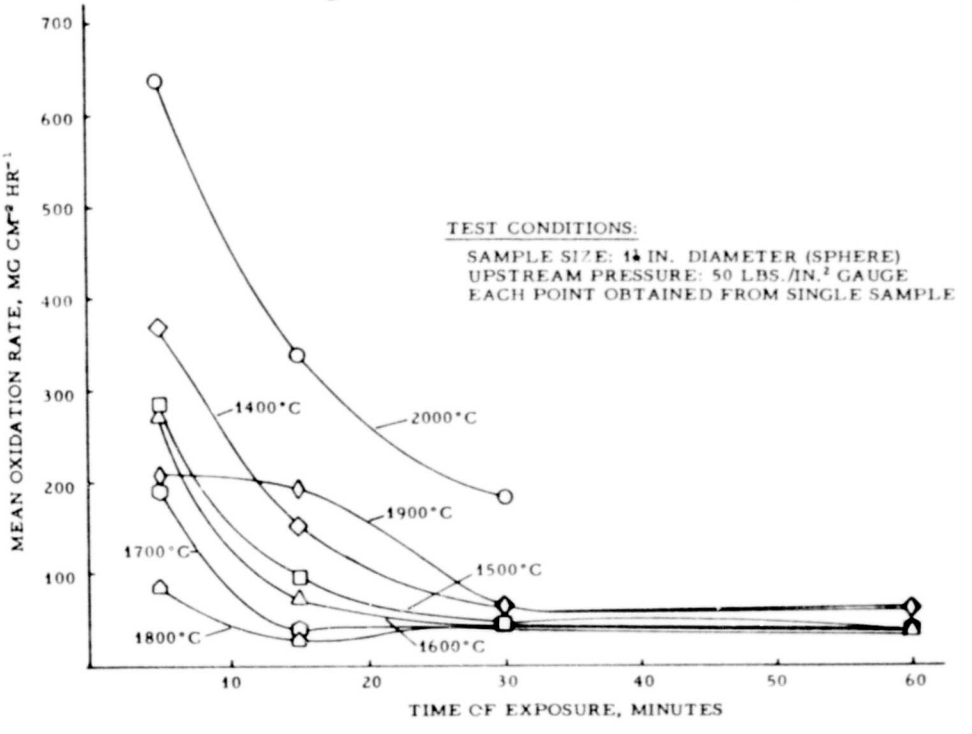

Figure 82. Oxidation Characteristics of JT-0981 Between 1400 and 2000°C, Mean Oxidation Rate Versus Time of Exposure

L-905

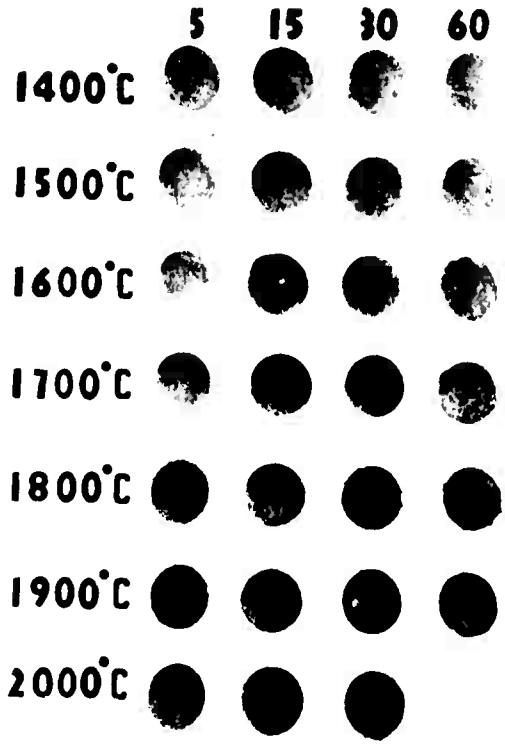

Figure 83. Appearance of JT-0981 Samples After Testing, Upper Numbers Indicating Time of Exposure in Minutes

After cooling to room temperature, coatings formed at 1800°C and above were found to be thin and readily chipped off the parent material. This does not reflect the adherence of these coatings at high temperatures, where they are known to be viscous and have never been observed to flake off during exposure.

5.1.1.8. Evaluation of Siliconized JT-0981

During the preliminary high-temperature screening described in Section 4.2., the ends of the resistance-heated test bars, close to the water-cooled copper terminals, gave a good indication of the low-temperature oxidation resistance of the composite. We noted that a number of the test bars deteriorated fastest in the lower temperature zones of the test bars. JT-0981 was one such composite.

Further studies, described in Section 5.1.1.2., indicated that JT-0981 has good resistance at temperatures above 1700°C, but that the performance deteriorated at the lower test temperatures. Figure 84 compares the performance of JTA and JT-0981.

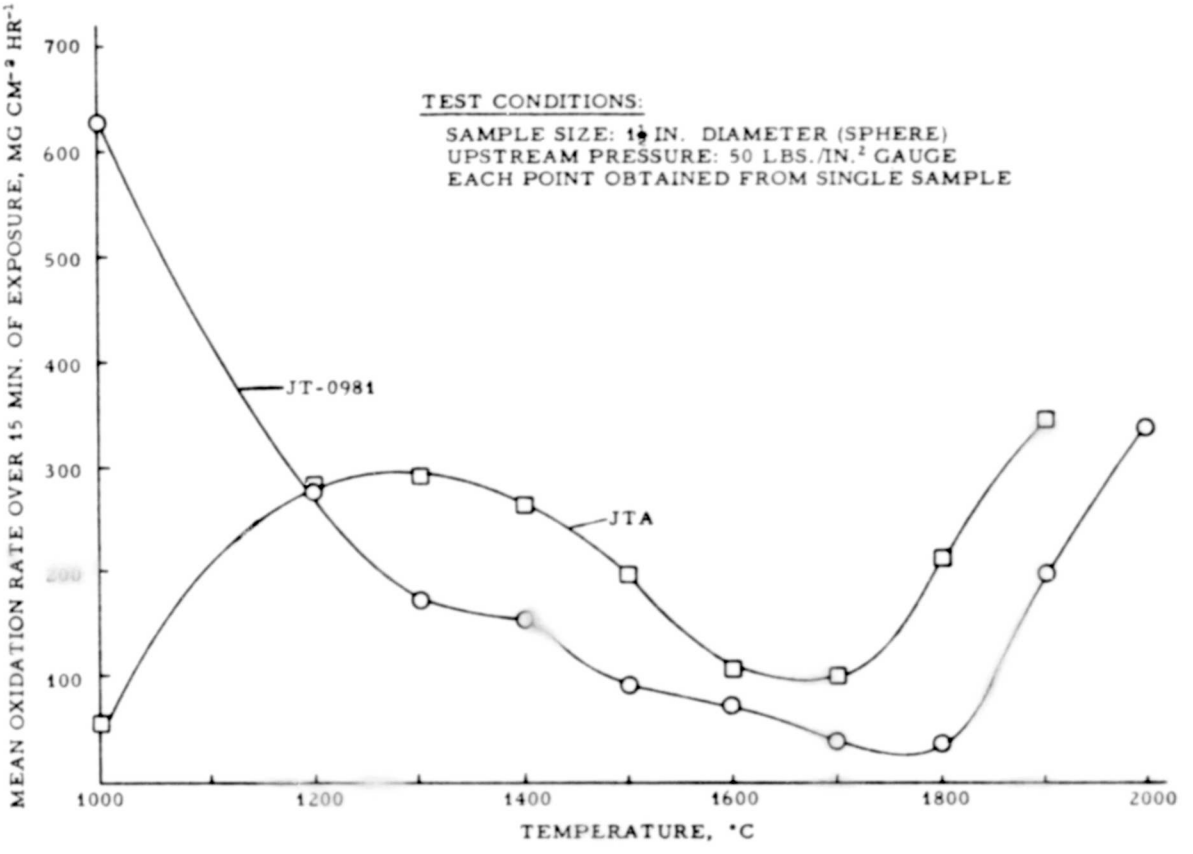

Figure 84. Comparison Between JTA and JT-0981, Mean Oxidation Rate Over 15 Minutes of Exposure Versus Temperature L-906

In many applications, the pieces would be exposed to both high and low temperatures. In the low-temperature range (to 1600°C), excellent protection for graphite can be provided by siliconizing the surface. During this treatment, silicon diffuses into the graphite and forms a silicon carbide coating on the graphite.

A similar procedure should be applicable for providing protection for the graphite-refractory composites. The coating for the composite, however, will consist of silicon carbide and the silicides of the metallic additives.

Several test spheres of JT-0981 were siliconized. Since JT-0981 is a C/Zr/Si system, the resulting coating was SiC and one or more of the several zirconium silicides.

Results of the oxidation tests on the siliconized and normal JT-0981 are compared in Table 9. Siliconizing appears to be a very effective method of eliminating the low-temperature deficiencies of the material.

Table 9. Comparison of Silicized and Unsilicized JT-0981

Temperature, °C	Per Cent Relative Weight Loss of 1½-Inch Diameter Sphere After 15 Minutes of Exposure	
	JT-0981	Silicized JT-0981
1000	8.236	−0.002
1200	3.738	−0.010
1300	2.358	−0.011
1400	2.086	−0.001
1500	1.250	+0.076
1600	0.956	+0.079
1700	0.536	+0.805
Upstream Pressure - 50 lbs./in.^{2} gauge		

5.1.2. Pressure Effects on Oxidation Rates

Modern applications of refractory composites are not limited to exposure at one atmosphere. Performance tests were carried out at various pressures to study the oxidation behavior of selected materials.

5.1.2.1. Description of Apparatus

Since the levitation apparatus was not easily adaptable to pressure variation, the resistance-heated apparatus shown in Figure 85 was constructed. It resembles the screening apparatus used in Section 4.2., except the specimen and electrodes are enclosed in a vessel which can be evacuated or pressurized. This apparatus suffers from the same drawback of non-isothermal conditions because of the cold contact ends and the results can not be used to calculate oxidation rates. Qualitative interpretations sufficient to appraise the pressure dependence should be possible.

An overall view of the apparatus is shown in Figure 86. Air was used as the oxidizer and the tests were carried out at constant pressure. The pressure level was maintained by controlling the flow through a leak line and the air in the vessel was continuously replaced.

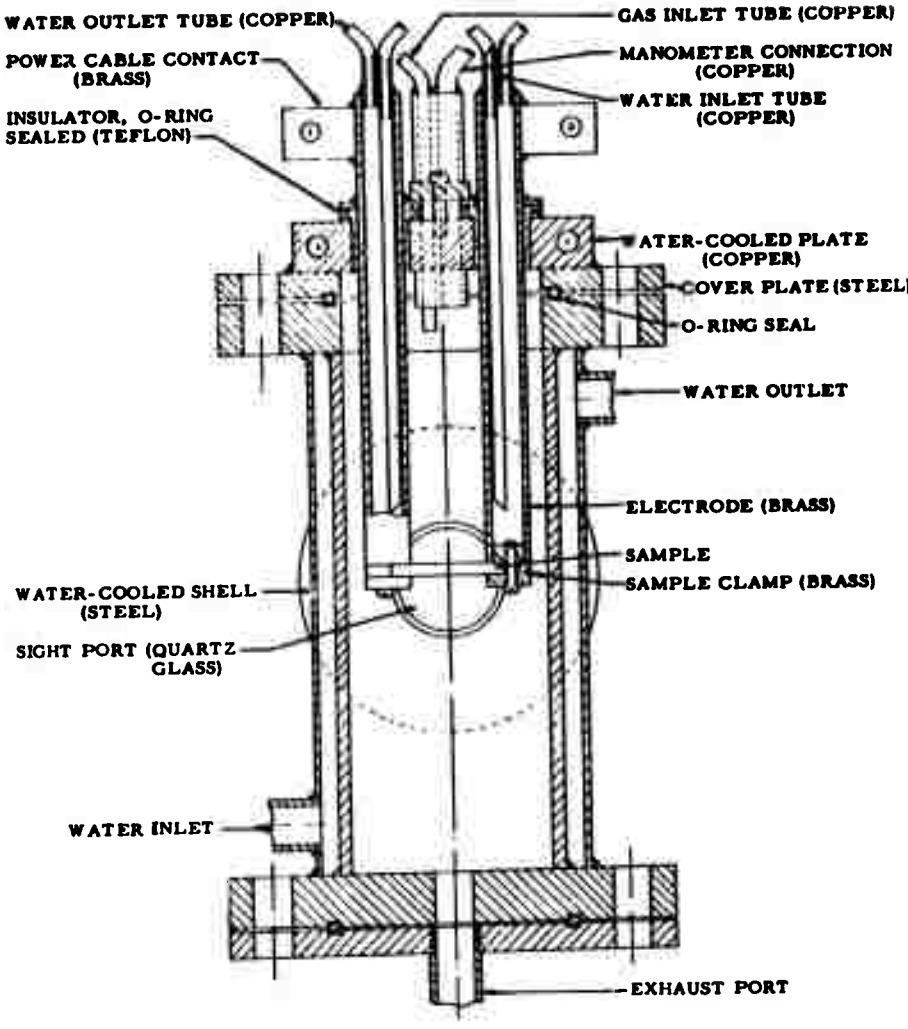

Figure 85. Oxidation Apparatus for Tests at Reduced and Elevated Pressures, Cross Section L-907

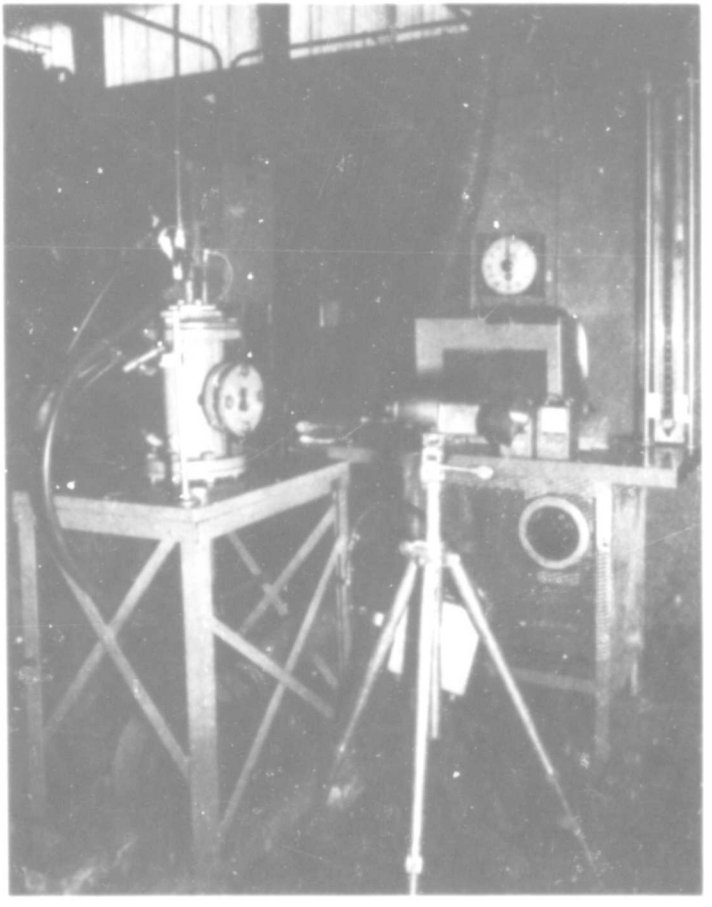

Figure 86. Oxidation Apparatus for Tests at Reduced and Elevated Pressures, Overall View

5.1.2.2. Evaluation of Grade ATJ Graphite

The oxidation behavior of ATJ graphite as a function of pressure was determined since it provided an indication of the effect of various concentrations on the graphite part of the composites.

Relative weight losses for 10-minute exposures are shown in Figure 87. Apparently, at the higher pressures, sufficient oxygen is present at the surface and the reaction is controlled by the surface oxidation rate. At 0.05 atmospheres, the oxygen transport to the surface appears controlling.

5.1.2.3. Evaluation of JTA

For comparison purposes, JTA was evaluated in this test apparatus. The results are shown in Figure 88. Each point represents a single

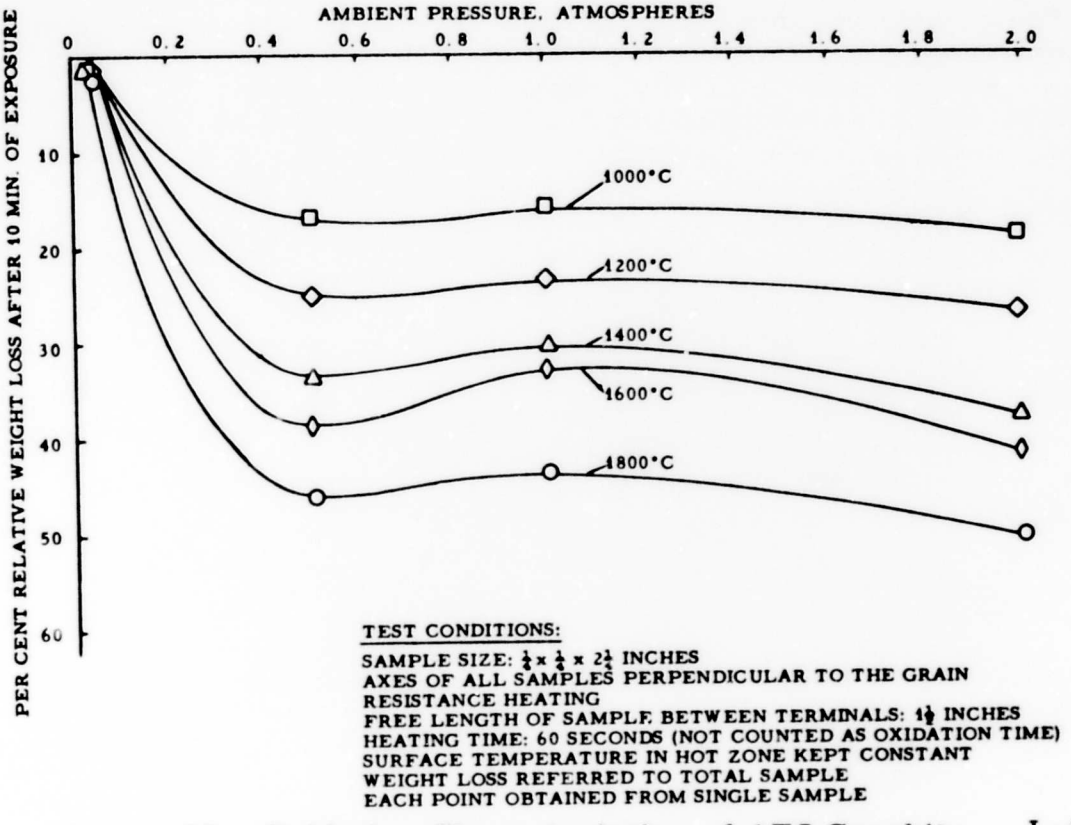

Figure 87. Oxidation Characteristics of ATJ Graphite as a Function of the Ambient Pressure L-908

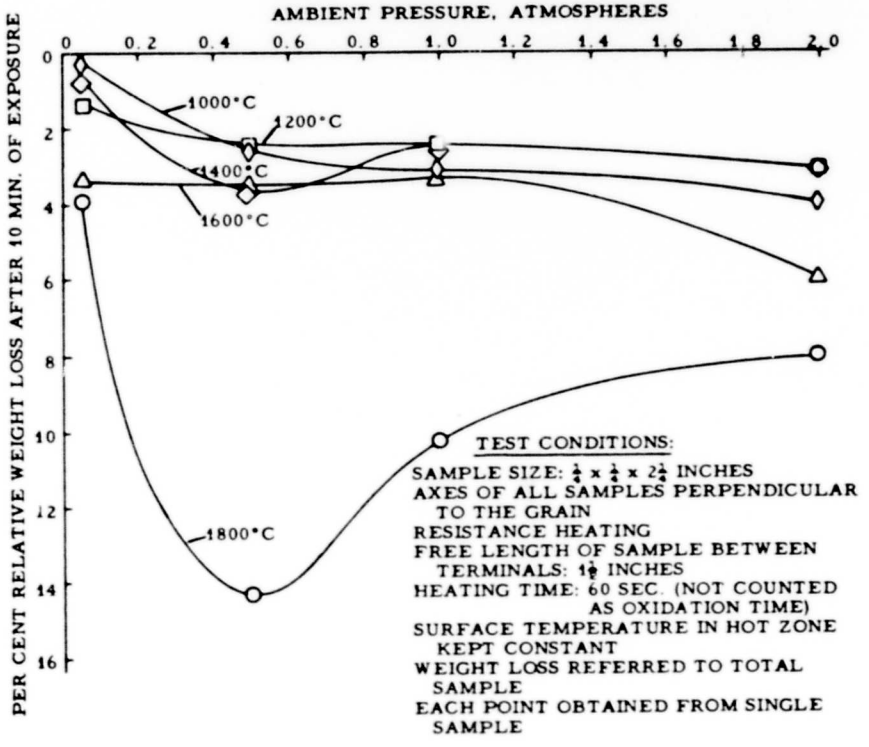

Figure 88. Oxidation Characteristics of JTA as a Function of the Ambient Pressure L-909

test. The complex nature of the mechanism for surface protection makes the interpretation of the data for JTA more difficult. At 1600°C, the rate does not appear to be affected by pressure. The higher value at two atmospheres could be attributed to greater losses of carbon during the initiation period but it may be just experimental variation. The 1800°C maximum at 0.5 atmosphere can be explained as a greater volatilization of the surface oxides formed. At the lower pressure a smaller amount of volatile oxide is formed while at the higher pressure the vaporization is suppressed.

Figure 89 shows hot zone cross sections of the JTA samples after testing. The oxide coatings formed at 1600 and 1800°C under a pressure of 0.05 atm. were powdery and easily blown off the substrate. Apparently at this low pressure the B_2O_3 - representing a major constituent of the coating, evaporates entirely leaving the other oxides poorly bonded together and to the base.

5.1.2.4. Evaluation of JT-0981

Apart from characterizing JT-0981 as one of the most promising high-temperature composites, the evaluation of its oxidation resistance as a function of the ambient pressure could be expected to have further significance. The absence of boron in this material was likely to permit determination of the role of B_2O_3 in the sensitivity of JTA to combinations of high temperature and moderately reduced pressure described in the preceding section.

Weight losses are not reported here because of the poor oxidation resistance of JT-0981 at low temperatures. The weight losses from the cooled sample ends greatly exceed those from the regions at nominal test temperature rendering such data misleading.

Figure 90 shows hot zone cross sections of the samples exposed to various air pressures at 1600 and 1900°C.

The 1800°C cross-section pictures show that oxygen attack is more severe at 0.5 atm. than at 1 atm. JT-0981 does not exhibit the same degree of sensitivity in such conditions as JTA. Comparison of Figures 89 and 90 indicate a larger gap is formed with the JTA and suggests that the boron in JTA is the main cause for the high weight loss during high-temperature, low-pressure exposures.

Findings of this type are a good demonstration of the necessity for tailoring graphite-refractory composites to specific environmental conditions.

5.2. Physical Properties

5.2.1. JTA

Some of the thermal and mechanical properties of JTA were measured under the previous contract.[1] These exploratory determinations

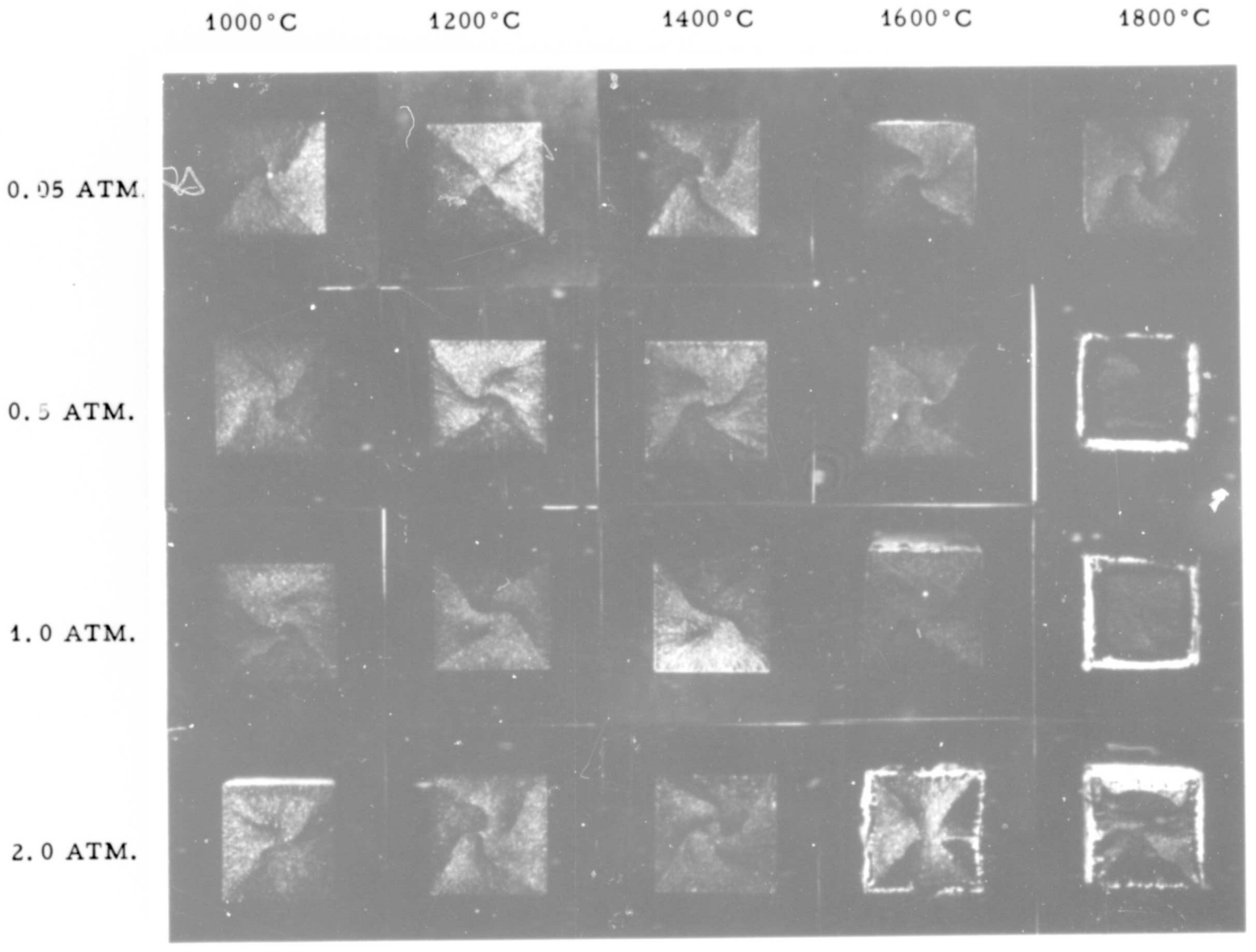

Figure 89. The Effect of Ambient Pressure on the Oxidation Behavior of JTA, Cross Sections of Samples After 10-Minute Exposures

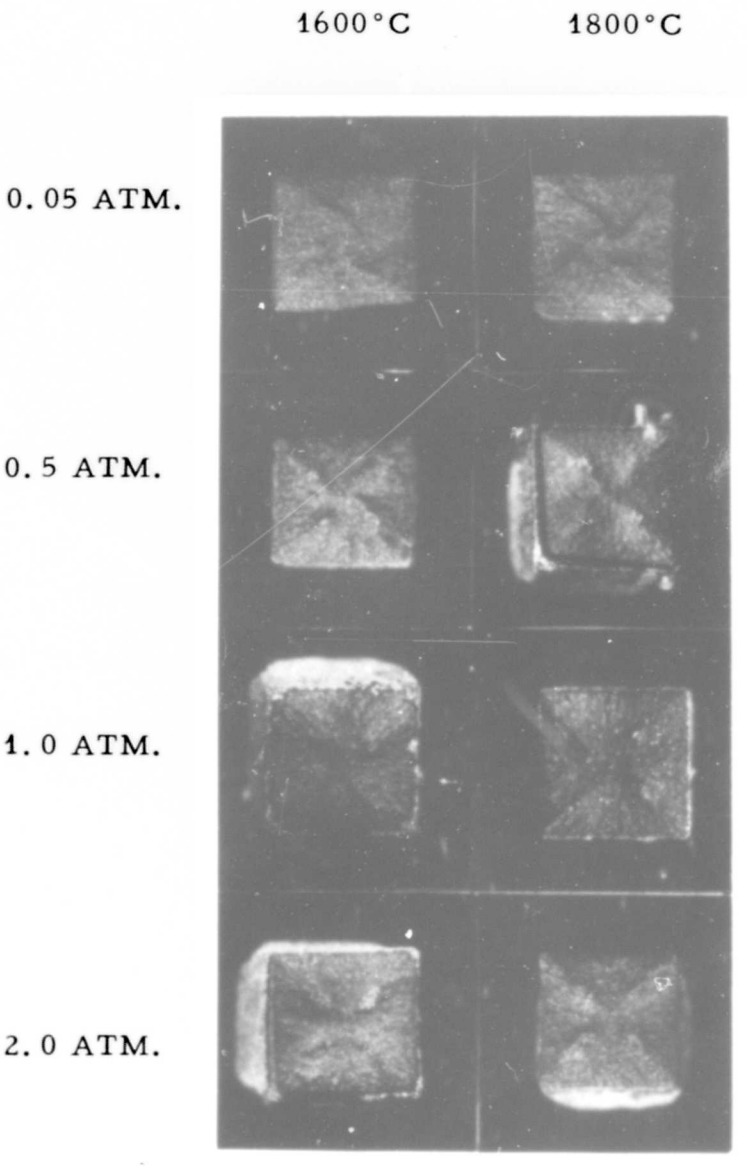

Figure 90. The Effect of Ambient Pressure on the Oxidation Behavior of JT-0981, Cross Sections of Samples After 10-Minute Exposures

were far from comprehensive, and were derived from small experimental lots and single samples. It was desirable to supplement this information with measurements on a number of samples. All evaluations presented here were carried out on samples cut from commercial blanks 5 inches in diameter by 5 inches long, and reasonably large numbers of samples were used wherever practical. The results of measurements at room temperature are compiled in Table 10.

Table 10. Room-Temperature Physical Properties of JTA

	$\overline{X}$*	Max.	Min.	σ*	N*
Bulk Density, g/cc	3.04	3.10	2.88	0.05	45
Young's Modulus, 10^6 lbs./in.^{2}					
With Grain	14.68	17.10	12.18	1.45	22
Across Grain	5.57	5.91	5.04	0.30	23
Tensile Strength, lbs./in.^{2}					
With Grain	10,520	12,085	8,235	2,025	3
Across Grain	4,920	5,100	4,685	195	4
Flexural Strength, lbs./in.^{2} Sample Size: $\frac{1}{2} \times \frac{1}{2} \times 5$ in.					
With Grain	17,160	19,960	14,535	1,434	22
Across Grain	7,995	8,695	5,520	780	23
Compressive Strength, lbs./in.^{2} Sample Size: 1 in. D. x 1 in. L.					
With Grain	25,950	30,100	21,800	2,300	16
Across Grain	34,350	38,000	29,900	2,600	16
Thermal Expansion, 10^{-6}/°C					
With Grain	3.63	4.34	3.23	0.47	8
Across Grain	4.36	4.43	4.27	0.06	8
Thermal Conductivity, $\frac{\text{cal-cm}}{\text{cm}^2 \text{ sec. °K}}$					
With Grain	0.344	0.346	0.313	0.022	4
Across Grain	0.195	0.210	0.182	0.010	6
Electrical Resistivity, 10^{-4} Ω-cm					
With Grain	1.78	1.90	1.65	0.08	22
Across Grain	3.95	4.61	3.46	0.41	23

* $\overline{X}$ = Average; σ = Standard Deviation; N = Number of Samples

The room-temperature stress-strain curves for JTA in tension are shown in Figure 91.

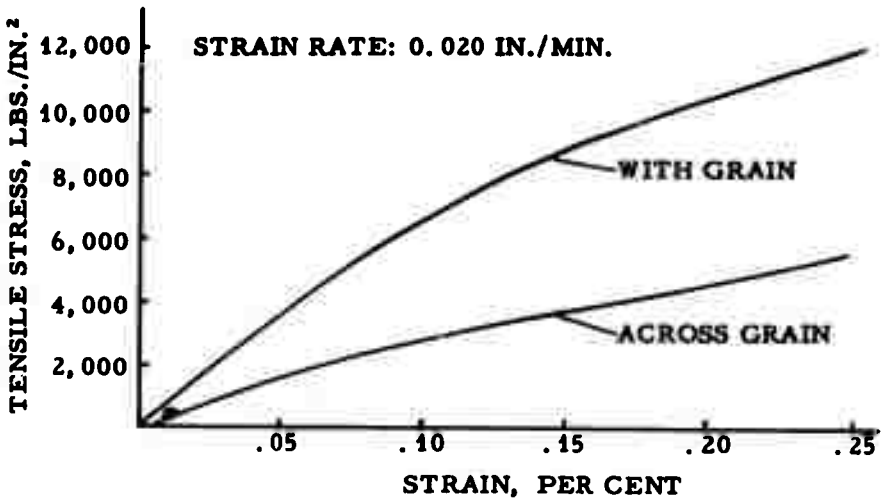

Figure 91. Tensile Stress-Strain Relationships for JTA at Room Temperature L-910

Elevated temperature, flexural strength, and thermal expansion are shown in Figures 92 and 93. Apart from oxidation resistance, strength is undoubtedly a main asset of JTA. Further, the moderately high thermal expansion of this material makes it an attractive substrate for numerous carbide coatings.

5.2.2. JT-0981

Room-temperature physical property determinations on JT-0981 are compiled in Table 11. Comparisons show that with the exception of electrical resistivity, these characteristics do not differ from those of JTA to any significant extent.

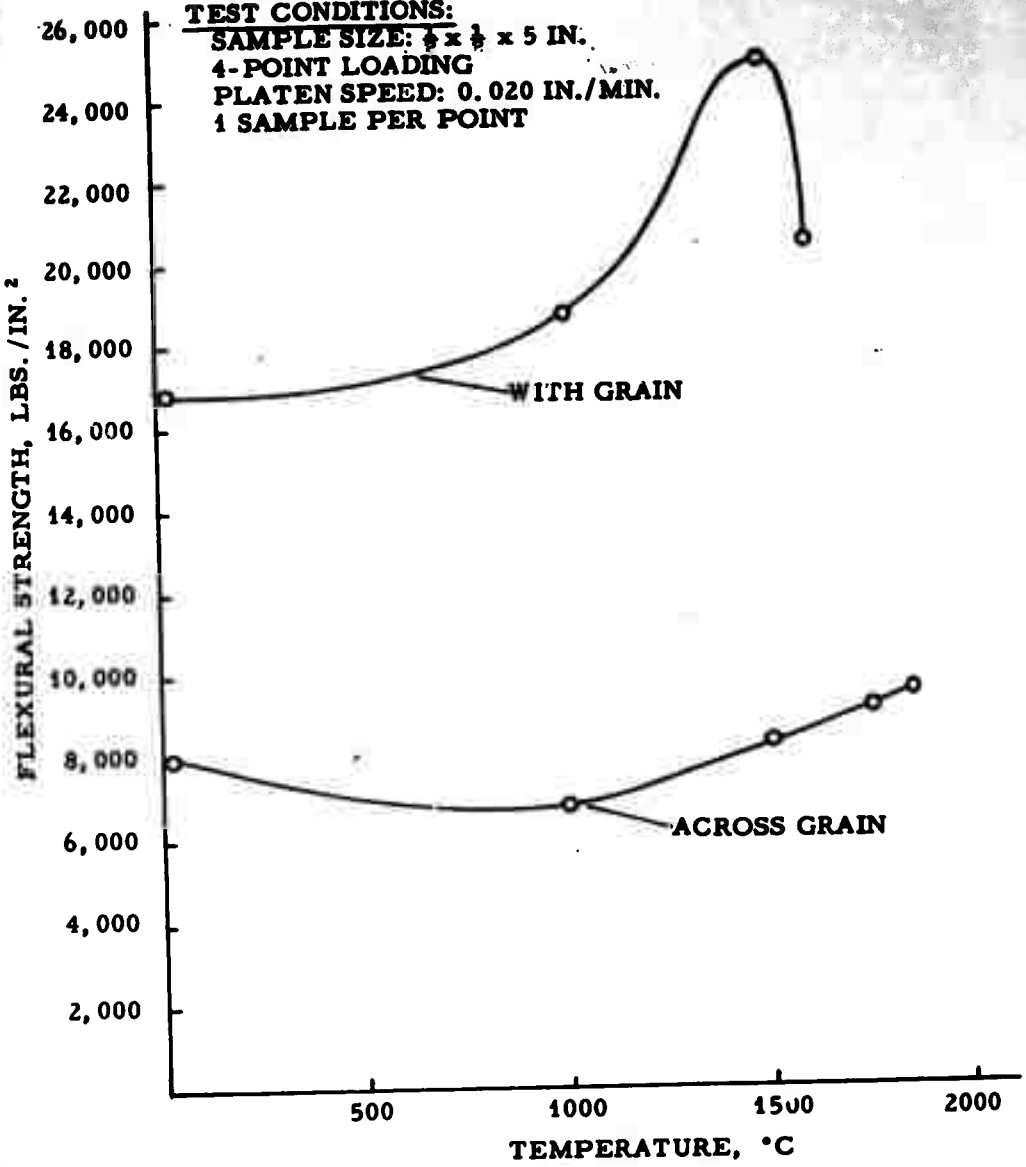

Figure 92. Flexural Strength of JTA Versus Temperature

L-911

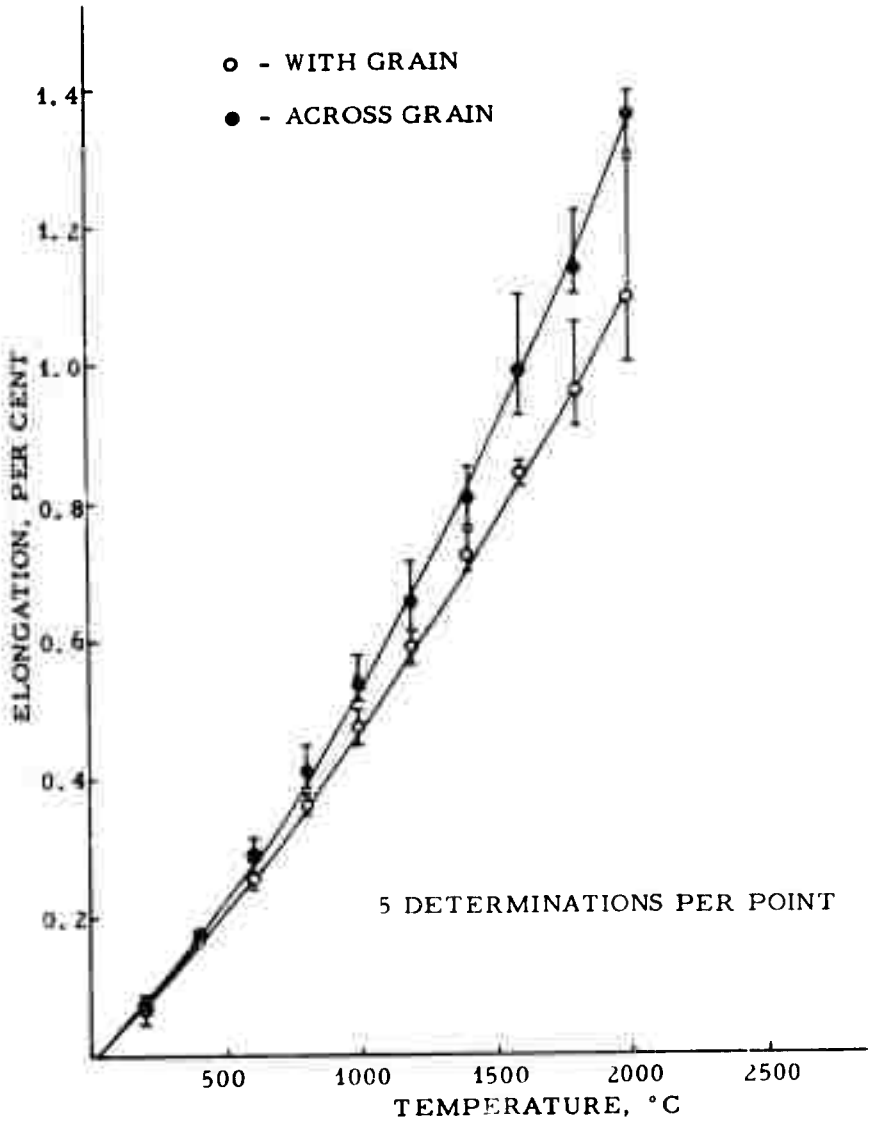

Figure 93. Thermal Expansion of JTA Versus Temperature L-167

Table 11. Room-Temperature Physical Properties of JT-0981

	$\overline{X}$*	Max.	Min.	σ*	N*
Bulk Density, g/cc	3.07	3.16	2.95	0.08	28
Young's Modulus, 10^6 lbs./in.^{2}					
With Grain	13.97	17.97	8.44	3.54	14
Across Grain	5.98	7.46	4.42	1.22	14
Tensile Strength, lbs./in.^{2}					
With Grain	8,720	10,400	7,010	1,695	3
Across Grain	4,760	5,195	4,465	384	3
Flexural Strength, lbs./in.^{2}, Sample Size: $\frac{1}{2}$ x $\frac{1}{2}$ x 5 in.					
With Grain	15,100	18,480	7,070	4,480	14
Across Grain	6,940	9,425	4,670	1,940	14
Compressive Strength, lbs./in.^{2}, Sample Size: 1 in. D. x 1 in. L.					
With Grain	32,150	38,900	20,700	6,550	8
Across Grain	32,000	43,500	22,000	7,750	8
Thermal Expansion, 10^{-6}/°C					
With Grain	3.34	3.63	3.10	0.26	4
Across Grain	3.75	3.87	3.51	0.16	4
Thermal Conductivity, $\frac{\text{cal-cm}}{\text{cm}^2 \text{ sec. } °K}$					
With Grain	0.352	0.378	0.325	-	2
Across Grain	0.228	0.240	0.217	-	2
Electrical Resistivity, 10^{-4} Ω - cm					
With Grain	5.71	8.00	4.74	0.81	14
Across Grain	11.08	13.88	6.05	2.28	14

* $\overline{X}$ = Average; σ = Standard Deviation; N = Number of Samples

6. APPLICATION TESTING OF SELECTED MATERIALS

In modern weapons technology, refractory materials are commonly used as leading edges and rocket motor components. Both applications involve exposure to high-velocity gas and conditions that can not be simulated by any of the test techniques described in the previous section. A series of plasma jet tests were considered to give a test more nearly comparable to actual use conditions.

Most plasma jet evaluations for comparing different materials are carried out with a constant gas enthalpy in a test series. Since the surface temperature may vary widely under these conditions because of variation in thermal properties of the samples, the second series of experiments reported was carried out at a constant temperature on the front surface of the sample.

A plasma test can provide a good simulation of the thermal conditions of a given flight. The simulation is not perfect since, with the available equipment, aerodynamic shear stresses on the flight surfaces can not be simultaneously duplicated. Many coatings of graphite-refractory composites exhibit a molten phase at high temperatures, and removal of the coating by the shear forces is important in the oxidation process. Contrary to the oxidation tests described in earlier sections, plasma exposures provide heating from the outside rather than internal heating, and can yield a qualitative indication of the stripping of the coating by aerodynamic forces.

6.1. Performance of ATJ Graphite, JTA, JT-0965, and JT-0981 in High-Velocity Air Plasma

6.1.1. ATJ and JTA Testing

The first plasma tests on JTA were carried out at the NASA Research Center at Langley Field, Virginia. The sample figuration is shown in Figure 94. The specimen was mounted on a water-cooled holder with its axis parallel to the plasma stream. In a subsonic air plasma with a theoretical free-stream temperature of 1925°C, the front surface of the sample reached a uniform equilibrium temperature of 1740°C. After four consecutive 6-minute exposures, the specimen retained its shape and lost less than 5 per cent of its weight. ATJ graphite in the same test showed a 50 per cent weight loss after 3 minutes.[6]

A cross section of the JTA sample after exposure is shown in Figure 95. In addition to impressive configuration stability, an extremely good bond was found between the coating and the parent material. A picture of the interface is shown in Figure 96. No gap development was in evidence. If there was any effect of the aerodynamic shear stresses during the exposure, it was to prevent bubble formation and ensure that whatever liquid appeared on the surface was spread out uniformly.

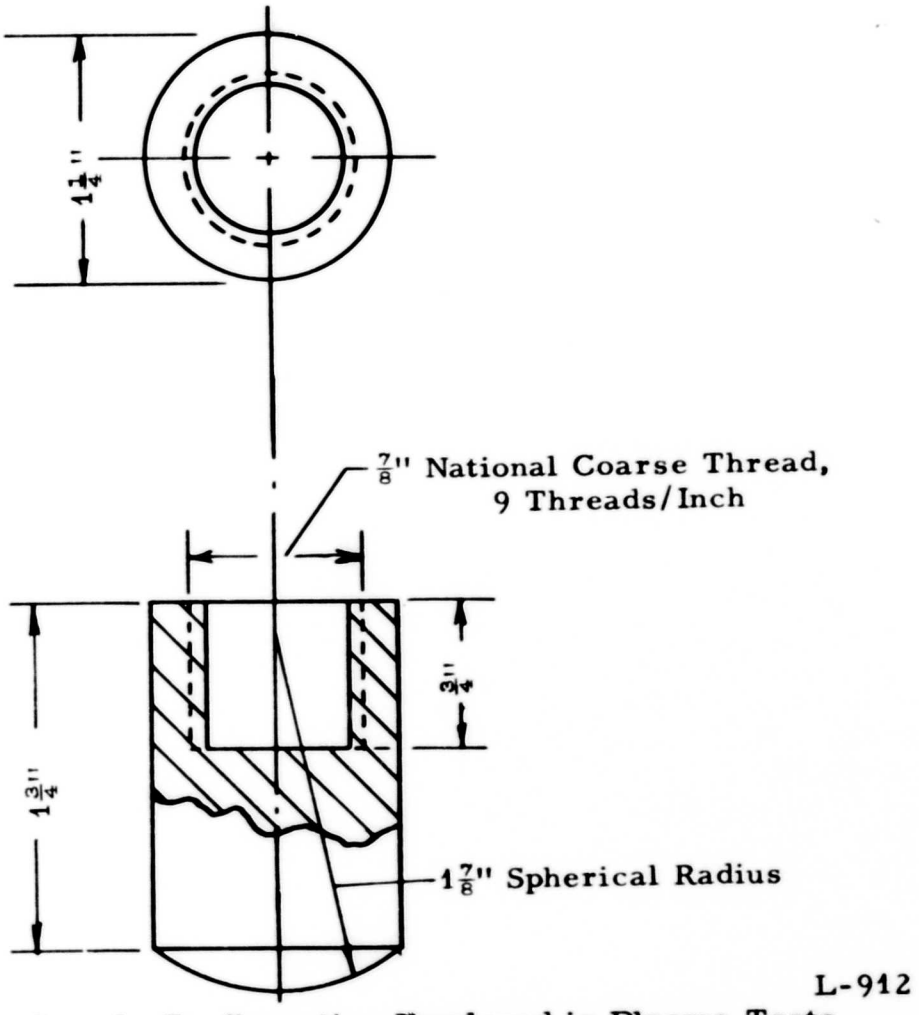

Figure 94. Sample Configuration Employed in Plasma Tests

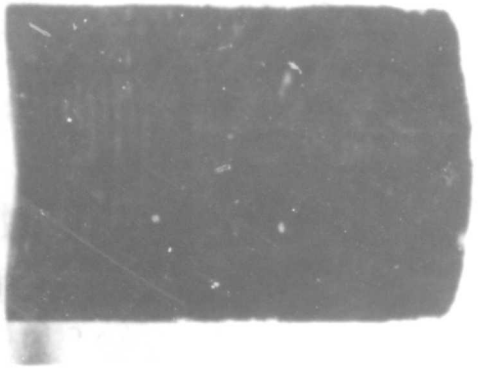

Figure 95. Cross Section of JTA Sample After Four 6-Minute Air Plasma Exposures at a Front Surface Temperature of 1740°C

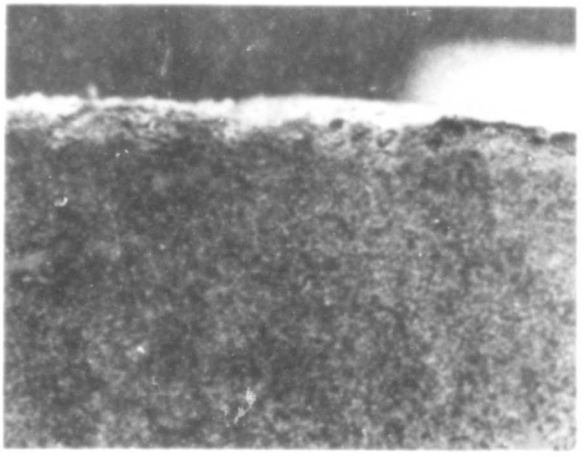

Figure 96. JTA Sample After Four 6-Minute Air Plasma Exposures at a Front Surface Temperature of 1740°C, Interface Between Coating and Parent Material, 4X

An extensive plasma test series was arranged at the Cincinnati Testing Laboratory, a Division of Studebaker Corporation. The sample configuration of Figure 94 was retained. The tests were to be performed at a front surface temperature of 1900°C. Subsonic, sonic and supersonic tests were planned to study the effect of various aerodynamic shear stresses produced by significantly different environmental conditions.

The results of the tests on JTA and ATJ graphite are compiled in Table 12. It is evident that within the range of these tests, increased aerodynamic shear stress at constant surface temperature did not cause an increase in oxidation with JTA. The decrease in the average oxidation rates with duration of the test follows since the rate of loss decreases drastically once the initial surface coating is formed. Figures 97 and 98 show the samples after testing to subsonic and sonic exposures, respectively. JTA is seen to have retained its shape.

Table 12. High Velocity Experiments with JTA and ATJ at 1900°C

Test No.	Sample Material	Test Gas Velocity	Density g/cc	Oxidation Rate * $Mg/cm^2/sec.$	Test Duration Sec.
1-1	ATJ	Subsonic	1.782	4.960	300
2-1	JTA	"	2.985	0.174	300
2-2	JTA	"	3.079	0.105	600
2-3	JTA	"	3.082	0.0934	1200
1-2	ATJ	Sonic	1.792	7.995	150
2-4	JTA	"	3.084	0.179	300
2-5	JTA	"	3.083	0.129	600
2-6	JTA	"	3.097	0.100	1200

* Based on front face area.

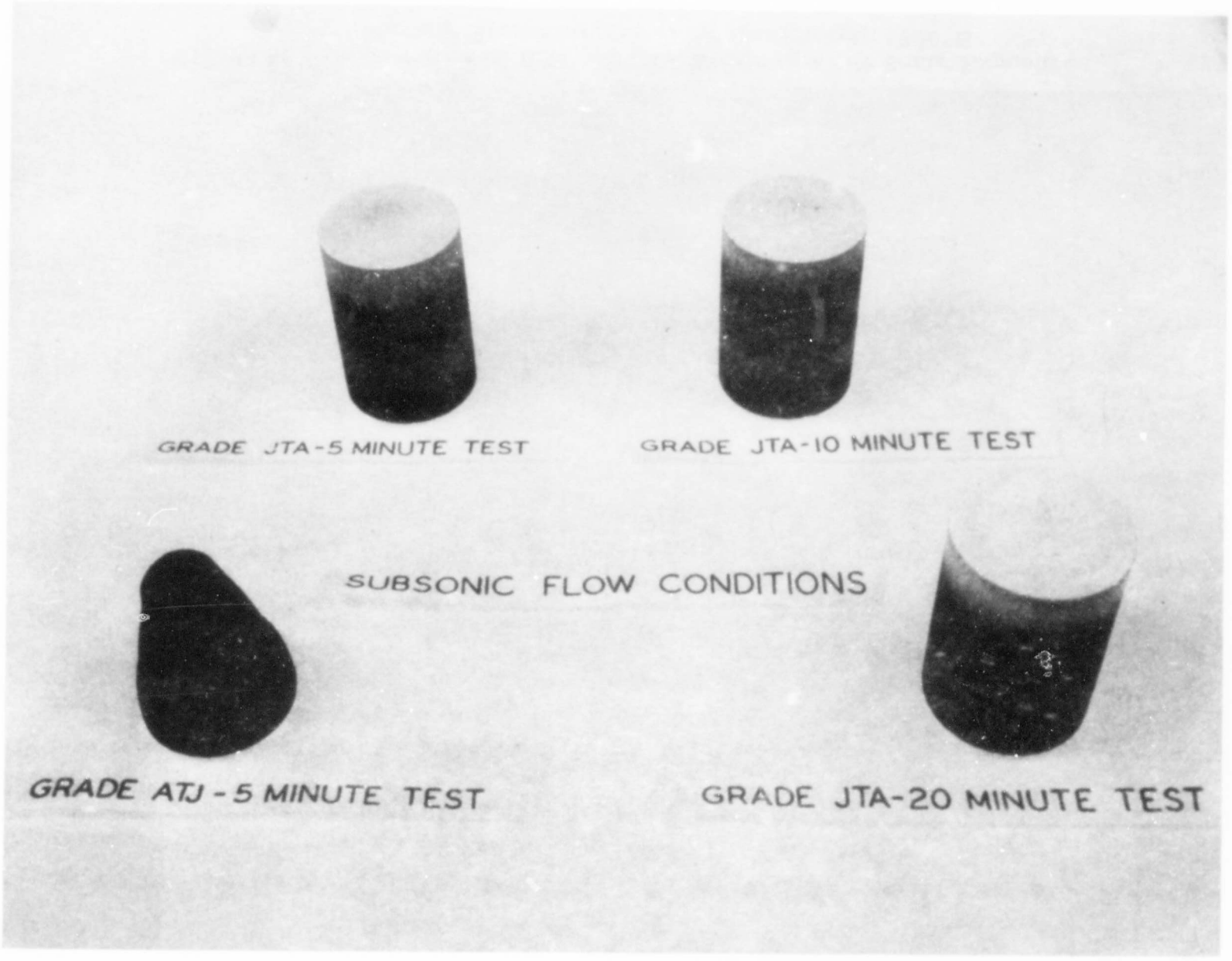

Figure 97. Appearance of ATJ and JTA Samples After Subsonic Exposures at Surface Temperatures of Approximately 1900°C

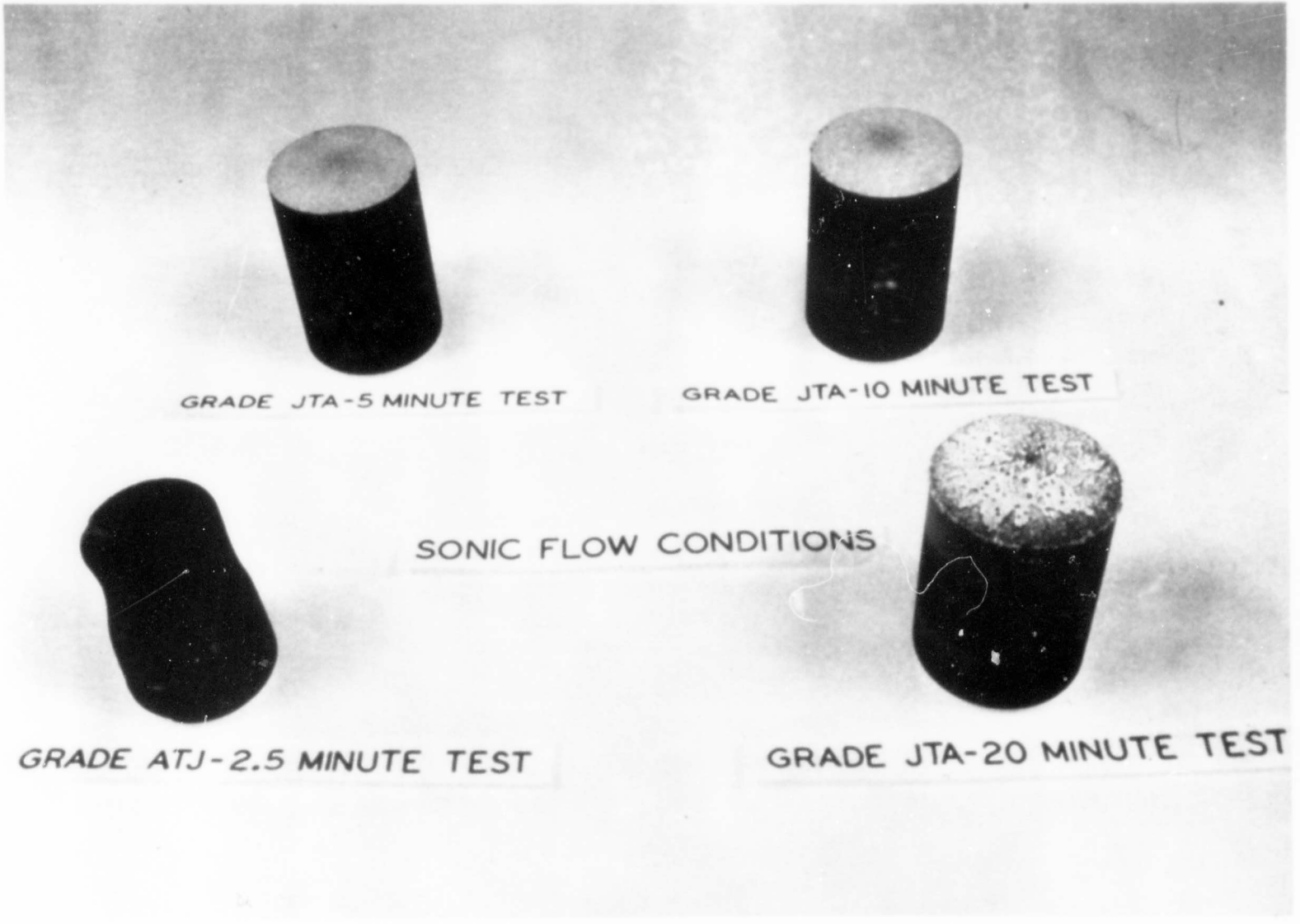

Figure 98. Appearance of ATJ and JTA Samples After Sonic Exposures at Surface Temperatures of Approximately 1900°C

Experiments to evaluate JTA under supersonic plasma conditions were unsuccessful since the desired surface temperature of 1900°C could not be reached. However, during calibration runs for the supersonic test condition the major problem encountered was higher than desired surface temperature (above 2000°C). After a cathode failure and subsequent replacement, the plasma generator could not maintain the sample surface temperature at 1900°C.

The high-temperature calibration runs did yield some qualitative information about JTA's behavior in supersonic plasma conditions. JTA did form a protective oxide coating. The coating did not sheer or flake off during the exposures in excess of 5 minutes. The coating was as tenaciously bonded after cooling to room temperature as the coatings formed under the other flow conditions.

The tests performed with the replacement cathode yielded a temperature of 1500°C and the results are shown in Table 13.

Table 13. High Velocity (Mach 3.5) Experiments with JTA and ATJ at 1500°C

Test No.	Sample Material	Test Gas Velocity	Density g/cc	Oxidation Rate* $Mg/cm^2/sec.$	Test Duration Sec.
1-3	ATJ	Supersonic	1.799	0.797	600
2-7	JTA	"	3.034	0.076	300
2-8	JTA	"	3.036	0.054	600

* Based on front face area.

6.1.2. JT-0965 and JT-0981 Testing

Laboratory oxidation tests indicated that JT-0965 and JT-0981 were superior in performance at high temperature to JTA. To test these materials further, a series of sonic tests at 2000°C and 2300°C was planned at Cincinnati Testing Laboratory. During the surface-temperature calibration runs it was noted that the protective coating was not being formed on the lower temperature side walls of the specimen. The oxidation rate on the unprotected surfaces was so much greater than from the test surface that any long-term weight loss data would be meaningless and further testing was stopped. The calibration runs did provide qualitative information on performance of the composites. An oxide coating formed at each exposure temperature. After cool down from a 2000°C exposure, JT-0965 had a hard, jagged oxide coating tenaciously bonded to the parent material. The JT-0981 did not have a well-bonded coating after the same treatment.

Both materials lost molten oxide from the front surface during the 2300°C calibration runs. The sample came up to temperature rapidly and was apparently unaffected until a large portion of the sample reached the front surface temperature, then small bubbles appeared on the front surface. The bubbles formed droplets which moved to the edge and were blown from the sample. Figures 99 to 102 show the appearance of specimens after the 2300°C runs.

6.2. Performance of JTA in Rocket Motors

The materials group of Thompson-Ramo-Wooldridge, Space Technology Laboratory at El Segundo, California has tested grade JTA as a nozzle insert material in a liquid propellant system with success. The firing parameters were a hydrazine-UDMH 50:50 mixture fuel, nitrogen-tetraoxide oxidizer, fuel-oxidizer ratio of 1.60 ±0.05 and a chamber pressure of 110 lbs./in.^{2} absolute which yields a flame temperature of 5200°F. Grade JTA is compared to a silica cloth phenolic system in Figure 103, illustrating the respective pressure-time curves.

The "knee" in the JTA curve probably occurred when the refractory additives were melting at a significantly rapid rate and allowed a continuous removal of a liquid surface coating.

Figure 99. Side View of JT-0965 After Sonic Air Plasma Exposure at a Front Surface Temperature of 2300°C, Test Duration, 200 Sec.

Figure 100. Front View of JT-0965 After Sonic Air Plasma Exposure at a Front Surface Temperature of 2300°C, Test Duration, 200 Sec.

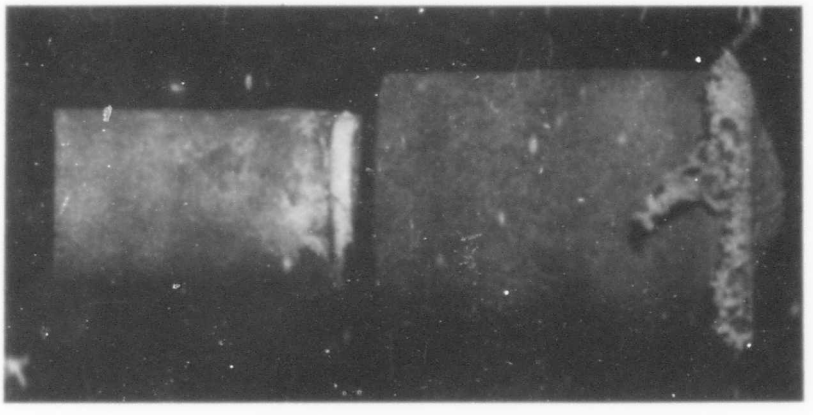

Figure 101. Side View of JT-0981 After Sonic Air Plasma Exposure at a Front Surface Temperature of 2300°C, Test Duration, 200 Sec.

Figure 102. Front View of JT-0981 After Sonic Air Plasma Exposure at a Front Surface Temperature of 2300°C, Test Duration, 200 Sec.

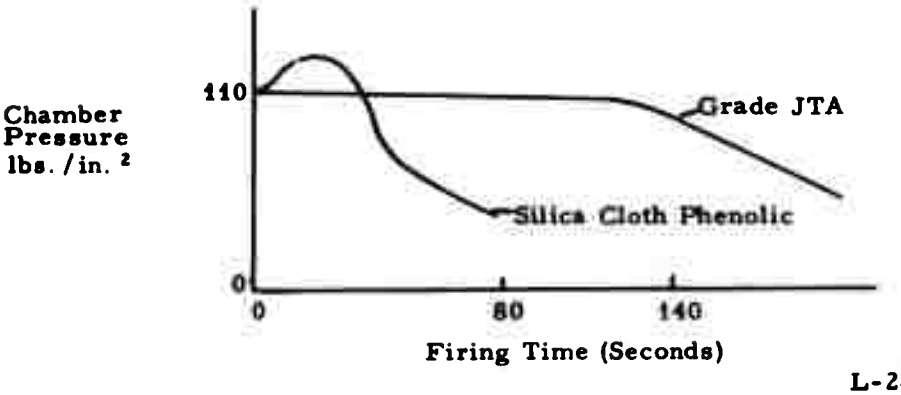

L-289

Figure 103. Performance of JTA as a Throat Insert in a Liquid Fuel Rocket Motor as Compared to Silica Cloth Phenolic Jsed Under Identical Conditions

7. RECOMMENDATIONS FOR FUTURE WORK

Further work in the development of graphite oxidation-resistant composites for use above 2000°C should be concentrated on systems containing hafnium or thorium. Substitution of hafnium for zirconium in composites with silicon and carbon permits the formation of a more adherent coating. Thorium oxide, although more difficult to handle, forms a strong bond with the graphite matrix material.

Graphite-refractory composites should be tailored to fit the specific requirements of the service environment. Further studies of the type reported in this document would aid in the development of the information to permit this tailoring.

Although these compounds were developed basically as oxidation-resistant materials, the high strength high conductivity of the materials should not be overlooked for use where the oxidation resistance is not the only consideration. The graphite-refractory composite may eventually assume the same role in graphite technology as is played by alloys in the metal technology.

8. REFERENCES

1. JANAF Thermochemical Tables, Thermal Research Laboratory, The Dow Chemical Company, Midland, Michigan (1963).

2. Kubaschewski, O., and E. L. Evans, "Metallurgical Thermochemistry," Pergamon Press, New York (1958).

3. Zeitsch, K. J. and J. Criscione, "Oxidation-Resistant Graphite-Base Composites," WADD Technical Report 61-72, Volume XXX.

4. Roth, R. S., and L. W. Coughanour, J. Research, Natl. Bur. of Standards, 55 [4] 212 (1955).

5. Brown, F. H., and P. Duwez, J. Am. Ceram. Soc., 38 [3] 98 (1955).

6. Manning, C. R., and E. E. Mathauser, "Investigation of Some New Materials for Aerospace Vehicle Applications," Paper Presented at the Sixth National SAMPE Symposium, Seattle, Washington, (November 1963).

BLANK PAGE